Unsymmetrically Substituted Group 13 and 15 Compounds in Intramolecular Frustrated Lewis Pair Synthesis

Aisling Frances Roper

Christ Church

Thesis submitted for the Degree of Doctor of Philosophy

Hilary Term 2024

Acknowledgements

Firstly, I would like to express my deepest thanks to my supervisor, Professor Simon Aldridge, whose palpable enthusiasm and second-to-none scientific knowledge have made every meeting, and the degree as a whole, both formative and fun.

Thanks also must go to my second supervisor, Professor Dermot O'Hare, for accepting my tendency to veer away from my project description with (for the most part) good grace.

It has been such a privilege to meet, and work with, some incredibly talented people in the Aldridge group and there are a many to whom I would like to give a massive thanks. Dr Josef Boronski, whose generous sharing of expertise was instrumental in the success of my chemistry. I am also so grateful for him for letting me stay in his spare room, and for being an enthusiastic fellow climber of Oxford rooftops. Agamemnon Crumpton, best computational collaborator, and originator of the iconic compliment "It's not a very nice thing to say, but you are a dreadful colleague". Jordan Dring, ultimate Part II, and most gracious completer of maybe 100 columns. Liam Griffin, king of ombré, owner of the coldest back in Oxford, and a man whose talents in chemistry are only surpassed by his ability to absolutely neck a pint. Dr Caitilín McManus, who made every lab day the best fun, and has continued to be a wonderful friend from Grenoble. Thank you for always being on the end of the phone for every up and down. Job Strujis (Dutch), a worthy inheritor to the title of best dressed member of S12. Lewis Wales, whose fumehood I already miss coming to for chats/ sharing of lab secrets/ my made up riff for 'the Six', it was *hilarious*.

From the O'Hare group, special thanks to Alex Evans, always a bright presence in the CRL. Our lengthy desk chats were high points of my day! Matt Haynes, fellow purveyor of the frequent insane events in the department. Gabija Navickaité, the path from tolerating each other to bestie has been beautiful and I look forward to its continual.

Thanks also to past and present members of the Aldridge group – Omar Apolinar, Dr Alexa Caise, Dr Mathias Ellwanger, Dr Andreas Heilmann, Dr Malte Fischer, Dr Andrey Protchenko, Dr Matt Roy, Dr Marcel Schropp, Dr Xiongfei Zheng and Dr Xueer Zhou.

In the wider Oxford chemistry ecosystem, thanks go to Martin Flerin, Tara Lurshay, Ben Shennan and Charlie Simms. I would like to thank the chemical crystallography department – Amber and Kirsten, for running a truly exhaustive training programme, and Keith for always letting me start my data collection early. I owe a great debt of thanks to the support staff in the CRL, especially Jude for repairing many seemingly un-fixable vacuum pumps, and Billy Fox for always amusing emails on the various goings on in and around the building.

Outside of the CRL, thanks must go to Dr Connor Ellis for being a lovely housemate to commiserate with over long days of failed reactions. Thank you to my greatest friend, my sister Caitlin. Thank you to my brother Jack, who is the funniest person I have ever met, and to my brother-in-law James, alter ego Cousin Robert. Finally, thank you to my endlessly supportive parents for giving me the confidence to always go for my dreams, it means everything to me.

Abstract

This thesis explores the viability of potential routes towards surface supported xanthene-based Frustrated Lewis Pairs (FLPs). This is carried out primarily through the synthesis of new Group 13 and 15 Lewis acids and bases, and their addition to xanthene precursors. The dihydrogen activation properties of the FLPs obtained is also examined. An introduction to relevant literature is made in **Chapter 1**, and experimental/characterisation methods are defined in **Chapter 2**. **Chapter 3** details the preparation of a series of heteroleptic *tris* aryl boranes. A robust synthetic route towards *bis* aryl methoxyboranes is introduced, and these compounds are used to prepare a selection of corresponding bromoboranes which are precursors to a series of triaryl boranes. Successful synthesis of desired *tris* as opposed to *tetra* substituted aryl boranes is highly dependent on the steric profile of the final substituent introduced. **Chapter 4** employs the bromoborane reagents prepared in the previous chapter for the synthesis of a series of FLPs varied at the Lewis acid moiety. Three of these systems are capable of reversible H_2 activation, two to a sufficient extent such that this equilibrium can be studied by variable temperature NMR spectroscopy. In contrast to previous reports of related species, the thermodynamic parameters underpinning hydrogenation cannot be described by a single linear van't Hoff plot. Instead, two disparate linear regimes are observed. A 'high temperature' series follows the expected trend of equilibrium moving towards the reaction product as temperature decreases. Below an inflection point, the opposite trend is seen – implying reversal of the reaction with temperature decrease. This unexpected reactivity was probed by quantum chemical calculations (carried out by Agamemnon Crumpton). These calculations suggest that below a certain temperature,

intermolecular aggregation of the FLPs is energetically preferred over hydrogenation, preventing facile hydrogen activation. The final results section, **Chapter 5**, looks at the construction of a range of xanthene-phosphines featuring substituents intended to be amenable to surface attachment. Following the preparation of these reagents, they are examined for their potential as precursors to model surface supported FLPs. It is found that placing a methoxy aryl group on a xanthene-phosphine inhibits subsequent functionalisation of the backbone to attain an intramolecular FLP. In contrast, introduction of a dimethylamino aryl lends the system to facile synthesis of FLPs furnished with three different functional groups on phosphorus. Whilst the pairs synthesised in this chapter did not prove suitable for attachment to a surface, the design principles gained from this work provide a clear direction for future synthetic strategies. The outlook is discussed in **Chapter 6**.

Abbreviations

°C	degrees Celsius
ΔG°	standard reaction free energy
ΔG‡	free energy of activation
ΔH°	standard reaction enthalpy
ΔH‡	enthalpy of activation
ΔS°	standard reaction entropy
ΔS‡	entropy of activation
approx.	approximately
Ar^F_6	3,5-*bis*(trifluoromethyl)phenyl
BAr^F_{18}	*tris*[3,5-bis(trifluoromethyl)phenyl]borane
Bcat	catecholborane
$B(C_6Cl_5)_3$	*tris*(pentachlorophenyl)borane
$B(C_6F_5)_3$, BCF	*tris*(pentafluorophenyl)borane
$[B(C_6F_5)_4]^-$	*Tetrakis*[3,5-*bis*(trifluoromethyl)phenyl]borate
BF_3	borontrifluoride
BMe_3	trimethylborane
Bpin	*bis*(pinacolato)diboron
ca.	circa
calc.	calculated
C_6Cl_5	pentachlorophenylborane
CO_2	carbon dioxide
C_6F_5	pentafluorophenylborane
$ClB(C_6Cl_5)_2$	*bis*(pentachlorophenyl)chloroborane
$ClB(C_6F_5)_2$	*bis*(pentafluorophenyl)chloroborane
d	doublet
Dipp	2,6-di*iso*propylphenyl
DFT	Density Functional Theory
equiv.	equivalent(s)
Et_2O	diethyl ether
Et_3PO	triethylphosphine oxide
FLP	Frustrated Lewis Pair
h	hour(s)
H_2	dihydrogen
$HB(C_6F_5)_2$	*bis*(pentafluorophenyl)borane
HBr	hydrogen bromide
$^iBu_3Al$	tri*iso*butylaluminium
^{i}Pr	*iso*propyl
$^iPr_3SnOTf$	tri*iso*propylstannyliium triflate
J	coupling constant
K	Kelvin
LA	Lewis acid

m	meta
m	multiplet
Mes	mesityl
min	minute(s)
^{n}BuLi	*n*-butyllithium
$^{n}Bu_3SnOTf$	tri-n-butyllstannyliium triflate
NaH	sodium hydride
N_2O	nitrous oxide
NMR	nuclear magnetic resonance
NOE	Nuclear Overhauser effect
o	ortho
p	para
Ph	phenyl
$[PhNHMe_2]Cl$	*N,N*-dimethylaniline hydrohloride
$PMes_3$	trimesitylphosphine
$PPhCl_2$	dichlorophenylphosphine
PPh_3	triphenylphosphine
$P^{t}Bu_3$	tri*tert*butylphosphine
$P^{t}BuCl_2$	dichloro*tert*butylphosphine
RT	room temperature
^{s}BuLi	secondary butyllithium
SPS	solvent purification system
^{t}Bu	tertiary butyl
^{t}BuLi	tertiary butyllithium
THF	tetrahydrofuran
TMS	triamethylsilane
TMEDA	*N,N,N,N*,-tetramethylethylenediamine
VT	variable temperature

Table of Contents

Chapter 1 – Introduction

1.1 Overview

Lewis acid-base theory is predicated on the principle that lone pair donation from an electron rich base to an electron poor acid yields a dative covalent bond, a motif implicit in the understanding of molecular interactions.[1] This paradigm was disrupted by the discovery that classical adduct formation can be prevented by peripheral steric bulk around one – or both – of the acid and base (**Figure 1.1**).[2] While bonding is prevented, close approach is not. The ensuing unquenched reactivity of proximate species can facilitate the activation of covalent bonds, such as in H_2.

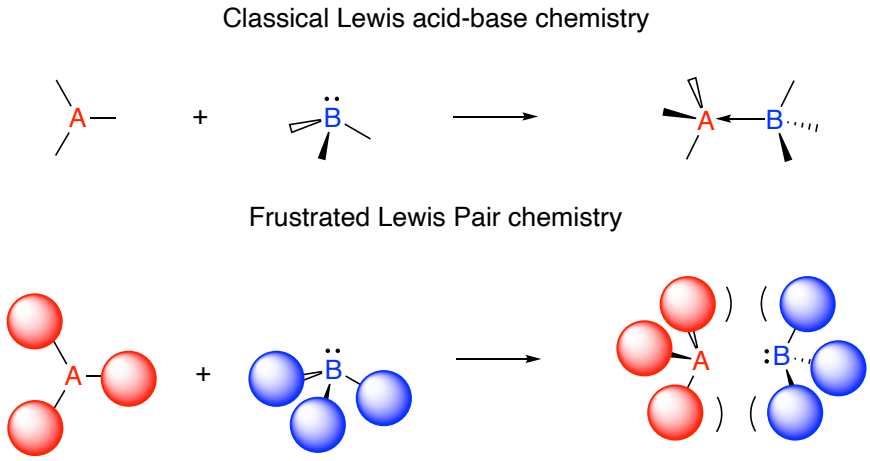

Figure 1.1 – Prevention of typical Lewis acid/base reactivity by substituent bulk.

This class of compounds is known as Frustrated Lewis Pairs (FLPs). The initial report using this vocabulary concerned an intramolecular phosphino-borane capable of reversible hydrogen splitting (**Scheme 1.1**), a process hitherto generally considered solely to be the domain of transition metal complexes.[3–6]

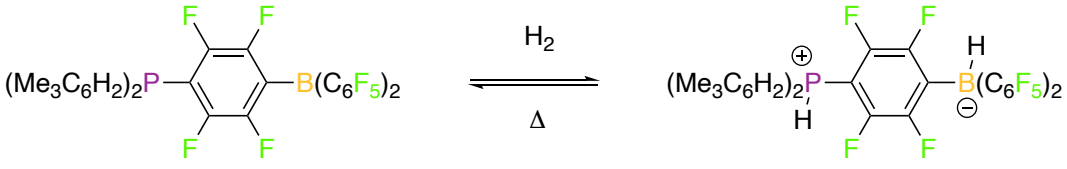

1.1 **1.2**

Scheme 1.1 – The first reported example of dihydrogen activation by an FLP.

The ability to replicate transition metal-like reactivity with compounds of the Main Group elements is a prized synthetic tool and this work provided new impetus in the field.

1.2 History and Development

Whilst they were not described as FLPs at the time, Brown observed in 1942 that sterically congested acid/base combinations fail to form dative adducts.[7] This was exemplified by the reactions of lutidine (2,6-dimethylpyridine) with BF_3 *versus* BMe_3 (**Scheme 1.2**); in the latter case a N→B bond is not observed on mixing the amine and borane due to steric congestion.

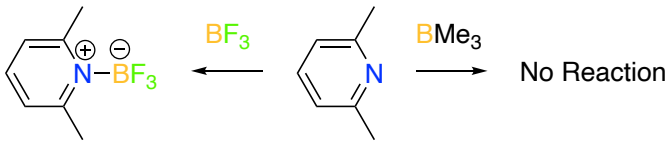

1.3 **1.4**

Scheme 1.2 – Reaction of lutidine with BF_3 versus BMe_3.

Reports of similar non-classical behaviour emerged in ensuing years, although without the linking vocabulary which is today associated with these systems.[8–10] For example, in 1959 Wittig and Benz reported the *ortho*-phenylene bridged phosphonium borate **1.7**, and seven years later Tochtermann observed C=C bond activation in butadiene by a mixture of triphenylborane and tritylsodium (**Scheme 1.3**).

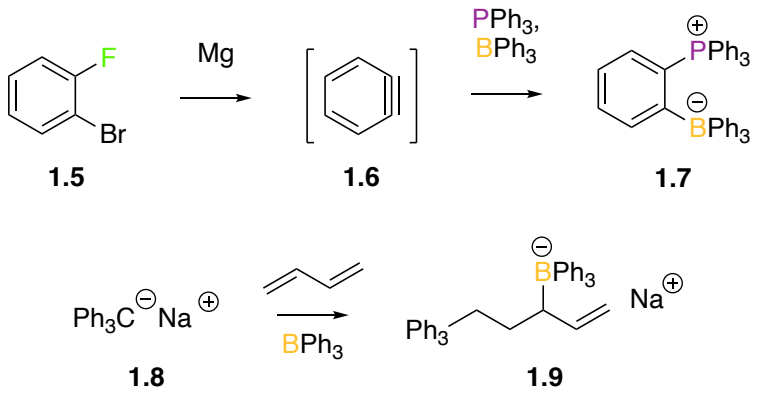

Scheme 1.3 - Early FLPs.

The 2006 work of Stephan *et al*., which conclusively articulated this family of compounds, led to a subsequent rapid development of understanding and scope, both in terms of acid/base combination and reactivity.[11] In the year after publication of their initial findings, the same group demonstrated dihydrogen activation with commercially available tri*tert*butylphosphine (P^tBu_3) or trimesitylphosphine ($PMes_3$), in combination with *tris*(pentafluorophenyl)borane $B(C_6F_5)_3$ (**Scheme 1.4**).[12]

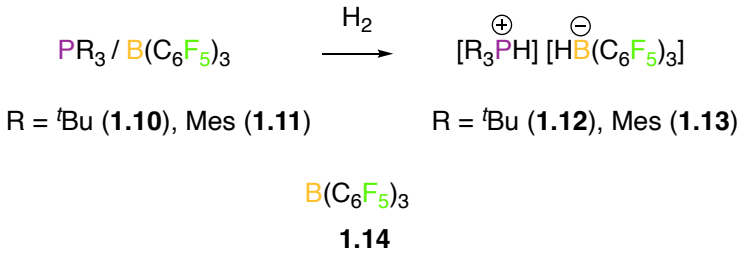

Scheme 1.4 – Irreversible dihydrogen activation by intermolecular FLPs.

Herein they showed that the principle of small molecule activation by sterically frustrated Lewis acid/base combinations could be applied to inter-, as well as intramolecular systems. Reaction of this same two-component system with alkenes yields different types of products depending on whether the olefinic species is free or incorporated in the phosphine (**Scheme 1.5**).[13] When one of the phosphine substituents is a terminal alkene, a 5-membered phosphorus-containing heterocycle with a pendant borane is formed. By contrast, ethylene, propylene or hex-1-ene participate in termolecular reactions with $B(C_6F_5)_3$ and P^tBu_3. The phosphine and

borane add to opposite ends of the double bond, with the same anti-Markovnikov regioselectivity as is observed in the hydroboration of alkenes.[14]

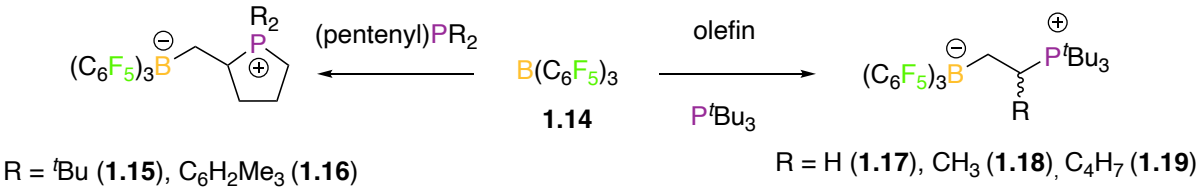

Scheme 1.5 – FLP-mediated olefin activation to yield either intramolecular cyclisation or intermolecular addition products.

Unequivocal separation of the Lewis acid and base might be assumed to be a reasonable pre-requisite for FLP-type reactivity. A counterpoint to this hypothesis was provided by Erker *et al.*, who studied hydrogen activation by an ethylene (—CH_2CH_2—) bridged system, **1.20**/**1.20'** which exists in equilibrium between its cyclic and open chain forms (**Scheme 1.6**).[15] The NMR spectroscopic data for this compound suggests a 4-membered heterocycle (**1.20**), however quantum chemical calculations indicate the existence of two energetically reasonable open-chain isomers, represented by **1.20'**, situated approx. 7 kcal mol^{-1} above **1.20**. The authors suggest that these isomers, in which the phosphine and borane are separated, are the active species for dihydrogen activation.

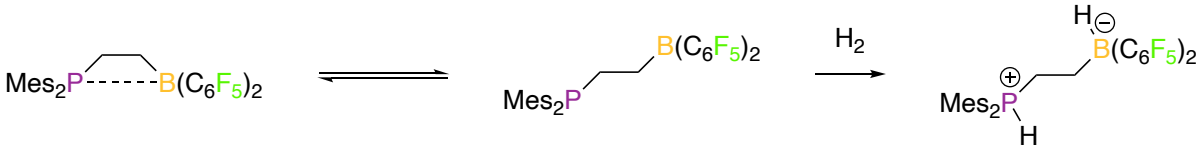

Scheme 1.6 – A cyclic intramolecular FLP in equilibrium with its hydrogen activating open chain isomer, and the hydrogenation product.

These landmark findings have been substantially built upon, and today 'FLP-like reactivity' is often used to describe synergistic donor/acceptor behaviour towards substrates such as nitriles and carbonyls.[16–20] This review of selected literature will largely focus on dihydrogen

activation as it relates towards hydrogenation, and the development of intramolecular pairs, as well as the outlook, specifically towards surface supported catalysis.[21–23]

1.3 Hydrogen Activation and Mechanism of Reactivity

Dihydrogen activation is the archetype of FLP reactivity, and the mechanism of heterolytic cleavage has been investigated since the infancy of the field.[24–29] Two pathways for this reaction were suggested in the first report (**Scheme 1.7**).[2] In these possible mechanisms, either a proton or hydride migrates from the base or acid to the *ipso*- carbon on the opposite side of the bridging fluoroaryl ring, followed by 1,2 hydrogen elimination to recover the "free" Lewis pair.

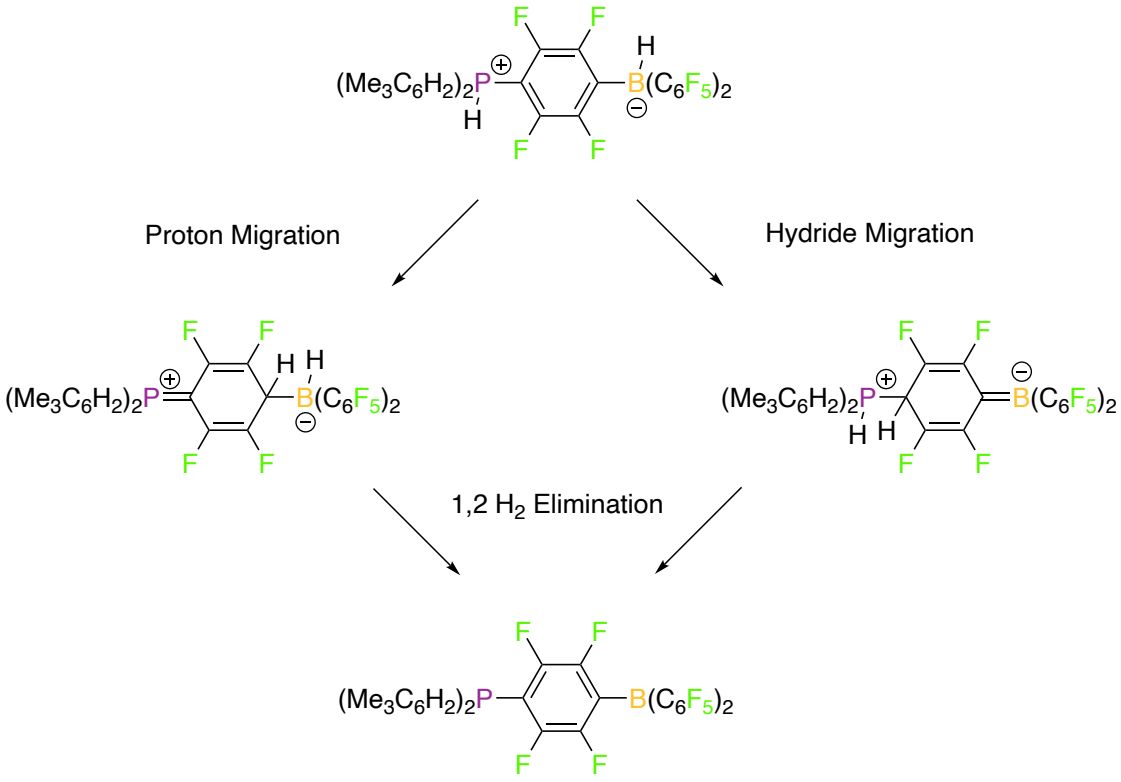

Scheme 1.7 – Initial postulated mechanism for hydrogen loss from an FLP.

In subsequent work, two potential reaction mechanisms for heterolytic hydrogen cleavage by a system composed of separate phosphine and borane compounds were postulated (**Scheme 1.8**).[12] One pathway draws analogies with the side-on donation/back donation interactions

typically seen in transition metal chemistry.[30] Alternatively, end-on base to substrate interaction coincident with hydrogen to acid donation was considered. No spectroscopic evidence for either intermediate was observed.

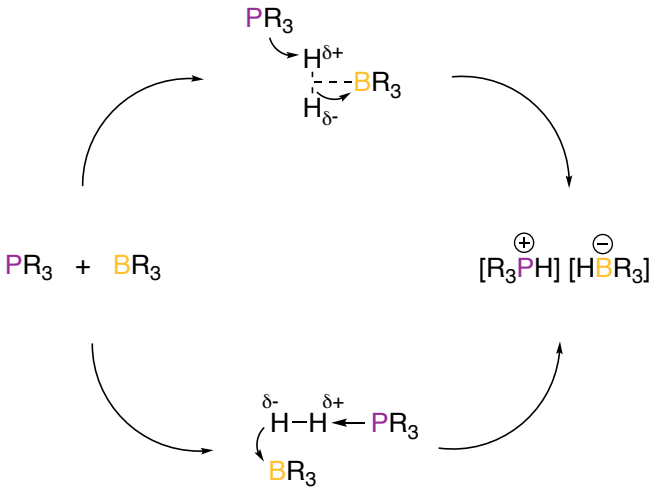

Scheme 1.8 – Suggested substrate orientations for hydrogen splitting.

Quantum chemical calculations have also been used to probe the activation of H_2 by P^tBu_3 or $PMes_3$ and $B(C_6F_5)_3$.[31] This study invoked the pre-association of the Lewis acid/base pair in an encounter complex which subsequently captures H_2 (**Figure 1.2**). Moreover, this idea possesses the advantage that an entropically unfavourable termolecular acid/base/substrate collision is circumvented.[32]

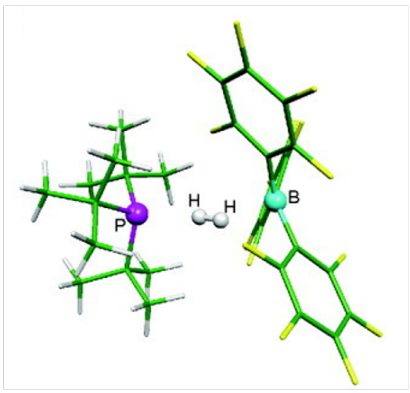

*Figure 1.2 – Computed hydrogen encounter complex. Reproduced with permission from 'Mechanism of Hydrogen Activation by Frustrated Lewis Pairs', Int. J. Quantum Chem., 2009, **109**, 2416–2425.*

In this model, non-covalent interactions (hydrogen bonds and dispersion forces) hold the reactive centres in the requisite orientation for a reaction to occur. The function of the frustration is that it facilitates a low energy conformation for interaction with dihydrogen. This induces polarisation of the molecule and cleavage of the H—H bond, in a concerted manner with the formation of P—H and B—H bonds.

For a system with a two-component active site, amenability towards the desired reactivity is contingent upon the combined strength of both components.[33] This can be well modelled for the reaction with dihydrogen, a simple substrate. In the case of FLPs, this means that the constituent acidity, basicity, and their ability to stabilise the transition state must overcome the energetic penalty involved in H—H bond breakage. Additionally, it is entropically unfavourable to capture a gas such as hydrogen. It is helpful in this discussion to consider inter and intramolecular systems separately, as was used in an examination of the thermodynamics of H_2 splitting (**Figure 1.3**).[34]

$$B + A + H_2 \rightarrow [BH]^+[AH]^- \quad (1)$$

$$B{\sim}A + H_2 \rightarrow [^+HB{\sim}AH^-] \quad (2)$$

Figure 1.3 – General equations for the activation of dihydrogen by inter and intramolecular FLPs where B denotes base, and A denotes acid.

Whereas cumulative acidic/basic strength correlates well with free energy for non-bonded intermolecular pairs, cooperativity in intramolecular systems influences reactivity. Moreover, the inherently smaller entropic loss upon binding to intramolecular FLPs might be enough to compensate for attenuated reactivity – suggesting a broader scope of possible substituents in pairs of this type.

1.3 Hydrogenation

1.3.1 Nitrogen Containing Substrates

A natural extension from hydrogen activation is hydrogenation, be it stochiometric or catalytic.[21] An early suggestion of FLP utility in these transformations was published in 2007, in which Stephan's original system was shown to catalyse the hydrogenation of bulky imines, nitriles and aziridines (**Scheme 1.9**).[35]

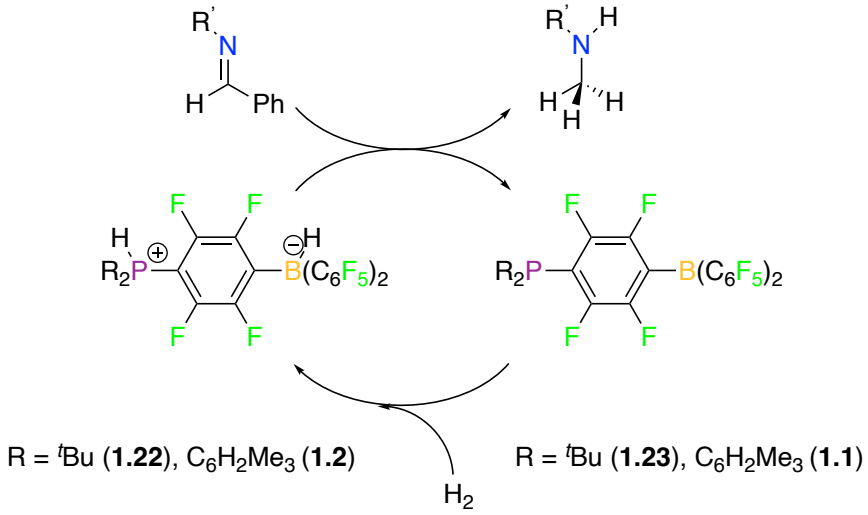

Scheme 1.9 – Catalytic cycle for imine hydrogenation by Stephan's FLP system.

Differing reduction rates among the imine substrates allowed for the elucidation of mechanistic information. The longer reaction times associated with more weakly basic N-donors implies that proton transfer from P to N is the rate determining step. This type of reactivity is limited to imines possessing sufficient bulk about the nitrogen centre, as the catalytic activity is suppressed by amine—borane adduct formation; this requirement can be mitigated by the introduction of $B(C_6F_5)_3$ to sequester the lone pair of N. In a similar fashion, Erker's alkane backbone system **1.20**/**1.20'** is able to catalytically hydrogenate bulky ketimines and enamines (**Scheme 1.10**).[36]

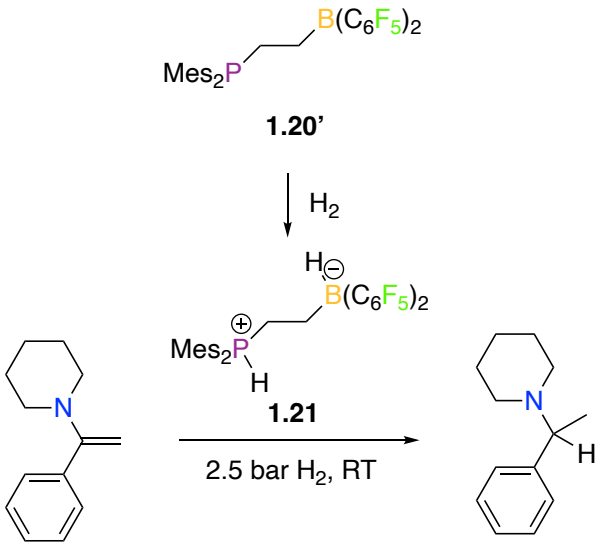

Scheme 1.10 – Hydrogenation of exemplar ketimine by an FLP.

As an aside, it is interesting to note that while the related alkenic equivalent **1.24** is itself inert towards hydrogen activation, H_2 cleavage can be induced by the addition of catalytic **1.20** (**Scheme 1.11**).

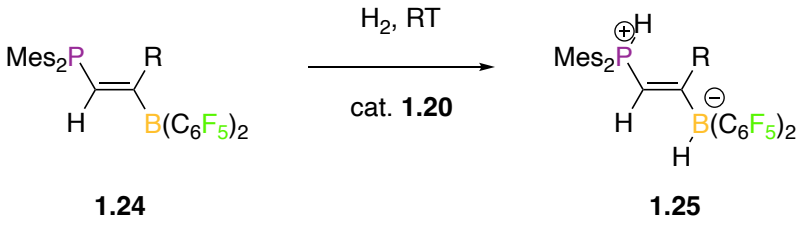

*Scheme 1.11 – Dihydrogen activation by FLP **1.24**, induced by **1.20**.*

A commonality to these initial examples is that the nitrogen centre is sterically encumbered, to avoid quenching the Lewis acid. However, intelligent design has allowed for hydrogenation of less bulky substrates as demonstrated by Soos *et al.* (**Scheme 1.12**)[37]

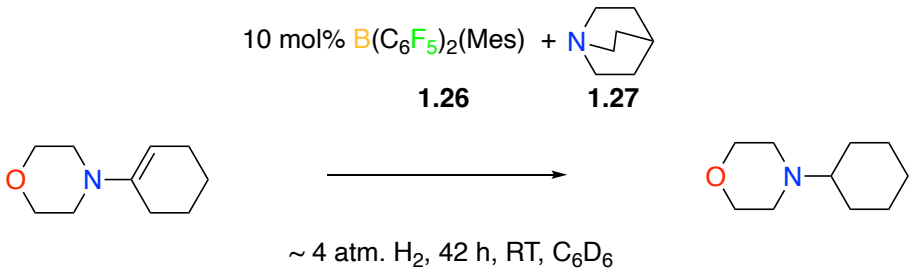

Scheme 1.12 – Exemplar sterically unhindered enamine reduced by an FLP catalyst.

This was achieved by increasing congestion about the borane Lewis acid to compensate for the corresponding decrease around the Lewis base. The non-polar unsaturated C=C bond in carvone was also reduced by the same FLP mixture (**Scheme 1.13**) although the reaction time was 6 days compared to 24 – 42 hours for imine substrates. This molecule was chosen as it is a typical test reaction for transition-metal catalysed hydrogenation.[38] Whereas a Raney Nickel catalyst reduces the carbonyl group, the opposite selectivity was seen when using **1.26**/**1.27**.

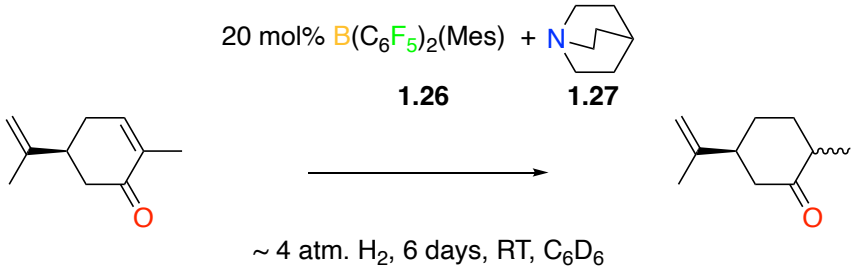

Scheme 1.13 – Chemoselective reduction of carvone by an FLP catalyst.

1.3.2 Reduction of Carbonyl Compounds

While the conversion of carbonyl compounds to alcohols is a useful synthetic transformation, the oxophilicity of typical boron-based Lewis acids poses a potential drawback in terms of their incorporation into a potential catalytic cycle due to propensity for catalyst poisoning.[39] Modifying the local environment about the Lewis acid to disfavour irreversible B—O bond formation is therefore important in efforts to carry out catalytic reduction processes involving oxygen containing molecules.[40–42]

This strategy was employed by Dorkó *et. al* for the reductive amination of carbonyls wherein a series of triaryl boranes were prepared with varying degrees protection afforded by *ortho*-halide substituents (**Figure 1.4**).[43] From **1.28** to **1.30**, shielding about the borane is systematically increased by the stepwise substitution of fluorine atoms with chlorine.

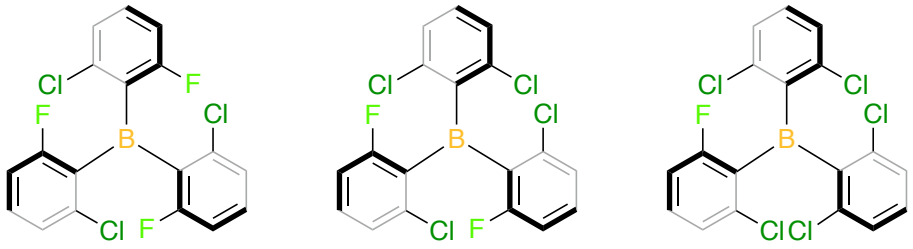

1.28 **1.29** **1.30**

Figure 1.4 – Homo and hetero diaryl boranes prepared.

More significant congestion about boron increases the reversibility of water binding such that the desired hydrogen activation is still feasible, albeit at elevated pressures of ca. 20 bar (**Scheme 1.14**).

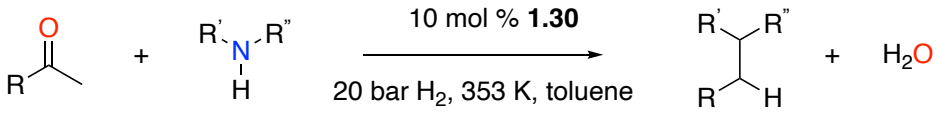

Scheme 1.14 – General scheme for reductive amination of carbonyls.

Alternatively, softer acids such as those based on tin can be employed to attain workable water tolerance. Ashley and co-workers were able to hydrogenate carbonyl compounds with an FLP composed of a trialkylstannane ($^{i}Pr_3SnOTf$) Lewis acid and a range of N-containing Lewis bases (**Scheme 1.15**).[44] They highlight that the thermal robustness of the trialkyl tin core is advantageous, given the elevated temperatures required (180 °C). The choice of Lewis acid was inspired by a report by Manners *et. al* which had explored the use of $^{n}Bu_3SnOTf$ in this capacity, albeit finding it lacking in reactive potency compared with $B(C_6F_5)_3$.[45]

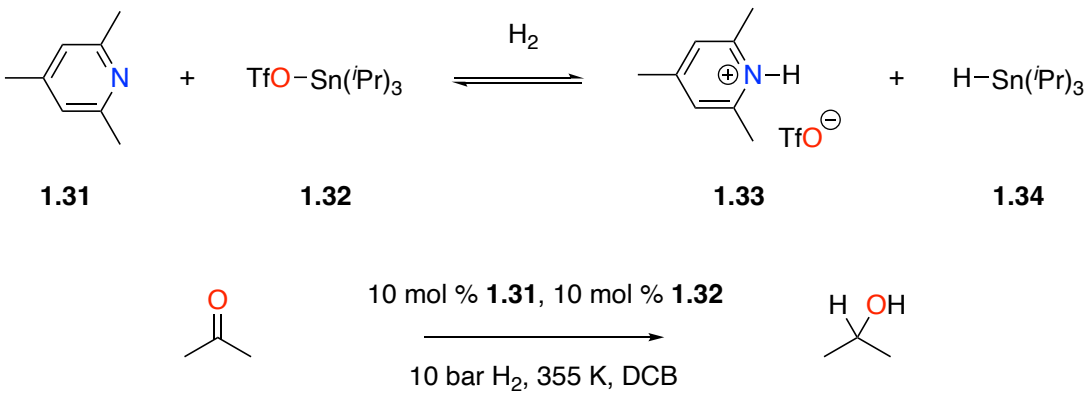

Scheme 1.15 – Generation of the FLP catalyst and a representative example of carbonyl reduction.

1.3.3 Non-Polar Unsaturated Bonds

Catalytic olefin hydrogenation by an FLP was achieved in 2012 by Greb *et. al* (**Scheme 1.16**).[46]

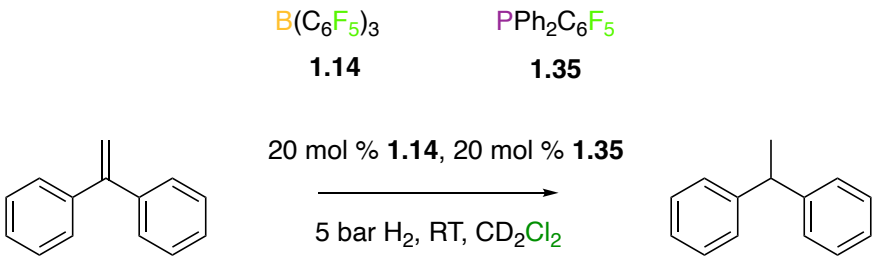

Scheme 1.16 – Representative example of catalytic olefin hydrogenation by an FLP.

The dependence of activity on the bulk about the basic centre implies, in a manner similar to imine reduction, that the reaction proceeds via initial protonation followed by hydride addition. Reversible dihydrogen cleavage by **1.14**/**1.35** is observed in the very low temperature range of -60 to -80 °C, although this equilibrium is not spectroscopically observed at room temperature. The substrate can be thought of as trapping the transient activated species, demonstrating that observable ambient temperature hydrogen splitting is not necessarily required for its delivery to small molecules.

Both computational and experimental probes of this transformation indicate that the pK_a of the protonated base is positively correlated with catalytic activity (**Graph 1.1**).[47] The authors of

this study concluded that the most important property of the Lewis base is its ability to facilitate substrate activation by proton transfer.

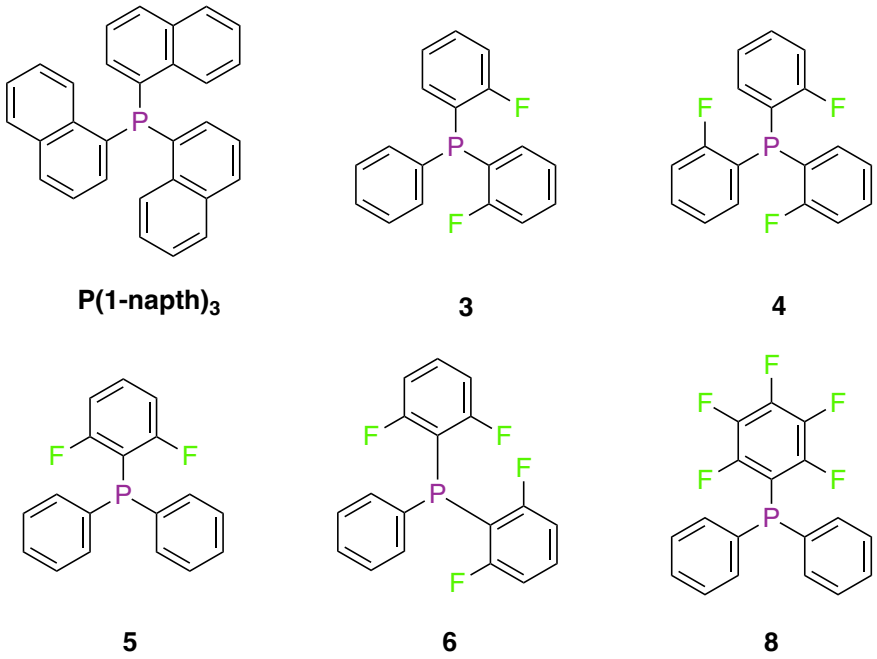

*Figure 1.5 – Lewis bases plotted on **Graph 1.1**.*

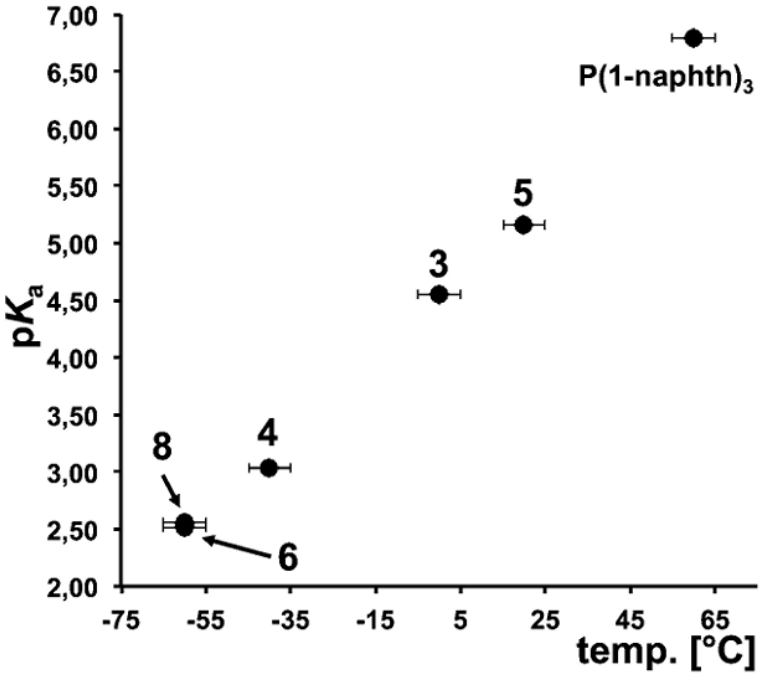

*Graph 1.1 – Relationship between basicity and catalytic activity in catalytic olefin hydrogenation by an FLP. Reproduced with permission from 'Electronic effects of triarylphosphines in metal-free hydrogen activation: a kinetic and computational study', Chem. Sci., 2013, **4**, 2788 – 2796.*

1.4 Intramolecular FLPs

Installation of both reactive moieties onto a single molecular scaffold is a rational synthetic strategy for FLPs, given this makes small molecule activation a bi- rather than termolecular event, corresponding to a lower entropic penalty. This suggest that intramolecular systems should exhibit superior catalytic activity to their intermolecular equivalents.[48] In this vein, a wide range of intramolecular FLPs have been synthesised and their reactivity explored.[49–51] Once this additional element of preorganisation is introduced, there are additional necessary considerations such as the distance between the Lewis acid and base, and the ease with which they can orient themselves in a conformation suitable for small molecule activation.[48] The choice of linker also has implications for the reactivity of the Lewis basic and acidic components, and synthetic strategies to arrive at these FLPs are typically more complex than the preparation of intermolecular analogues.[52]

1.4.1 Geminal FLPs

The geminal methylene-bridged phosphinoborane **1.36** has proven to be effective in the activation of both hydrogen and carbon dioxide at ambient pressure, along with *tert*butyl isocyanate (**Scheme 1.17**).[53]

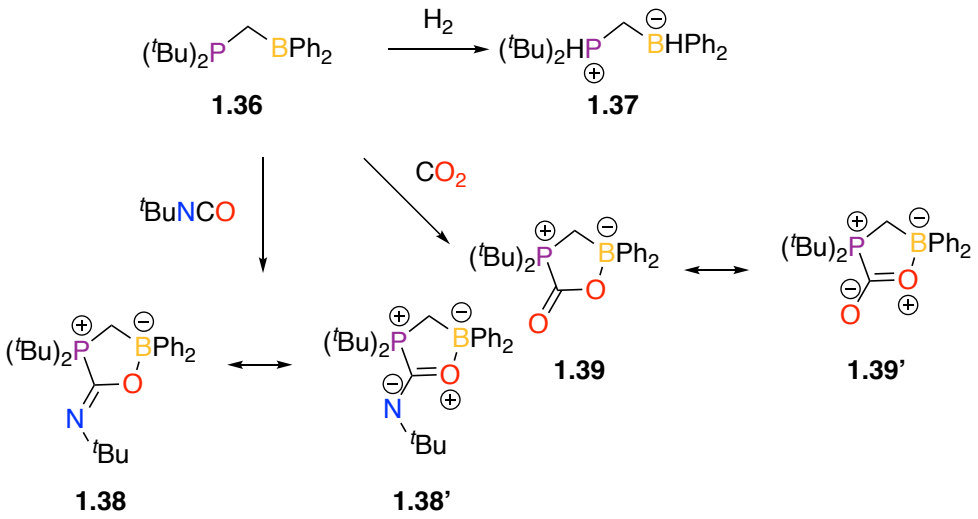

Scheme 1.17 – Hydrogen, carbon dioxide and isocyanate activation by an FLP.

Notably, the classical fluoroaryl borane substituents are absent in **1.36**, although the phosphine component does possess two strongly donating alkyl substituents which contribute significantly to the overall Lewis acid/base strength of the system.

1.4.2 Phenylene-linked and Vicinal FLPs

Rigid *ortho*-phenylene linkers have been studied as the backbone to amino boranes.[54] In 2013, a catalyst based on this structural motif was reported by Chernichenko and co-workers, for the hydrogenation of alkynes to *cis*-alkenes, with the active species generated *in situ* by hydrogenation of the parent precatalyst **1.40** (**Scheme 1.18**).[55]

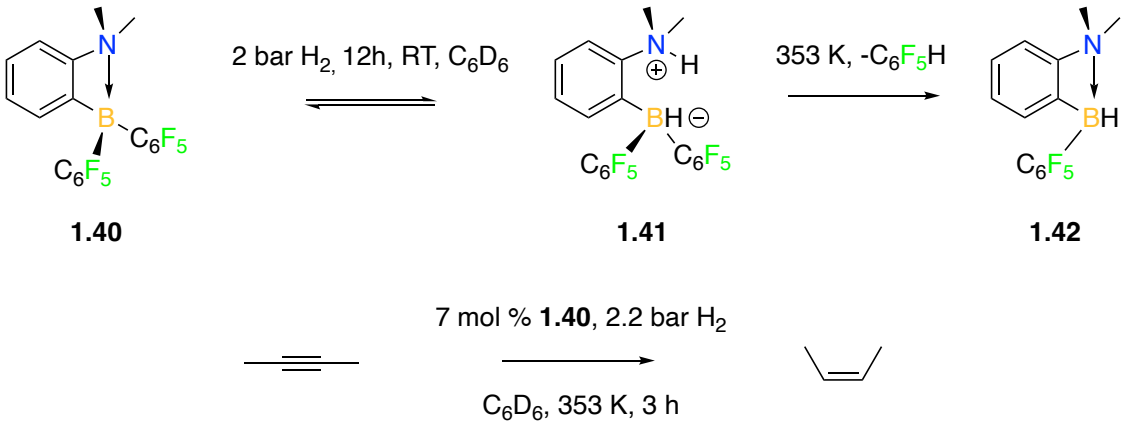

*Scheme 1.18 – Generation of active catalyst **1.42** from **1.40** and representative example of alkyne hydrogenation.*

The lability of the pentafluorophenyl group, while useful here for catalyst formation, prevents this study being extended to the hydrogenation of alkenes. The active species **1.42** first binds the substrate *via* the borane moity (**Scheme 1.19**). The resultant vinylborane activates dihydrogen to produce a species (**1.44**) analogous to **1.41**, differing only in that one of the pentafluorophenyl groups is replaced by an alkenic fragment.

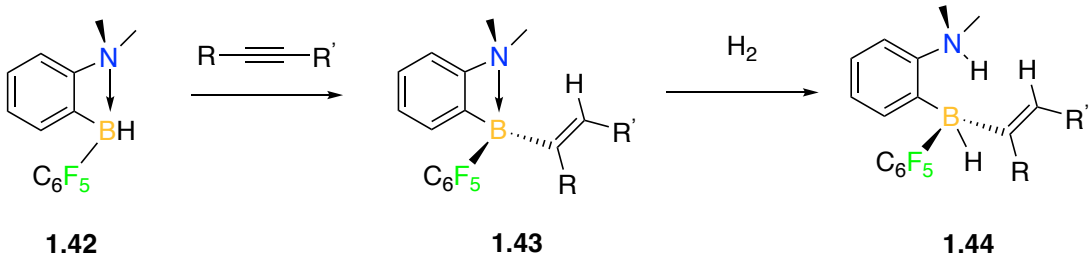

*Scheme 1.19 – Substrate binding by FLP hydrogenation catalyst **1.42**.*

At this point there are two competing pathways: one involving expulsion of a *cis*-alkene, which restarts the catalytic cycle, and one in which the pentafluorophenyl substituent on the borane is instead released (**Scheme 1.20**). It was found that this degradation pathway was favoured in alkene reduction attempts.

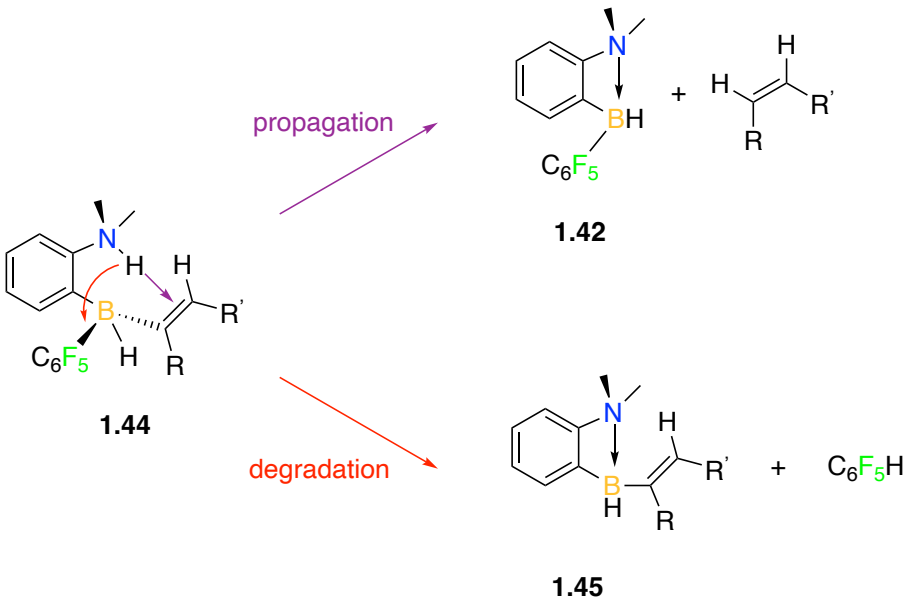

Scheme 1.20 – Competing propagation and degradation pathways within an FLP-mediated catalytic cycle for the hydrogenation of alkynes.

By exploiting a norbornane framework, a vicinal P/B FLP **1.48** with diverse reactivity has been constructed (**Scheme 1.21**).[56] A potential issue with any linked pair is that they might participate in an equilibrium with a species in which the acid and base interact intramolecularly, quenching each other, with the non-reactive form being a thermodynamic sink. The synthesis of **1.48** exploits the well-established stereochemistry of hydroboration reactions: Piers' borane

is added to dimesitylnorbornenylphosphine to yield an FLP with a phosphorus to boron separation of 3.878(1) Å, which is too wide for any such P→B interaction. The vinyl linker is also rigid, and the Lewis acid and base conformationally locked.

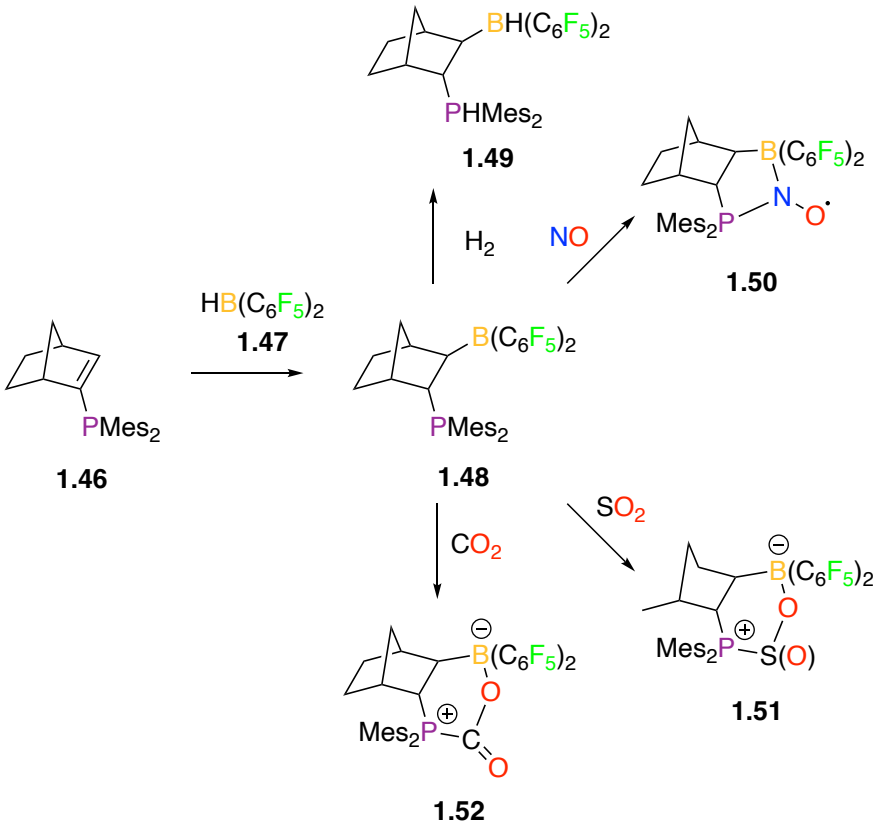

Scheme 1.21 – Synthesis and reactivity of an FLP with a norbornene backbone.

Regarding coordinative quenching, the Lewis acid to base distance is an important concern, although conversely a system in which the acid and base are held too far apart for any co-operative behaviour is also undesirable. This phenomenon was exploited by Aldridge and co-workers where, despite seemingly possessing requisite cumulative strength, a pair based on a dibenzofuran backbone is unable to activate hydrogen whilst similar xanthene-based systems can (**Figure 1.6**).[57] An intermolecular reaction pathway is not observed for **1.53** presumably because a termolecular collision is not sufficiently kinetically favourable.

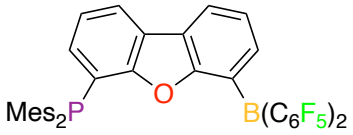

1.53

Figure 1.6 – Dibenzofuran FLP unable to facilitate hydrogen splitting.

1.4.3 Xanthene-Based FLPs

The 9,9-dimethyl xanthene scaffold has been widely explored in Main Group synthesis as the ligand environment for the stabilisation of low-valent metal and metalloid centres.[58–60] However, its primarily desirable feature in Frustrated Lewis Pair chemistry is the ca. 4.2 Å distance between acid and base functions when they are selectively installed in the 1 and 8 positions *via ortho*-directed metalation by the central oxygen atom. The initial report on FLPs of this type described how modulating Lewis basic strength yields reversible, rather than irreversible, hydrogen activation (**Scheme 1.22**).[61] Thermodynamically, these differences relate to the more weakly donating aryl phosphine which renders hydrogen loss favourable at room temperature. The dimesitylphosphine species **1.55** can also reversibly capture nitrous oxide (**Scheme 1.23**), with a corresponding yellow to colourless colour change that can be used for N_2O sensing.

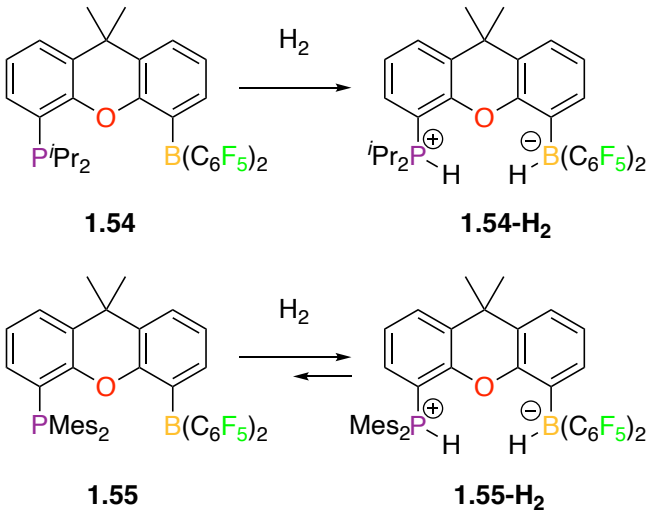

Scheme 1.22 – Reversible and irreversible dihydrogen activation by dimethyl xanthene FLPs.

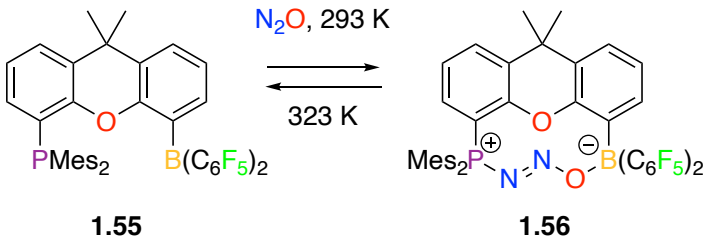

1.55 **1.56**

*Scheme 1.23 – Reversible capture of nitrous oxide by FLP **1.56**.*

Similarly, the related diphenylphosphine functionalised xanthene FLP **1.57** was shown to be catalytically competent in the dehydrocoupling of amine boranes (**Scheme 1.24**).[61] Here, the propensity of the hydrogenated catalyst to lose hydrogen was found to be key to the desired reactivity. Attenuation of basic strength by employment of an aryl, rather than an alkyl phosphine, facilitated catalytic activity.

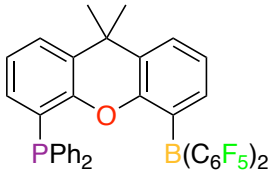

1.57

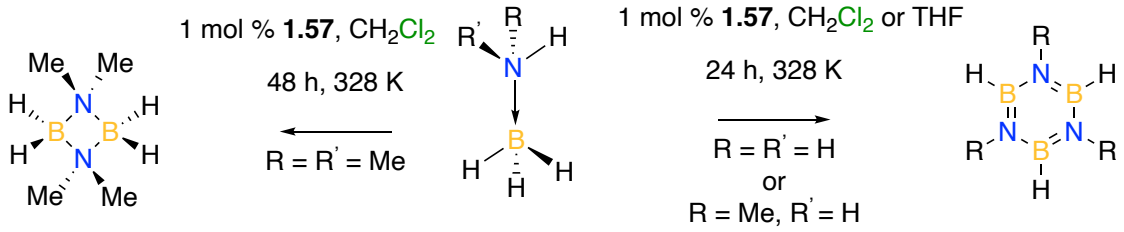

*Scheme 1.24 – Structure of FLP **1.57** and its catalytic activity in dehydrogenation of amine and ammonia-boranes.*

Subsequently this same intramolecular FLP was found to stoichiometrically C—H activate phenylacetylene.[62] The activated product of this reaction (**1.58**), in equilibrium with free FLP and alkyne, takes up two further equivalents of phenylacetylene. A borane heterocycle **1.59** is formed with a migrated C_6F_5 group *meta* to boron, and two pendant phenyl rings at the *para*- and other *meta* position, along with a bridge to the phosphine derived from the final molecule of alkyne (**Scheme 1.25**).

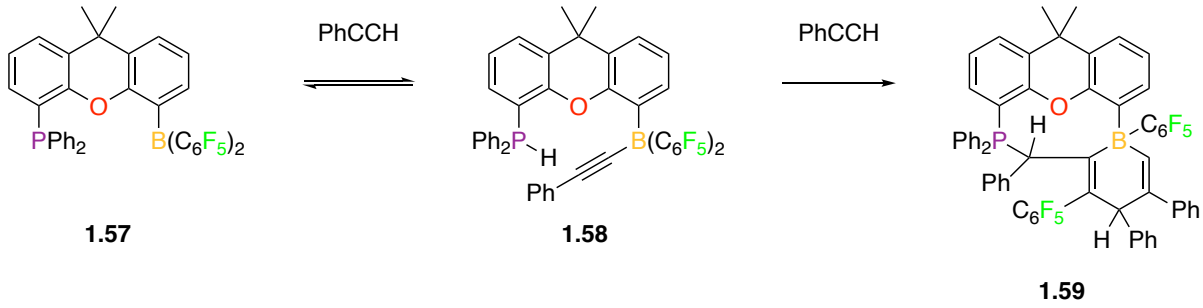

*Scheme 1.25 – Irreversible uptake of phenylacetylene by **1.57**.*

The more basic dimesityl phosphine FLP **1.55** facilitates simple irreversible C—H activation without the complication of heterocycle formation (**Scheme 1.26**), demonstrating that the onwards reactivity shown in **Scheme 1.25** is as a result of an equilibrium being established in the initial C—H activation step.

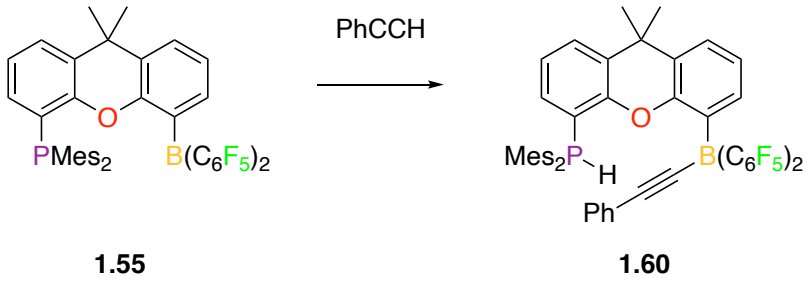

*Scheme 1.26 – C—H activation of phenylacetylene by FLP **1.55**.*

Additionally, these compounds were investigated with respect to their potential as hydroboration catalysts. Reaction of **1.55** with excess pinacol- or catecholborane induces migration of the fluoroarylborane to the phosphine, and its replacement on the backbone with a –Bpin or –Bcat unit (**Scheme 1.27**). The activity is thus realised, and **1.63** or Piers' borane generated from **1.63** is the active species in catalytic hydroboration of internal alkynes PhCCMe and PhCCPh.

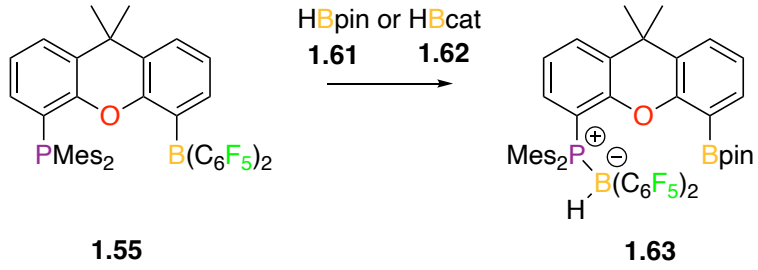

1.55 **1.63**

*Scheme 1.27 – Generation of FLP hydroboration catalyst from reaction of **1.55** with HBpin or HBcat.*

Given the limitations in catalytic processes discussed earlier associated the oxophilicity of boron, it is a natural extension to probe xanthene-based systems regarding their reactivity towards O—H bonds (**Scheme 1.28**).[63] As expected, in the case of $^{t}BuC_6H_4OH$ protonation at phosphorus is observed along with co-ordination of the remaining alcohol fragment to the borane. When a phosphine of lower basicity is studied (*i.e.* **1.57** as opposed to **1.55**), proton transfer back to the alcohol oxygen (**1.66**) is seen in equilibrium with the phosphonium/aryloxide zwitterionic form (**1.65**).

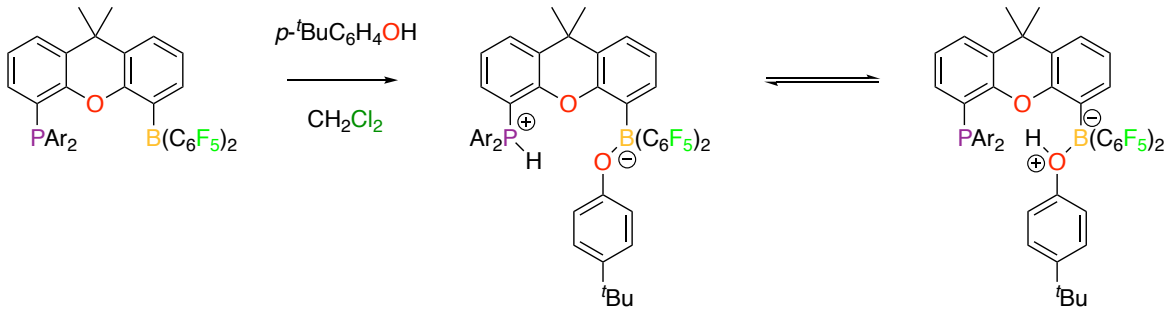

Ar = Mes (**1.55**) or Ph (**1.57**) Ar = Mes (**1.64**) or Ph (**1.65**) Ar = Ph (**1.66**)

*Scheme 1.28 – Activation of the O—H bond in 4-tert-butylphenol by FLP **1.55** or **1.57** and equilibrium between **1.65** and **1.66**.*

Quantum chemical calculations suggest that **1.66** is only slightly more stable than **1.65** at room temperature, by 2.0 kcal mol^{-1}. A low energy transition state can be located for proton migration with a barrier height of only 2.2 kcal mol^{-1}.

Xanthene and related backbone systems have also been investigated computationally as potential catalysts for the hydrogenation of carbon dioxide (**Figure 1.7**).[64] The postulated pathway is shown in **Scheme 1.29**.

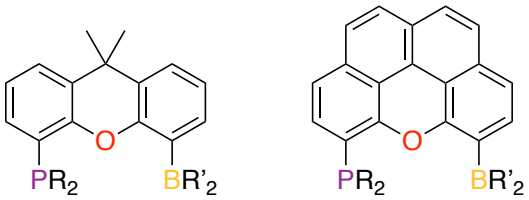

1.67 **1.68**

Figure 1.7 – General structure of computationally probed FLPs with xanthene and related backbones.

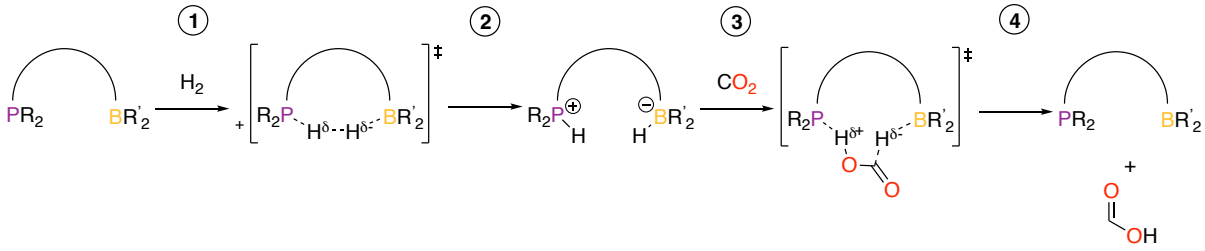

Scheme 1.29 – Mechanistic pathway for the hydrogenation of CO_2 by intramolecular FLPs.

Looking at the experimentally studied xanthene backbone FLP **1.55** (R = Mes, R' = C_6F_5), which is known to reversibly activate hydrogen at room temperature (Step **1**), the free energy barrier to this reaction was calculated as 11.6 kcal mol^{-1}, in keeping with a room temperature process. The barrier height for association of a molecular of CO_2 with the hydrogenated FLP (Step **3**) is far higher, at 34.6 kcal mol^{-1} (**Scheme 1.29**), which would suggest somewhat forcing conditions are required for this transformation – in keeping with other literature on carbon dioxide activation by FLPs. Comparing this to a naphtho analogue (R = Mes, R' = C_6F_5) with the general structure represented by **1.68**, hydrogen activation (Step **1**) is thermodynamically more uphill, at 15.6 kcal mol^{-1}. However, association of CO_2 with the hydrogenated FLP (Step **3**) is more feasible, with a 23.0 kcal mol^{-1} energy requirement.

These reactivity differences might be rationalised by the relative flexibilities of the backbones as described by the coplanar angle between the two aryl rings (**Figure 1.8**) and how this impacts their ability to stabilise transition states; this concept is raised by the authors although not meaningfully discussed.

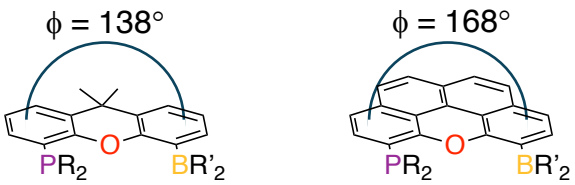

Figure 1.8 – Coplanar angle between the two aryl rings appended to the Lewis acidic and basic moieties.

The diverse and tuneable manifold of reactivity demonstrated by xanthene-based pairs make them a logical landscape upon which to develop FLP chemistry for more applicational endeavours, such as heterogeneous catalysis.

1.5 Heterogeneous FLPs

As the remit of FLP chemistry expands, industrial applications are a natural investigative focus. Heterogeneous catalysts are often favoured over homogeneous ones in industry due to advantages such as decreased reactor fouling, ease of product separation and ability to be used in flow chemistry.[65–67] Catalytic species covalently anchored to supports are critically important in this area and will be the focus of this discussion.

O'Hare and co-workers reported a silica supported FLP, characterised primarily by solid-state NMR spectroscopy. This system is bound directly through the acidic component, and cleaves hydrogen at 65 °C (**Scheme 1.30**).[68] The generation of this species follows a simple synthetic pathway – treatment of silica with Piers' borane followed by the addition of P^tBu_3 to yield a biphasic system. Whilst this is a convenient preparation, the strength of the Lewis acidic active site is dampened by bonding to a surface oxygen atom, as opposed to the typical electron withdrawing halogenated aryl rings.[69]

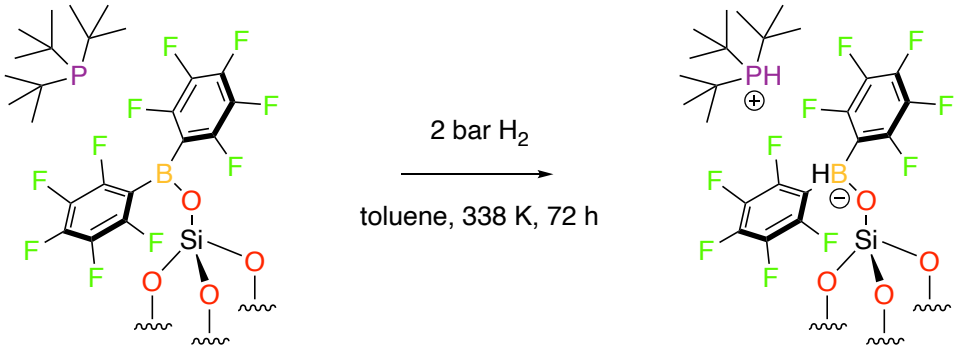

1.69 **1.70**

Scheme 1.30 – Silica supported intermolecular FLP.

The potential for adverse surface interactions can be attenuated by the introduction of a spacer between the Lewis acid or base and surface support. A range of these remotely supported acids and bases have been prepared *via* reactions of functionalised silica nanopowders with the corresponding allyltriethoxysilane (**Scheme 1.31**).[70] These are combined with a complementary solution phase acid or base, to yield systems which in all cases bind carbon dioxide at -64 °C under inert atmosphere conditions. Additionally, the hydrogenated products, when attainable, can facilitate the reduction of CO_2 to formic acid. Given the ubiquity of carbon dioxide as a potent greenhouse gas, this is an encouraging potential application of supported FLPs.

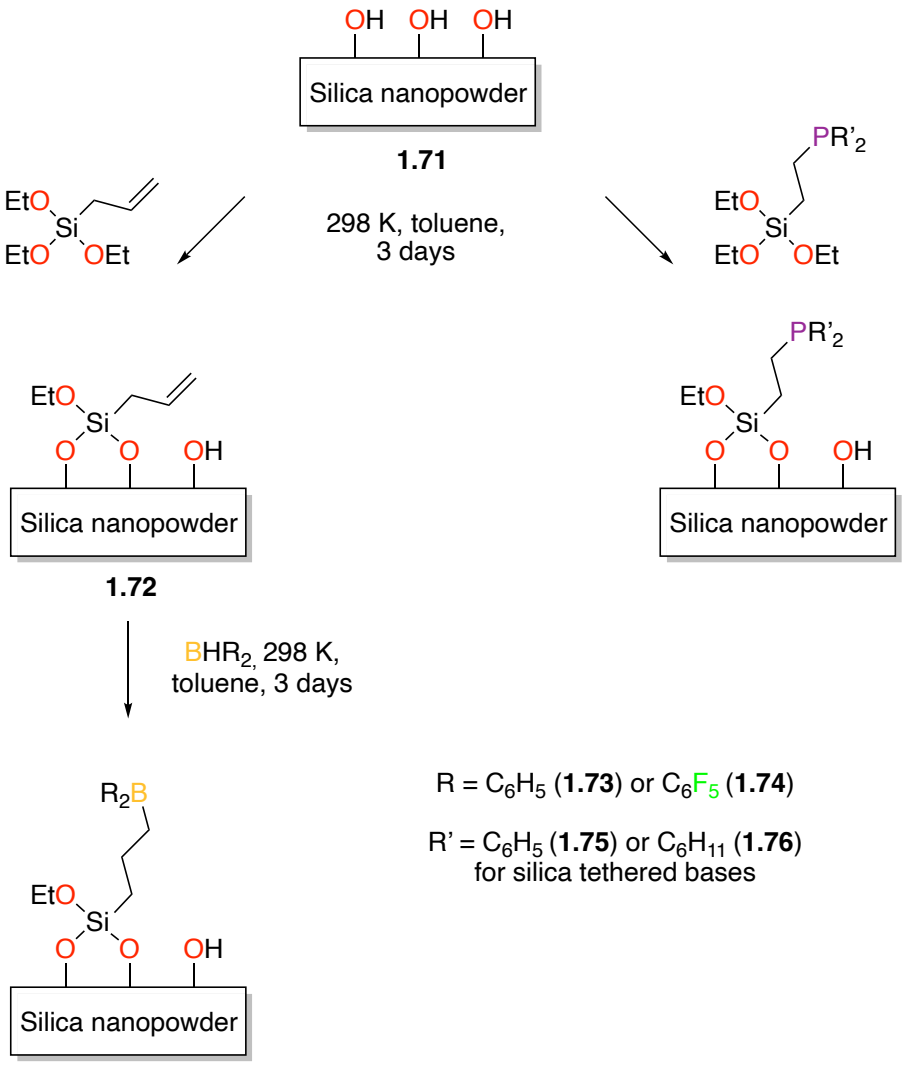

Scheme 1.31 – Preparation of silica supported acids and bases.

Similarly, FLPs can be secured *via* an aryl substituent on the base (**Scheme 1.32**).[71] In this example, treatment of dehydroxylated silica with $^{i}Bu_3Al$ yielded functionalised sites for reaction with the spacer. Reduction of the resultant surface followed by substitution using $P(C_6H_4OH)Ph_2$ (**1.78**) anchored the base, which then forms a weakly bound P—B adduct with $B(C_6F_5)_2R$ (where R = C_6F_5 (**1.80**) or H (**1.81**)). The hydrogen activation properties of these systems are realised by dissociation of the P—B bond and can be applied to the *Z*-selective hydrogenation of internal alkynes, most successfully for 3-hexyne with a selectivity up to 87%. Notably, the molecular analogue of **1.81** *i.e.* $HB(C_6F_5)_2/PPh_3$ is inactive for hydrogenation of 3-hexyne.

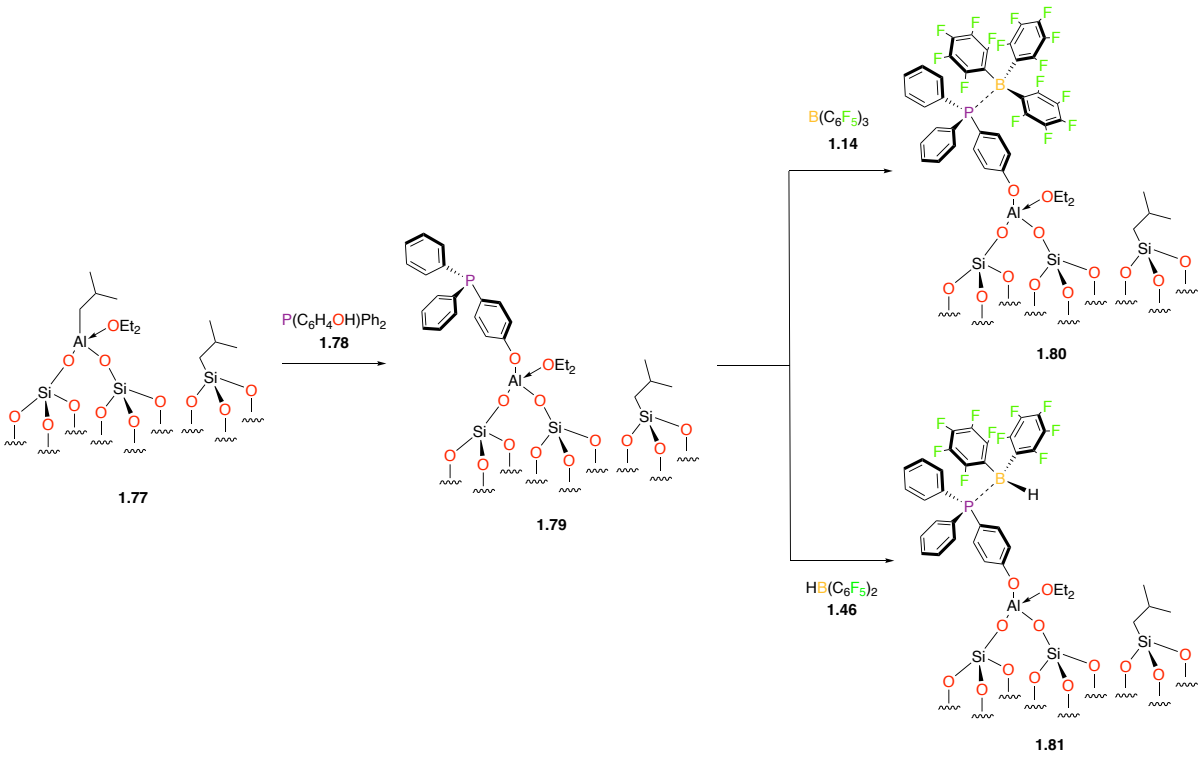

*Scheme 1.32 – Synthesis of base tethered FLPs **1.82** and **1.83** which were investigated for hydrogenation catalysis.*

A further example of catalytic hydrogenation by a solid Lewis base in conjunction with solution Lewis acid exploits the combination of a solid polyamine with *tris*(pentafluorophenyl)borane (**Figure 1.9**).[72] Whilst the ability to effect catalytic (rather than stoichiometric) hydrogenation is developmentally interesting, the substrate scope is limited to diethyl benzylidenemalonate and high pressures of hydrogen are also required (> 20 bar).

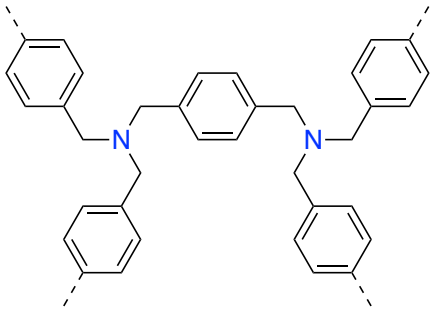

1.82

$B(C_6F_5)_3$

1.14

Figure 1.9 – 'Semi solid' FLP composed of solid polyamine with tris(pentafluorophenyl)borane.

An ambient temperature, low pressure hydrogen activation by immobilised pairs, as reported by Thomas *et al.*, have more potential applications.[73] Triaryl phosphines have been embedded into microporous polymer networks (**Figure 1.10**) and, in combination with *tris*(pentafluorophenyl)borane, are able to cleave dihydogen. One could envisage, therefore, their application in hydrogenation catalysis.

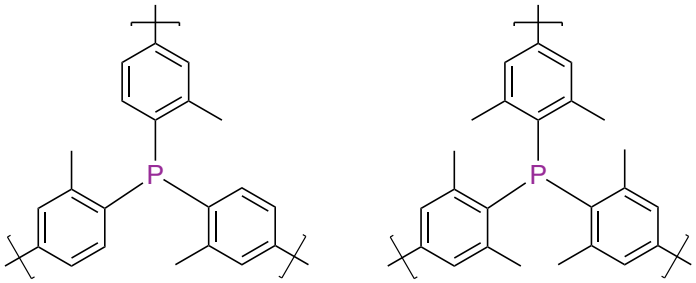

1.83 **1.84**

$B(C_6F_5)_3$

1.14

Figure 1.10 – Triaryl phosphines embedded into polymer networks for use in combination with tris(pentafluorophenyl)borane.

The examples discussed here are all intermolecular Frustrated Lewis Pairs, where one heterogenized component reacts alongside the other in solution phase. Whilst synthetically non-trivial, full heterogenization of both components might enhance their potential catalytic utility. There remains significant investigative space in this area to explore the potential remit of surface supported FLPs.

1.6 Project Aims and Outline

At the outset of this project there was not, to our knowledge, a well-characterised surface supported intramolecular FLP. Therefore, we sought to explore synthetic routes towards such systems, covalently bound to a surface *via* a molecular tether, guided by the existing promise of xanthene-backbone FLPs. Three potential sites for tethering were envisaged (**Figure 1.11**).

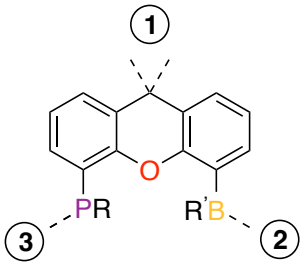

Figure 1.11 – 9,9-Dimethylxanthene with potential sites for molecular tethers indicated.

1.6.1 Backbone Tethered Pairs

Route 1: Modification of the xanthene backbone to maintain the integrity of the active site is perhaps the most intuitive means of incorporating a molecular tether, and this route was duly explored. However, preliminary investigations indicated that replacing the methyl groups in the 9 position with either a protected alcohol or carboxylic acid yields a xanthene derivative which is not amenable to the subsequent addition of a phosphine or borane. Despite these substitutions appearing trivial, functionalisation of the 4 and 5 positions using metalating agents was no longer possible in our hands. The importance of the methyl groups at C-9 in governing the desired reactivity is perhaps reflected in the relative sparsity of literature concerning alternatives at this position. It is worth noting also that 9,9-dimethylxanthene has been functionalised at the 2 and 7 positions, most commonly with *tert*-butyl groups, which might suggest the potential for incorporation of a molecular tether at either or both points. However, looking at work by Adams *et. al*, on the attempted synthesis of perfluoroalkylated derivatives of xantphos **1.85** – **1.87** (**Figure 1.12**), and their lack of success therein, this was also disregarded as a pathway.[74]

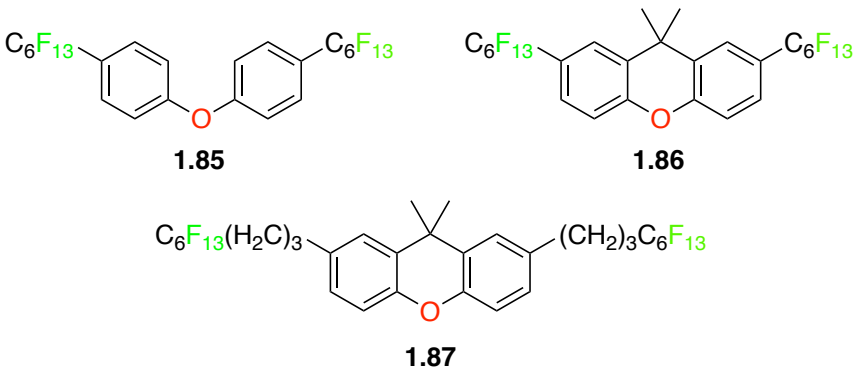

Figure 1.12 – Derivatised 9,9,-dimethylxanthene species which were unamenable to further substitution.

1.6.2 Borane Tethered Pairs

Route 2: A second avenue to be investigated involved functionalising the system to introduce a tether at the borane moiety. This was envisaged *via* the synthesis of borane reagents with the general form shown (**Figure 1.13**).

X = leaving group
Y = electron withdrawing group
Z = electron withdrawing group featuing a molecular tether

Figure 1.13 – General structure of target boranes.

Given the dominance of $B(C_6F_5)_3$ and derivatives thereof in FLP chemistry, the use of new Lewis acids in this capacity would form a significant body of exploratory synthetic work. Therefore, this was sub-divided into two distinct projects. Chapter 3 concerns the synthesis of hetero-diaryl bromoboranes both with and without tethering groups, and their use in the construction of *tris* heteroleptic boranes. Chapter 4 applies these reagents in the synthesis of xanthene-backbone FLPs. In addition, their dihydrogen activation properties are explored to evaluate their potential for hydrogenation catalysis.

1.6.3 Phosphine Tethered Pairs

Route 3: The well documented steric and electronic tunability of phosphines in homogeneous transition metal catalysis gives credence to a tethering route *via* functionalised phosphines. Chapter 5 explores the construction of a range of xanthene phosphines and their modification with tethering groups. These systems are then studied with respect to their potential as precursors for solution and solid phase FLP chemistry.

1.7 References

1 A. D. McNaught and A. Wilkinson, *The IUPAC Compendium of Chemical Terminology*, International Union of Pure and Applied Chemistry (IUPAC), 2019.

2 G. C. Welch, R. R. San Juan, J. D. Masuda and D. W. Stephan, *Science (80-.).*, 2006, **314**, 1124–1126.

3 J. R. Shapley, R. R. Schrock and J. A. Osborn, *J. Am. Chem. Soc.*, 1969, **91**, 2816–2817.

4 R. R. Schrock and J. A. Osborn, *J. Am. Chem. Soc.*, 1976, **98**, 2134–2143.

5 J. A. Osborn, G. Wilkinson and J. F. Young, *Chem. Commun.*, 1965, 17–17.

6 J. A. Osborn, F. H. Jardine, J. F. Young and G. Wilkinson, *J. Chem. Soc. A Inorganic, Phys. Theor.*, 1966, 1711–1732.

7 H. C. Brown, H. I. Schlesinger and S. Z. Cardon, *J. Am. Chem. Soc.*, 1942, **64**, 325–329.

8 W. Tochtermann, *Angew. Chemie Int. Ed. English*, 1966, **5**, 351–371.

9 D. J. Parks and W. E. Piers, *J. Am. Chem. Soc.*, 1996, **118**, 9440–9441.

10 G. Wittig and E. Benz, *Chem. Ber.*, 1959, **92**, 1999–2013.

11 D. W. Stephan and G. Erker, *Angew. Chemie Int. Ed.*, 2010, **49**, 46–76.

12 G. C. Welch and D. W. Stephan, *J. Am. Chem. Soc.*, 2007, **129**, 1880–1881.

13 J. S. J. McCahill, G. C. Welch and D. W. Stephan, *Angew. Chemie Int. Ed.*, 2007, **46**, 4968–4971.

14 H. C. Brown, *Tetrahedron*, 1961, **12**, 117–138.

15 P. Spies, G. Erker, G. Kehr, K. Bergander, R. Fröhlich, S. Grimme and D. W. Stephan, *Chem. Commun.*, 2007, 5072–5074.

16 Y. C. Chan, Y. Bai, W. C. Chen, H. Y. Chen, C. Y. Li, Y. Y. Wu, M. C. Tseng, G. P. A. Yap, L. Zhao, H. Y. Chen and T. G. Ong, *Angew. Chemie Int. Ed.*, 2021, **60**, 19949–19956.

17 P. Xu, Y. Yao and X. Xu, *Chem. – A Eur. J.*, 2017, **23**, 1263–1267.

18 E. R. M. Habraken, A. R. Jupp, M. B. Brands, M. Nieger, A. W. Ehlers and J. C. Slootweg, *Eur. J. Inorg. Chem.*, 2019, **2019**, 2436–2442.

19 N. Zwettler, S. P. Walg, F. Belaj and N. C. Mösch-Zanetti, *Chem. – A Eur. J.*, 2018, **24**, 7149–7160.

20 F. G. Fontaine and É. Rochette, *Acc. Chem. Res.*, 2018, **51**, 454–464.

21 J. Lam, K. M. Szkop, E. Mosaferi and D. W. Stephan, *Chem. Soc. Rev.*, 2019, **48**, 3592–

3612.
22 N. Li and W.-X. Zhang, *Chinese J. Chem.*, 2020, **38**, 1360–1370.
23 D. W. Stephan, *Acc. Chem. Res.*, 2015, **48**, 306–316.
24 S. Grimme, H. Kruse, L. Goerigk and G. Erker, *Angew. Chemie - Int. Ed.*, 2010, **49**, 1402–1405.
25 L. Liu, L. L. Cao, Y. Shao, G. Ménard and D. W. Stephan, *Chem*, 2017, **3**, 259–267.
26 A. R. Jupp, *Dalt. Trans.*, 2022, **51**, 10681–10689.
27 F. Holtrop, C. Helling, M. Lutz, N. P. Van Leest, B. De Bruin and J. C. Slootweg, *Synlett*, 2022, **34**, 1122–1128.
28 L. Liu, B. Lukose, P. Jaque and B. Ensing, *Green Energy Environ.*, 2019, **4**, 20–28.
29 T. Özgün, K. Bergander, L. Liu, C. G. Daniliuc, S. Grimme, G. Kehr and G. Erker, *Chem. - A Eur. J.*, 2016, **22**, 11958–11961.
30 Y. Kan and Q. Zhang, *Nanostructured Mater. Next-Generation Energy Storage Convers. Hydrog. Prod. Storage, Util.*, 2017, 43–84.
31 A. Hamza, A. Stirling, T. A. Rokob and I. Pápai, *Int. J. Quantum Chem.*, 2009, **109**, 2416–2425.
32 G. Skara, F. De Vleeschouwer, P. Geerlings, F. De Proft and B. Pinter, *Sci. Reports 2017 71*, 2017, **7**, 1–15.
33 F. G. Fontaine, M. A. Courtemanche, M. A. Légaré and É. Rochette, *Coord. Chem. Rev.*, 2017, **334**, 124–135.
34 T. A. Rokob, A. Hamza and I. Pápai, *J. Am. Chem. Soc.*, 2009, **131**, 10701–10710.
35 P. A. Chase, G. C. Welch, T. Jurca and D. W. Stephan, *Angew. Chemie - Int. Ed.*, 2007, **46**, 8050–8053.
36 P. Spies, S. Schwendemann, S. Lange, G. Kehr, R. Fröhlich and G. Erker, *Angew. Chemie - Int. Ed.*, 2008, **47**, 7543–7546.
37 G. Eros, H. Mehdi, I. Pápai, T. A. Rokob, P. Király, G. Tárkányi and T. Soós, *Angew. Chemie Int. Ed.*, 2010, **49**, 6559–6563.
38 A. F. Barrero, E. J. Alvarez-Manzaneda, R. Chahboun and R. Meneses, *Synlett*, 1999, **1999**, 1663–1666.
39 D. J. Parks, W. E. Piers, M. Parvez, R. Atencio and M. J. Zaworotko, *Organometallics*, 1998, **17**, 1369–1377.
40 J. Li, C. G. Daniliuc, G. Kehr and G. Erker, *Angew. Chemie*, 2019, **131**, 6809–6813.
41 J. Li, C. Mück-Lichtenfeld, C. G. Daniliuc, G. Kehr and G. Erker, *Angew. Chemie Int. Ed.*, 2020, **59**, 12477–12483.
42 D. W. Stephan, *Chem. Soc. Rev.*, 2023, **52**, 4632–4643.
43 É. Dorkó, M. Szabó, B. Kótai, I. Pµpai, A. Domjµn, T. Soós, É. orkó, D. Soós, M. Szabó and A. Domjµn, *Angew. Chemie*, 2017, **129**, 9640–9644.
44 D. J. Scott, N. A. Phillips, J. Oshua, S. Sapsford, A. C. Deacy, M. Atthew, J. Fuchter and A. E. Ashley, *Angew. Chemie*, 2016, **128**, 14958–14962.
45 G. R. Whittell, E. I. Balmond, A. P. M. Robertson, S. K. Patra, M. F. Haddow and I. Manners, *Eur. J. Inorg. Chem.*, 2010, **2010**, 3967–3975.
46 L. Greb, P. Oña-Burgos, B. Schirmer, S. Grimme, D. W. Stephan and J. Paradies, *Angew. Chemie Int. Ed.*, 2012, **51**, 10164–10168.
47 L. Greb, S. Tussing, B. Schirmer, P. Oña-Burgos, K. Kaupmees, M. Lõkov, I. Leito, S. Grimme and J. Paradies, *Chem. Sci.*, 2013, **4**, 2788–2796.
48 D. J. Scott, M. J. Fuchter and A. E. Ashley, *Chem. Soc. Rev.*, 2017, **46**, 5689–5700.

49 A. Stute, G. Kehr, C. G. Daniliuc, R. Fröhlich and G. Erker, *Dalt. Trans.*, 2013, **42**, 4487–4499.

50 J. H. W. LaFortune, A. Trofimova, H. Cummings, S. A. Westcott and D. W. Stephan, *Chem. – A Eur. J.*, 2019, **25**, 12521–12525.

51 G. Kehr, S. Schwendemann and G. Erker, in *Topics in Current Chemistry*, Springer, Berlin, Heidelberg, 2012, pp. 45–83.

52 T. Özgün, K. Y. Ye, C. G. Daniliuc, B. Wibbeling, L. Liu, S. Grimme, G. Kehr and G. Erker, *Chem. – A Eur. J.*, 2016, **22**, 5988–5995.

53 F. Bertini, V. Lyaskovskyy, B. J. J. Timmer, F. J. J. De Kanter, M. Lutz, A. W. Ehlers, J. C. Slootweg and K. Lammertsma, *J. Am. Chem. Soc.*, 2012, **134**, 201–204.

54 M. A. Courtemanche, A. P. Pulis, É. Rochette, M. A. Légaré, D. W. Stephan and F. G. Fontaine, *Chem. Commun.*, 2015, **51**, 9797–9800.

55 K. Chernichenko, Á. Madarász, I. Pápai, M. Nieger, M. Leskelä and T. Repo, *Nat. Chem. 2013 58*, 2013, **5**, 718–723.

56 M. Sajid, G. Kehr, T. Wiegand, H. Eckert, C. Schwickert, R. Pöttgen, A. J. P. Cardenas, T. H. Warren, R. Fröhlich, C. G. Daniliuc and G. Erker, *J. Am. Chem. Soc.*, 2013, **135**, 8882–8895.

57 Z. Mo, E. L. Kolychev, A. Rit, J. Campos, H. Niu and S. Aldridge, *J. Am. Chem. Soc.*, 2015, **137**, 12227–12230.

58 A. Nicolay, M. S. Ziegler, L. Rochlitz and T. D. Tilley, *Polyhedron*, 2020, **180**, 114420.

59 J. Hicks, P. Vasko, J. M. Goicoechea and S. Aldridge, *Nature*, 2018, **557**, 92–95.

60 X. Zheng, A. Heilmann, C. McManus and S. Aldridge, *Chem. – A Eur. J.*, 2021, **27**, 3159–3165.

61 Z. Mo, A. Rit, J. Campos, E. L. Kolychev and S. Aldridge, *J. Am. Chem. Soc.*, 2016, **138**, 3306–3309.

62 P. Vasko, I. A. Zulkifly, M. Á. Fuentes, Z. Mo, J. Hicks, P. C. J. Kamer and S. Aldridge, *Chem. - A Eur. J.*, 2018, **24**, 10531–10540.

63 P. Vasko, M. Á. Fuentes, J. Hicks and S. Aldridge, *Dalt. Trans.*, 2019, **48**, 2896–2899.

64 M. Delarmelina, J. W. de M. Carneiro, C. R. A. Catlow and M. Bühl, *Catal. Commun.*, 2022, **162**, 106385.

65 A. R. Jupp and D. W. Stephan, *Trends Chem.*, 2019, **1**, 35–48.

66 L. Zhang, M. Zhou, A. Wang and T. Zhang, *Chem. Rev.*, 2020, **120**, 683–733.

67 J. M. Thomas and R. Raja, *Top. Catal.*, 2006, **40**, 3–17.

68 J. Y. Xing, J. C. Buffet, N. H. Rees, P. Nørby and D. O'Hare, *Chem. Commun.*, 2016, **52**, 10478–10481.

69 R. J. Mayer, N. Hampel and A. R. Ofial, *Chem. – A Eur. J.*, 2021, **27**, 4070–4080.

70 K. Mentoor, L. Twigge, J. W. H. Niemantsverdriet, J. C. Swarts and E. Erasmus, *Inorg. Chem.*, 2021, **60**, 55–69.

71 K. C. Szeto, W. Sahyoun, N. Merle, J. L. Castelbou, N. Popoff, F. Lefebvre, J. Raynaud, C. Godard, C. Claver, L. Delevoye, R. M. Gauvin and M. Taoufik, *Catal. Sci. Technol.*, 2016, **6**, 882–889.

72 A. Willms, H. Schumacher, T. Tabassum, L. Qi, S. L. Scott, P. J. C. Hausoul and M. Rose, *ChemCatChem*, 2018, **10**, 1835–1843.

73 M. Trunk, J. F. Teichert and A. Thomas, *J. Am. Chem. Soc.*, 2017, **139**, 3615–3618.

74 D. J. Adams, D. J. Cole-Hamilton, D. A. J. Harding, E. G. Hope, P. Pogorzelec and A. M. Stuart, *Tetrahedron*, 2004, **60**, 4079–4085.

Chapter 2 – Experimental Methods

2.1 Manipulation of air sensitive compounds

Most of the compounds described in this thesis are highly air and moisture sensitive, and manipulation was enabled by the use of a Schlenk line or inert atmosphere glovebox. A Schlenk line is a dual vacuum-inert gas manifold consisting of two manifolds connected by double oblique glass stopcocks. One manifold is connected to the inert gas supply (argon in this case) at one end and vented through a mercury bubbler at the other. The second manifold is connected to a high vacuum pump, *via* a liquid nitrogen-cooled trap, and monitored using a pressure gauge, showing that pressure was maintained at *ca*. $2x10^{-2}$ mbar. This set-up allows vessels attached *via* tubing to be easily placed under vacuum or argon. All glassware used was dried overnight in a 200 °C oven, or flame dried using a Bunsen burner. Glassware was kept oxygen free by connecting to the Schlenk line and undertaking at least three cycles of vacuum pumping to *ca.* $4x10^{-2}$ mbar and refilling with argon. Liquid transfer was carried out by cannula or syringe. Solvents were dried by passage through activated alumina columns and degassed before use. Diethyl ether and hydrocarbon solvents were stored over a K mirror, THF was stored over an Na mirror, dichloromethane was stored over 4 Å molecular sieves. A glovebox, maintained under a nitrogen atmosphere, was used for the storage and manipulation of air and moisture sensitive solids. The atmosphere was purified with an activated copper catalyst and 4 Å molecular sieves. Gases were introduced by degassing solutions using three freeze–pump–thaw cycles, before filling the headspace of the reaction vessel with the chosen gas. N_2O and CO_2 were stored in gas cylinders equipped with a regulator. H_2 was collected from a hydrogen manifold Schlenk line at 1 atm. pressure and stored in a Teflon valve ampoule over P_2O_5.

2.2 Spectroscopy and analytical techniques

2.2.1 NMR spectroscopy

NMR spectra were measured in C_6D_6 or C_7D_8 which were dried over 3 Å molecular sieves, with the solvent stored under nitrogen in a Teflon valve ampoule. NMR samples were prepared under nitrogen in sample tubes fitted with J. Young Teflon valves and NMR spectra measured on a Bruker Avance III HD Nanobay 400 MHz NMR spectrometer equipped with a 9.4 T magnet or a Bruker Avance III NMR 500 MHz NMR spectrometer equipped with a 11.75 T magnet and a ^{13}C detect cryoprobe. ^{1}H and ^{13}C NMR spectra were referenced internally to residual protio-solvent (^{1}H) or solvent (^{13}C) resonances and are reported relative to tetramethylsilane ($\delta = 0$ ppm). Variable temperature ^{31}P spectra were referenced relative to an internal standard of Ph_3PO in C_7D_8, contained within a flame-sealed capillary. Chemical shifts are quoted in δ (ppm) and coupling constants in Hz.

2.2.2 Elemental analysis

Elemental analyses were carried out by London Metropolitan University. Air and moisture sensitive samples were packed in a sealed glass capillary under argon or in a vial within a vial, sealed with Parafilm, under a nitrogen atmosphere.

2.2.3 DFT calculations

All computational work reported here was performed by Agamemnon Crumpton (University of Oxford, Aldridge group) using ORCA (Revision 5.0.3).[1–3] The meta-generalized-gradient approximation (mGGA) functional R2-SCAN[4,5] was employed in conjunction with the Def2-TZVPPms3[6] basis set with the D4 dispersion correction,[7,8] and employing the geometrical counterpoise correction gCP[9] (together known as the R2SCAN-3c method).[6] Benzene

solvation was modelled with CPCM. The nature of the stationary points (minima) was confirmed by full frequency calculations and are characterized by zero imaginary frequencies.

2.2.4 X-ray crystallography

Single-crystal X-ray diffraction data were measured using an Oxford Diffraction Supernova dual-source diffractometer equipped with a 135 mm Atlas CCD area detector. Crystals were selected under Paratone-N oil, mounted on Micromount loops and quench-cooled using an Oxford Cryosystems open flow N_2 cooling device.[10] Data was collected at 150 K using mirror monochromated Cu ($\lambda = 1.5418$ Å) K_α radiation. All crystallographic data were processed using the CrysAlisPro[11] package, including unit cell parameter refinement and inter-frame scaling (which was carried out using SCALE3 ABSPACK within CrysAlisPro). Equivalent reflections were merged, and diffraction patterns processed with the CrysAlisPro suite. Structures were subsequently solved using ShelXT 2018 and refined on F^2 using the ShelXL 2018 package and XSeed.[12,13]

2.3 References

1 F. Neese, *Wiley Interdiscip. Rev. Comput. Mol. Sci.*, 2012, **2**, 73–78.

2 F. Neese, F. Wennmohs, U. Becker and C. Riplinger, *J. Chem. Phys.*, 2020, **152**, 224108.

3 F. Neese, *Wiley Interdiscip. Rev. Comput. Mol. Sci.*, 2018, **8**, e1327.

4 J. W. Furness, A. D. Kaplan, J. Ning, J. P. Perdew and J. Sun, *J. Phys. Chem. Lett.*, 2020, **11**, 8208–8215.

5 J. W. Furness, A. D. Kaplan, J. Ning, J. P. Perdew and J. Sun, *J. Phys. Chem. Lett.*, 2020, **11**, 9248.

6 S. Grimme, A. Hansen, S. Ehlert and J. M. Mewes, *J. Chem. Phys.*

7 E. Caldeweyher, C. Bannwarth and S. Grimme, *J. Chem. Phys.*, 2017, **147**, 034112.

8 E. Caldeweyher, S. Ehlert, A. Hansen, H. Neugebauer, S. Spicher, C. Bannwarth and S. Grimme, *J. Chem. Phys.*, 2019, **150**, 154122.

9 H. Kruse and S. Grimme, *J. Chem. Phys.*, 2012, **136,** 154101.

10 B. J. Cosier and A. M. Glazer, *J. Appl. Crystallogr.*, 1986, **19**, 105–107.

11 A. Rothkirch, G. D. Gatta, M. Meyer, S. Merkel, M. Merlini and H. P. Liermann, *J.*

Synchrotron Radiat., 2013, **20**, 711–720.

12 G. M. Sheldrick, *Acta. Crystallogr. Sect. A Found. Crystallogr.*, 2007, **64**, 112–122.

13 L. J. Barbour, *J. Supramol. Chem.*, 2001, **1**, 189–191.

Chapter 3 – Synthesis of Heteroleptic Triaryl Boranes

3.1 Introduction

For reactivity studies involving sterically hindered Group 13 Lewis acids, electron-withdrawing haloaryl substituents are natural choices to enhance electrophilicity of the vacant *p*-orbital.[1,2] Syntheses of homoleptic triaryl boranes are well established, often *via* the use of Grignard or organolithium reagents.[3–6] In contrast, generalised routes to unsymmetrically substituted boranes are often considered non trivial. Using hard nucleophiles in combination with symmetrical BX_3 starting materials tends to lead to unselective substitution and mixtures of products.[7]

3.1.1 Aryl Boranes of the Type BR_2R'

Species of the type BR_2R' are far more common than BRR'R". Several boranes featuring this structural motif were prepared by Ashley and co-workers in 2011, featuring a mixture of perfluoro (C_6F_5) and perchloro (C_6Cl_5) aryl rings (**Scheme 3.1**).[7]

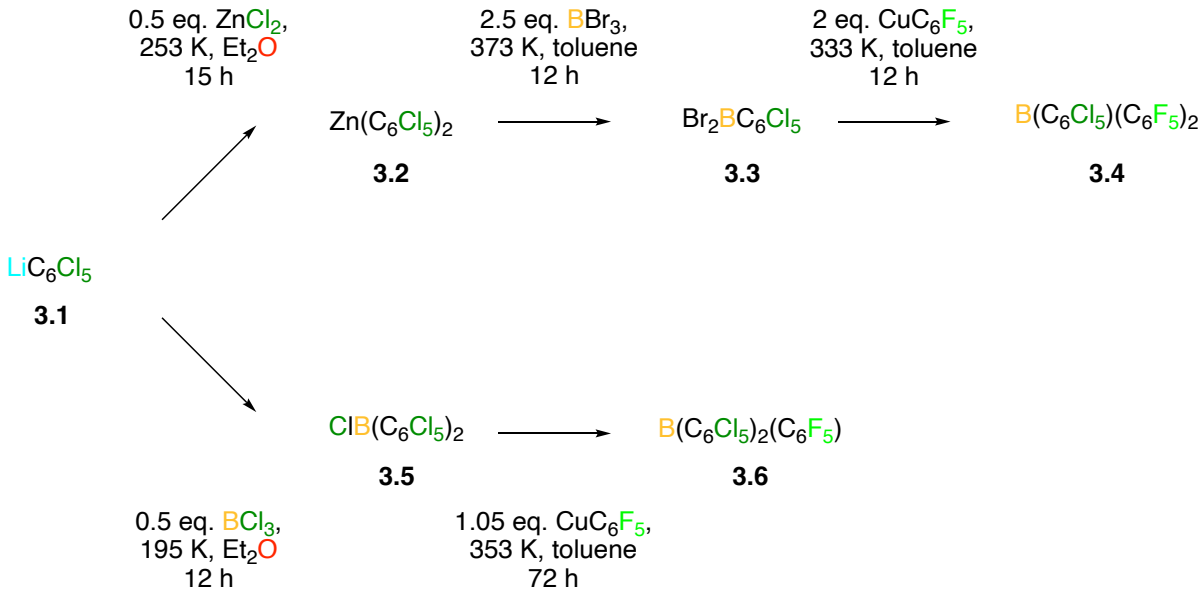

Scheme 3.1 – Syntheses of boranes of the type BR_2R' where R, R' = C_6F_5, C_6Cl_5.

Either one or two pentachlorophenyl rings can be introduced using a trihaloborane starting material. The use of a copper-based transfer reagent in the desired stoichiometry then enables incorporation of the final pentafluorophenyl ring or rings *via* metathesis. With these boranes in hand, the authors investigated how systematic variation of chlorinated and fluorinated substituents can be used to vary Lewis acidic strength. As the number of perfluorinated aryl groups increases, so does acidity, as the boron atom is less efficiently shrouded by the *ortho*-atoms of the aromatic rings. This runs counter to an electronic description of the electron-withdrawing capability of perchlorinated versus perfluorinated aryl groups. Additionally, the reduction potential becomes less negative with stepwise substitution of C_6Cl_5 rings (**Figure 3.1**) from **3.4** to **3.6** to **3.7** (*tris*pentachlorophenyl borane $B(C_6Cl_5)_3$), which would suggest superiority of C_6Cl_5 as an electron withdrawing group.

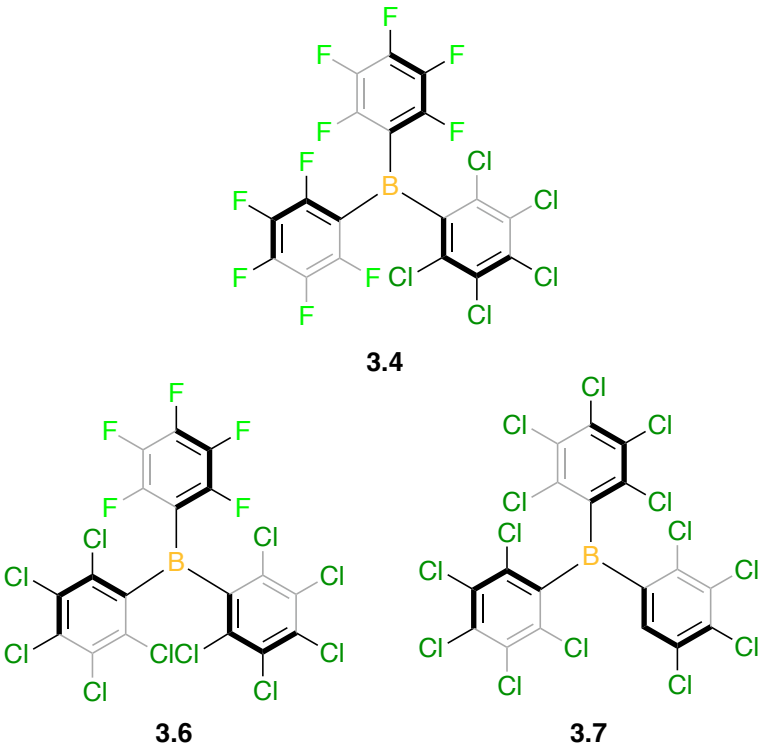

Figure 3.1 – Bulky, electron deficient, perchlorinated boranes.

The two conflicting sources of evidence led the authors to conclude that physical means such as the Gutmann-Beckett or Childs' method, in accounting for both steric and electronic effects, allow for most accurate determination of chemical reactivity.

Zinc and copper haloaryls have been used by Wildgoose *et al.* to synthesise similar boranes featuring the 3,5-bis(trifluoromethyl)phenyl group (Ar^{F}_{6}) (**Scheme 3.2**).[8]

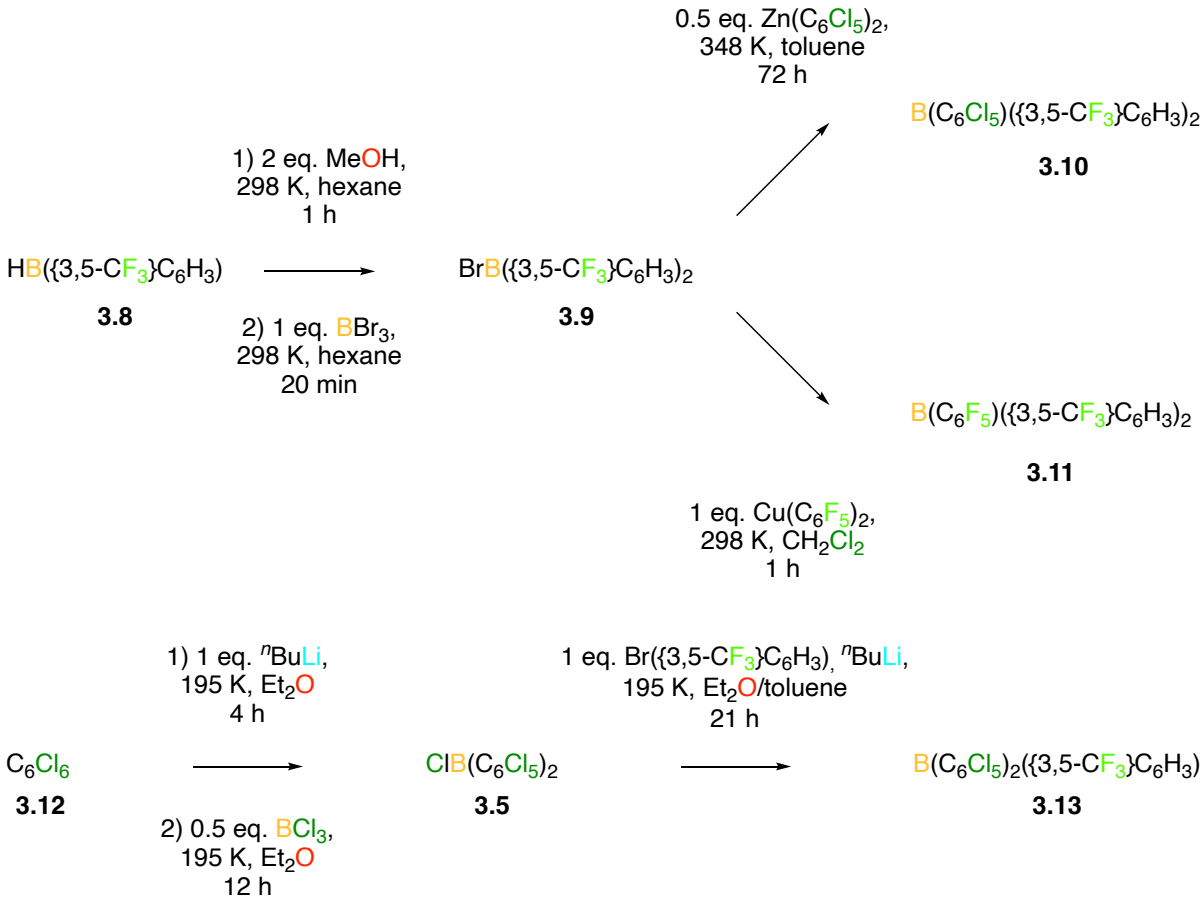

Scheme 3.2 – Alternate synthesis of BR_2R' boranes where R, R' = C_6F_5, C_6Cl_5, $Ar^F{}_6$.

In this study it was suggested that solid-state structures can be used to gain insight into relative acidity. These boranes possess a trigonal planar geometry at boron, with the rings adopting a paddlewheel structure to minimise steric strain arising from interactions between the aryl groups (**Figure 3.2**).

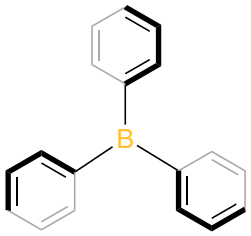

3.14

Figure 3.2 – Illustration of general paddlewheel structure with aryl rings twisted out of the BC_3 plane which is defined by boron and its three bonded carbon atoms. Triphenylborane has been used for clarity.

A correlation is seen between size of the *ortho-* atoms (increasing from hydrogen to fluorine to chlorine) and the degree to which the aryl groups twist out of the BC_3 plane. More significant twisting allows for direct donation of electron density from a lone pair on an atom in the *ortho-* position into the vacant $2p_z$ orbital on boron, thereby modulating Lewis acidity. Conversely, greater out of plane twisting angles decrease overlap between the boron $2p_z$ orbital and the aromatic π system. Less efficient donation from the aromatic ring would be expected to lead to increased Lewis acid strength, so presumably there is a balance of these competing effects. *Ortho*-groups are also relevant in terms of ensuring the formation of *tris* as opposed to *tetra* substituted products. This was demonstrated by the 2021 work of Marder *et al*. (**Scheme 3.3**).[9] A diverse collection of *para-* functionalised aryls was explored, summarised in **Table 3.1**.

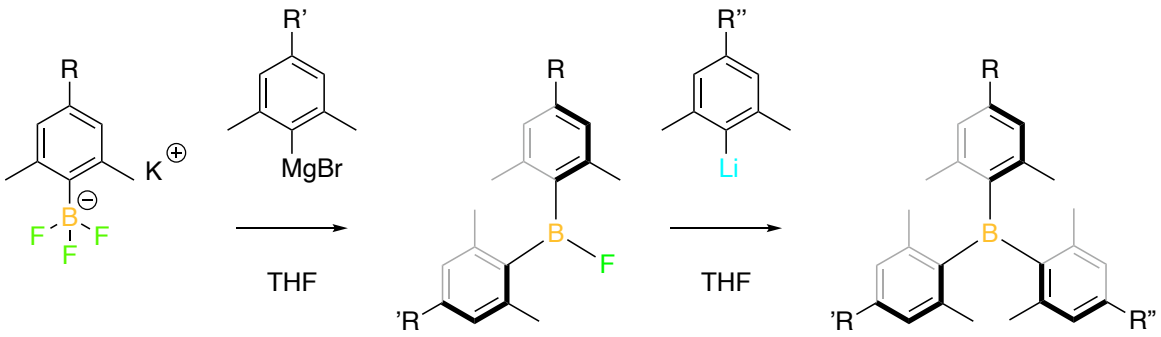

Scheme 3.3 – Synthesis of heteroleptic ortho- methylated boranes.

R	R'	R''
H	Br	Me
H	Br	Me
Me	Br	H
Br	H	Me
H	Br	$SiMe_3$
H	Me	NMe_2
H	Me	NMe_2
H	NMe_2	Me
H	NMe_2	Me

Table 3.1 – Para- functional groups employed in the work of Marder.

Using potassium (2,6-dimethylphenyl)trifluoroborate as the starting material, the second aryl group was introduced using an excess of Grignard reagent while the third requires a more reactive lithiated arene. All substituents possess two *ortho*- methyl groups, presumably to provide steric protection so that a *tris*, as opposed to *tetra* substituted motif is favoured. Given the work of Wildgoose detailing acidity attenuation due to electron donation, a similar effect might be expected, amplified by the positive inductive nature of alkyl groups, although the properties of these boranes were not explored in depth in this report.

3.1.2 Heteroleptic Triaryl Boranes BRR'R"

Recent work by Legare (2023) has exploited a number of different aryl difluoroboranes for the preparation of triarylboranes, some of which have three different groups bound to the central boron atom.[10]

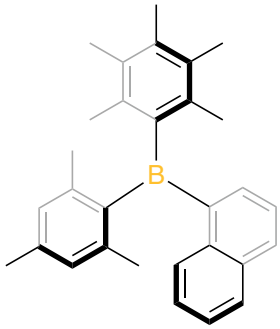

3.15

Figure 3.3 – Structurally characterised hetero triaryl borane reported by Legare and co-workers.

The crystallographically characterised borane **3.15** (**Figure 3.3**) features mesityl, naphthalene and pentamethylbenzene substituents in a classical *tris*borane paddlewheel geometry.

Triaryl boranes have found wide ranging applications due to their diverse optical and electronic properties.[11] However, given the traditional reactivity of boranes is predicated on the availability of the vacant p-orbital, heteroleptic triaryl boranes with at least one electron withdrawing substituent would appear to be more useful synthetic targets for reactivity exploration. Fluorinated triaryl boranes have been studied as hydrosilylation and hydroboration catalysts for a variety of unsaturated substrates.[12–14] Such demonstrably useful species therefore appear to be a rational starting point for further exploration.

In addition to studies on *bis* heteroleptic species (**Scheme 3.2**), another report by Wildgoose introduced a synthetic pathway to heteroleptic triaryl boranes featuring electron withdrawing groups (**Scheme 3.4**).[15]

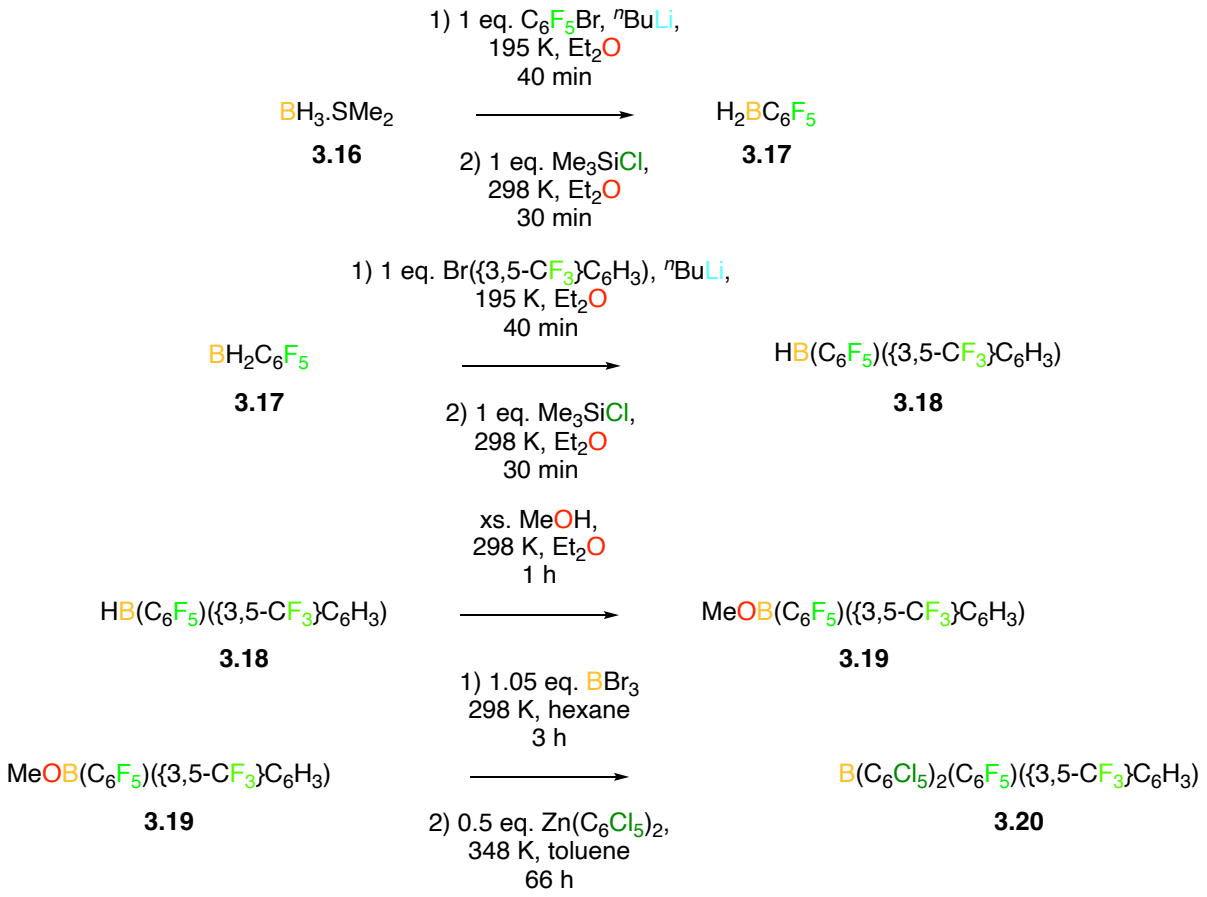

Scheme 3.4 – Synthetic route to heteroleptic triaryl boranes reported by Wildgoose et al.

The authors detailed the introduction of the first two aryl rings *via* lithiation and subsequent hydride abstraction. The resulting diaryl hydroborane could then be converted first into the methoxyborane, then the bromoborane, before the final aryl substituent was added using a zinc transfer reagent. However, given the relative scarcity of these reports, significant challenges remain and there is space for a more widely applicable synthetic route towards heteroleptic tri substituted boranes.

3.2 Aims

The work described in this chapter aimed to develop a synthetic route to heteroleptic triaryl boranes with substituents solely introduced by salt metathesis using metalated aryls. Metalation

as a means of derivatisation is one of the most widely used reactions in chemical synthesis – meaning any method developed in this manner could have broad reaching applicability. The long-term goal was to apply this synthesis towards new FLPs with tuneable electronic and steric profiles. However, a methodology was targeted in the first place towards 'simple' new boranes to examine their discrete chemical reactivity.

Borane properties are conferred by the degree to which their substituents withdraw or donate electron density, and by their steric profiles. A range of aryl groups was therefore explored. The two most commonly used boron precursor choices used in the literature are borane dimethyl sulfide ($BH_3.SMe_2$) or (2,6-dimethylphenyl)trifluoroborate derivatives. The former was chosen here, as the latter enforces a mesityl-derived functional group from the outset.

3.3 Results and Discussion

3.3.1 Synthesis of Diaryl Methoxyboranes

Initial work looked to replicate and expand upon the procedures of Wildgoose *et al.* to generate all the permutations of heterodiaryl methoxyboranes furnished with C_6Cl_5, C_6F_5 and $Ar^F{}_6$ rings (**Figure 3.4**).

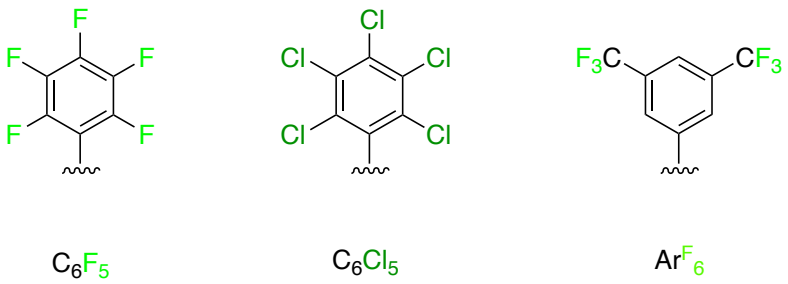

Figure 3.4 – Bulky electron withdrawing aryl groups.

At the outset, it became clear that the literature synthesis is not reproducible in our hands, as adding the borane dimethyl sulfide, Ar_2BH, precursor to C_6F_5Li or C_6Cl_5Li (**Scheme 3.4**) gives the corresponding homodiaryl borane in all cases and conditions trialled. In the case of C_6F_5Li, the planar methoxyborane product **3.i** was crystallographically characterised after quenching with methanol (**Figure 3.5**). X-ray quality crystals are obtained in 54 % yield from a dichloromethane solution.

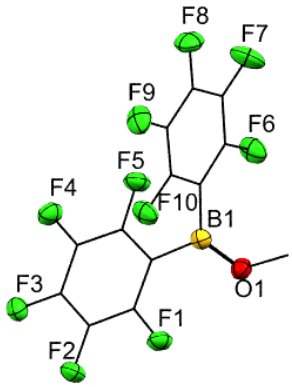

*Figure 3.5 – Molecular structure of **3.i** as determined by X-ray crystallography. Ellipsoids are shown at 50% probability. Carbon atoms are shown in wireframe format and hydrogen atoms are omitted for clarity.*

Modification of this procedure to make the lithiated arene the limiting reagent allows for the stepwise coordination of aryl rings to the boron centre. (**Scheme 3.5**).

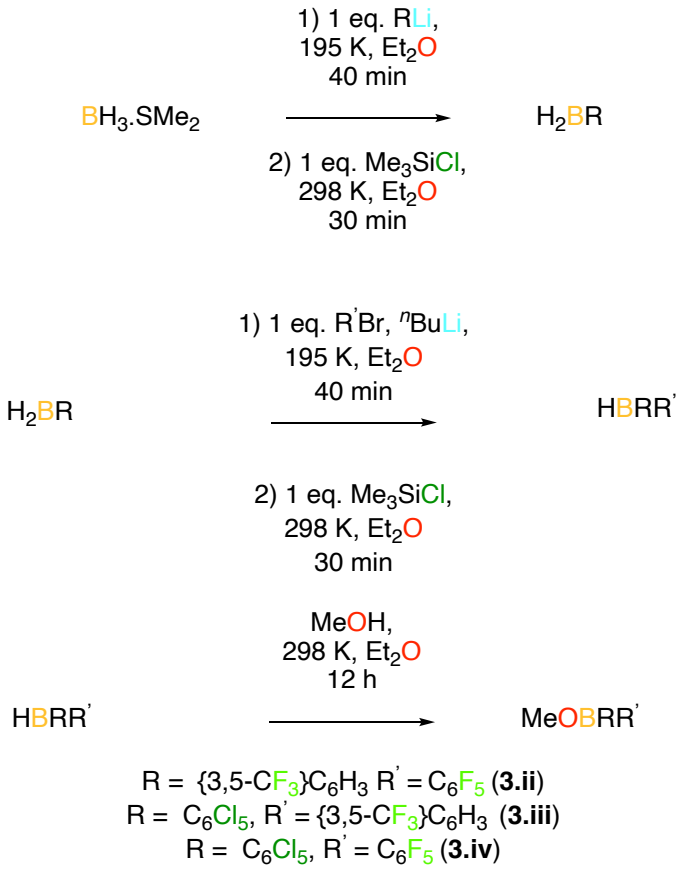

Scheme 3.5 –Synthesis of hetero diaryl methoxyboranes.

Crystals of the Ar^F_6/C_6F_5 methoxyborane **3.ii** (for which spectroscopic data was previously reported) were grown from cold dichloromethane, allowing its structure to be unambiguously confirmed by X-ray crystallography (**Figure 3.6**).

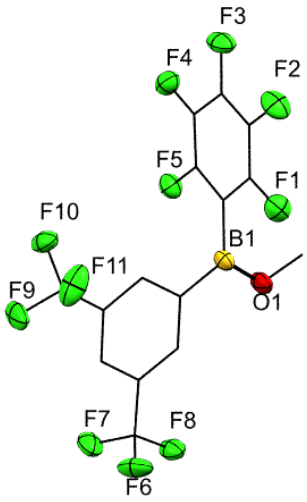

*Figure 3.6 – Molecular structure of **3.ii** as determined by X-ray crystallography. Ellipsoids are shown at 50% probability. Carbon atoms are shown in wireframe format and hydrogen atoms are omitted for clarity.*

The yield obtained is similar to that reported in the literature (61 % as opposed to 58 % reported). Spectroscopic data is also in agreement with the literature report. A resonance is seen in the ^{11}B NMR spectrum at 42.1 ppm. Within the ^{19}F NMR spectrum the signal corresponding to the six Ar^F_6 fluorine atoms lies at -62.9 ppm and the C_6F_5 fluorine resonances are found at -131.5, 148.6 and -159.3 ppm. Using this compound as a starting point raised two questions: can alternative aryl rings be added and, if they can, is the order of addition important? Extending the synthetic procedure to the corresponding Ar^F_6/C_6Cl_5 borane **3.iii**, answered both points, with X-ray quality crystals grown by similar means from cold dichloromethane (**Figure 3.7**).

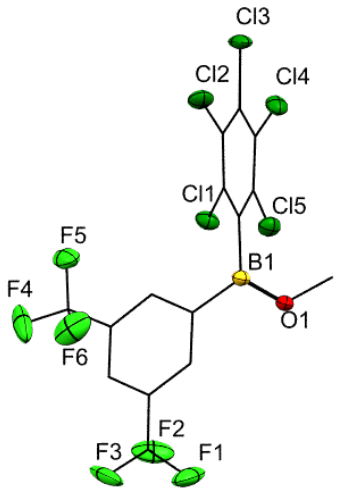

*Figure 3.7 – Molecular structure of **3.iii** as determined by X-ray crystallography. Ellipsoids are shown at 50% probability. Carbon atoms are shown in wireframe format and hydrogen atoms are omitted for clarity.*

The ^{11}B NMR spectrum is very similar to that of **3.ii**, with a characteristic broad signal at 42.3 ppm. The ^{19}F NMR spectrum features a singlet at -62.4 ppm, corresponding to the two CF_3 groups, which is reminiscent of the same environment in **3.ii**. The ^{1}H NMR spectrum features only three resonances: two in the aryl region at 8.26 and 7.84 ppm due to the aromatic $Ar^F{}_6$ protons *ortho*- and *para*- to boron, and one at 3.18 ppm arising from the methoxy group. Importantly from a synthetic perspective, the electron withdrawing aryl groups can be added in either order to yield the same product with a consistently good crystalline yield of 84 %.

A mixed borane furnished with one C_6Cl_5 and one C_6F_5 group may also be attained (**3.iv** – 81 % yield). The ^{11}B chemical shift is similarly diagnostic (40.0 ppm) and there are three multiplets ($J \sim 6$ Hz) in the ^{19}F NMR spectrum at -130.9, -147.9 and -161.6 ppm. As expected, the ^{1}H NMR spectrum features only a single methoxy proton peak at 3.27 ppm. X-ray quality crystals of **3.iv** were obtained from a cold dichloromethane solution (**Figure 3.8**).

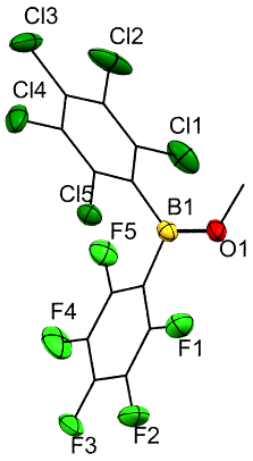

*Figure 3.8 – Molecular structure of **3.iv** as determined by X-ray crystallography. Ellipsoids are shown at 50% probability. Carbon atoms are shown in wireframe format and hydrogen atoms are omitted for clarity.*

Stoichiometric control is crucial in this synthetic approach, as exemplified by attempts to lithiate bromopentafluorobenzene (C_6F_5Br) *in situ* in the presence of $BH_3.SMe_2$. This produces a homoleptic *bisa*ryl product $(C_6F_5)_2BH$, which means that the first substituent to be added must be available as a stable lithiate, in order for it to be added as the limiting reagent. In practice, 'stable' is reasonably ill defined, and appears only to exclude C_6F_5Li – a species which detonates above -40 °C.

A route to a system featuring a dimethylamino group in the *para* position was also sought in order to allow access to the related quaternary ammonium derivative. It was hypothesised that this group would confer strong Lewis acidity, based on a comparison of the Hammett constants of fluorine ($\sigma_p = 0.06$) and chlorine ($\sigma_p = 0.227$) to trimethylammonium ($\sigma_p = 0.820$).[16] It has also been experimentally demonstrated in work by Gabbai and co-workers, which described acidity enhancement of mesityl boranes by the systematic replacement of the mesityl with cationic anilinium group (**Figure 3.9**).[17]

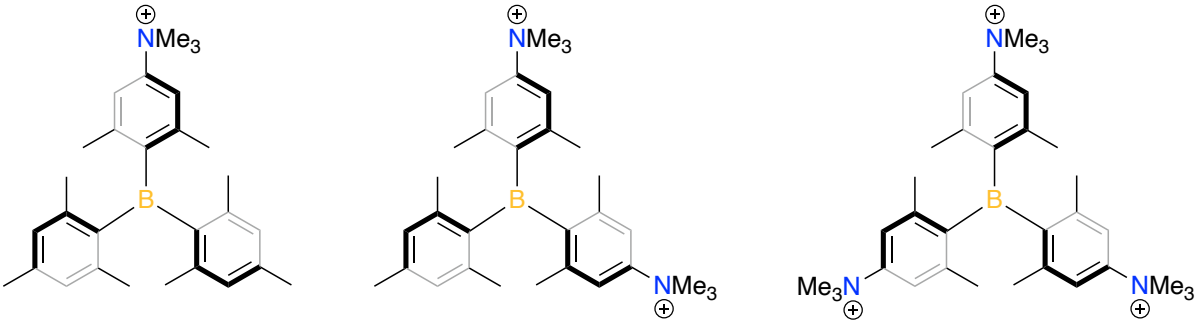

Figure 3.9 – Acidity enhancement by peripheral decoration of boranes with ammonium functions.

The process illustrated in **Scheme 3.5** was therefore extended to the aryl group $C_6F_4NMe_2$. Attempted syntheses of the $C_6Cl_5/C_6F_4NMe_2$ and $C_6F_5/C_6F_4NMe_2$ boranes (**Figure 3.10**) indicated the primary consideration in designing the reaction sequence must be stability of a given substituent towards subsequent lithiation.

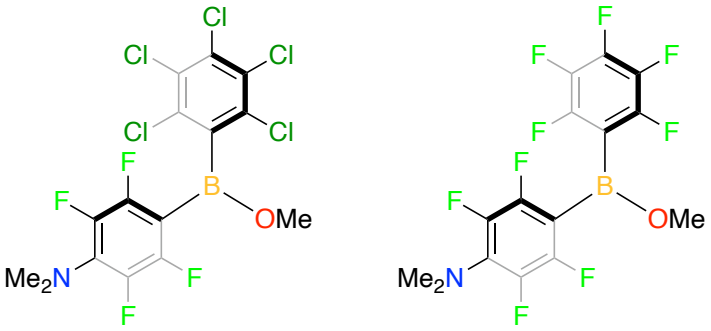

3.v **3.v'**

Figure 3.10 – Proposed para-aniline methoxyboranes.

For example, a mixed $C_6F_5/C_6F_4NMe_2$ borane **3.v'** does not appear attainable by this route (**Scheme 3.5**) because $BH_2C_6F_4NMe_2$ is not amenable to nucleophilic attack by ArLi; and the C_6F_5 group cannot be added first for the reasons outlines above. By introducing the C_6Cl_5 group in the first step, the $C_6Cl_5/C_6F_4NMe_2$ methoxyborane **3.v** could however be synthesised (albeit in a modest yield of 30 %) and characterised crystallographically (**Figure 3.11**).

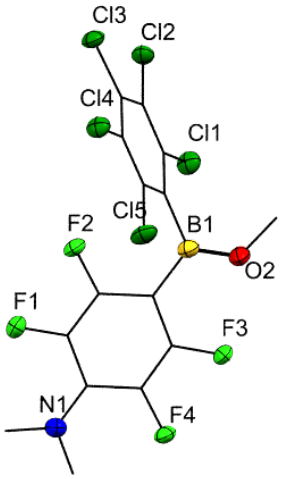

*Figure 3.11 – Molecular structure of **3.v** as determined by X-ray crystallography. Ellipsoids are shown at 50% probability. Carbon atoms are shown in wireframe format and hydrogen atoms are omitted for clarity.*

Spectroscopically, the ^{1}H NMR spectrum of **3.v** shows a resonance at 3.34 ppm corresponding to the three methoxy group protons, and a triplet due to the tertiary amine protons at 2.43 ppm. The splitting presumably arises from long-range coupling to the aryl fluorine atoms. Within the ^{11}B NMR spectrum a peak is seen at 40.3 ppm. Two resonances are observed in the ^{19}F NMR spectrum, at -132.8 (*ortho*- to B) and -153.0 ppm (*meta*- to B).

3.3.2 Comparison of Solid-State Structures

Based on the protocol suggested by Wildgoose, of deviation from planarity having implications for acidity in triaryl boranes, we wondered whether any similar inferences could be drawn from the structurally characterised diaryl boranes **3.i** – **3.v**. Ring twist was calculated as the interplanar angle between boron and its appended atoms (BOC_2), and the least squares planes of the aryl rings.

	Ring Twist / °				Mean / °
Borane	Ar^F_6	C_6F_5	C_6Cl_5	$C_6F_4NMe_2$	
3.i		69.2 42.8			56.0
3.ii	84.7	22.4			53.6
3.iii	21.9		84.7		53.3
3.iv		46.3	76.2		61.3
3.v			76.3 89.3	7.4 8.7	45.4

Table 3.2 – Summary of deviation angles from BOC_2 plane.

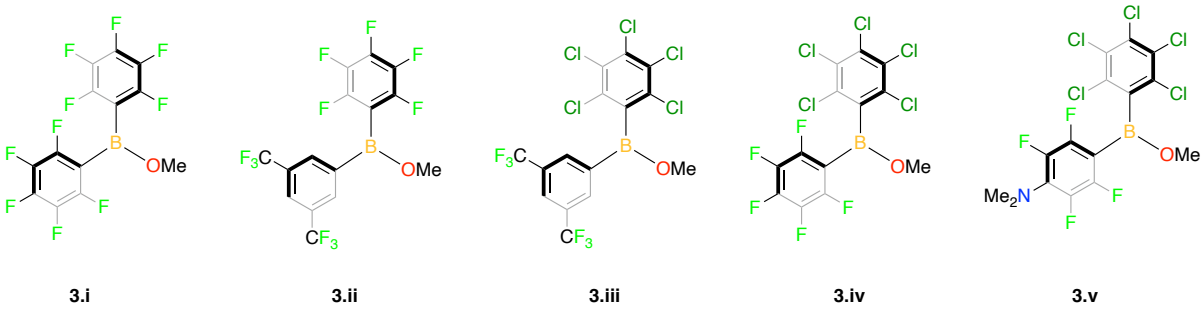

*Figure 3.12 – Methoxyboranes **3.i - 3.v**.*

For **3.ii** and **3.iii**, the average deviation from the plane is similar. Intuitively, one would expect that the ring with larger *ortho-* substituents would deviate more significantly out of the BOC_2 plane. Whereas the situation is as expected for **3.iii**, the opposite is the case for **3.ii**. It does not appear that *ortho-* groups are the sole governing factor in solid state geometry for these boranes, as if this were the case, we would expect **3.iv** and **3.v** to be structurally similar, although they are not.

3.3.3 Generation of Bromoborane Transfer Reagents

With a selection of methoxyboranes in hand, subsequent work examined whether they could be used as transfer reagents of a BRR' centre to other functional groups. This was envisaged by bromination (**Scheme 3.6**) followed by reaction with a further lithiated nucleophile.

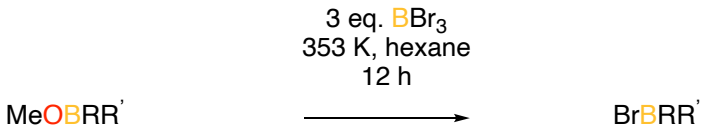

Scheme 3.6 – Synthesis of bromoboranes from methoxyboranes.

The conditions required for bromination of methoxyboranes **3.ii** – **3.v** are forcing, with heat, long reaction times, and an excess of boron tribromide all required to drive the reaction to completion. These reactions were monitored primarily by ^{1}H NMR spectroscopy as the disappearance of the peak around 3.2 ppm corresponding to the methoxy group protons is highly diagnostic of conversion to the corresponding bromoborane. Additionally, the singular resonance in the boron spectrum moves downfield from around 40 to around 60 ppm, due to the replacement of a methoxy group with a more poorly π donating halogen.

Bromoboranes BrB(C_6Cl_5)(C_6F_5) (**3.vi**) and BrB(C_6F_5)(C_6H_3 3,5-CF_3) (**3.vii**) are oils and were used for onward reactions without further purification, assuming quantitative conversion on the basis of NMR spectroscopy. However, the isolation of the BrB($Ar^F{}_6$)(C_6Cl_5) (**3.viii** – 81 % yield) and BrB($C_6F_5NMe_2$)(C_6Cl_5) (**3.ix** – 73 % yield) as off-white powders proved to be facile.

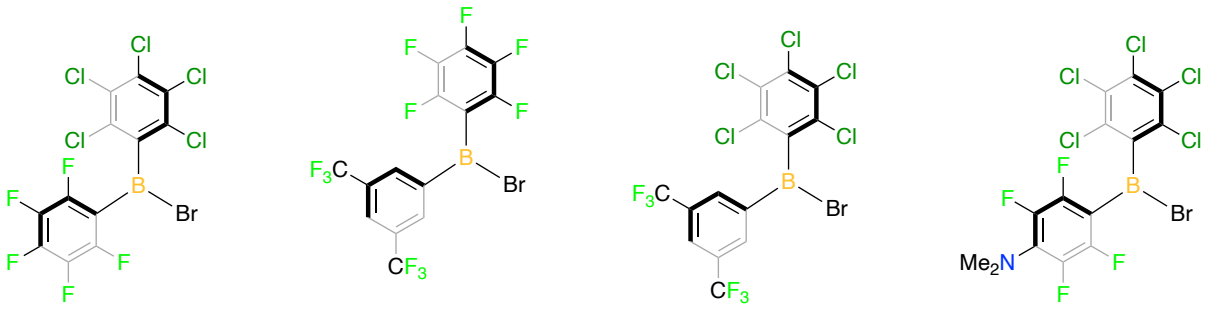

*Figure 3.13 – Bromoboranes **3.vi - 3.ix**.*

Presence or exclusion of the pentafluorophenyl group appears to be decisive here in determining physical state of the bromoborane. Given that diaryl haloboranes featuring the 3,5-bis(trifluoromethyl)phenyl and pentachlorophenyl groups are free flowing solids (**3.9** and **3.5**), whereas *bis*(pentafluorophenyl) chloroborane is somewhat oily, this stands in agreement to the expected physical characteristics of this borane.[18]

Although bromination/lithiation as a strategy for synthesising a bromo diarylborane has been seen before, the work of Wildgoose involved addition of the final substituent using a zinc transfer reagent. The breadth of systems which can be functionalised by lithiation is wide, which would bring this alternative methodology far closer to being a general synthesis.

3.3.4 Synthesis of Heteroleptic Triaryl Boranes

Boranes furnished with a pentachlorophenyl group were used to test the viability of a lithiation route, as the steric bulk of C_6Cl_5 was thought to give the best possible chance of generating the desired three co-ordinate product. Unfortunately, aryl lithiates such as PhLi, LiC_6H_4*p*NMe_2 and LiC_6H_4*p*OMe (**Scheme 3.7**) favour the addition of two equivalents to the boron centre even when $BrB(C_6Cl_5)(C_6F_5)_2$ **3.vi**, the most congested boron centre, is used.

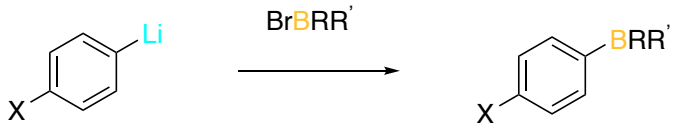

X = H, NMe_2, OMe

R = C_6Cl_5, R' = C_6F_5
R = C_6Cl_5, R' = {3,5-CF_3}C_6H_3

Scheme 3.7 – Attempted syntheses of heteroleptic triaryl boranes.

Looking at functionalisation of the existing boranes **3.vi**, **3.viii** and **3.ix**, reaction with mesitylithium, however, proceeds well to yield a single three co-ordinate borane product, even when two equivalents of lithiate are added (**Scheme 3.8**).

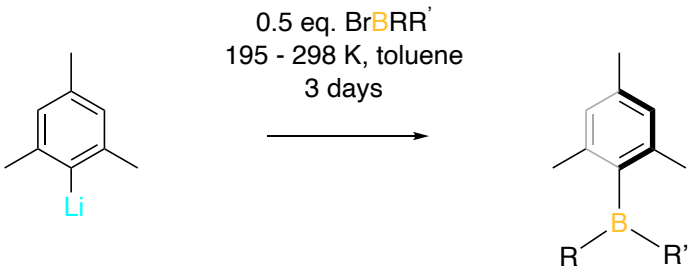

R = C_6Cl_5, R' = C_6F_5 (**3.x**) 35 % yield
R = C_6Cl_5, R' = {3,5-CF_3}C_6H_3 (**3.xi**) 10 % yield
R = C_6Cl_5, R' = $C_6F_4NMe_2$ (**3.xii**) 41 % yield

Scheme 3.8 – Synthesis of mesityl boranes.

Preparation of these mesityl boranes **3.x** – **3.xii** can be tracked primarily by the diagnostic fluorine NMR resonances. Replacement of the bromide with the mesityl group is most facile for the C_6Cl_5/C_6F_5 system **3.vi**, requiring only 30 min of heating (80 °C) to yield **3.x** (**Figure 3.14**).

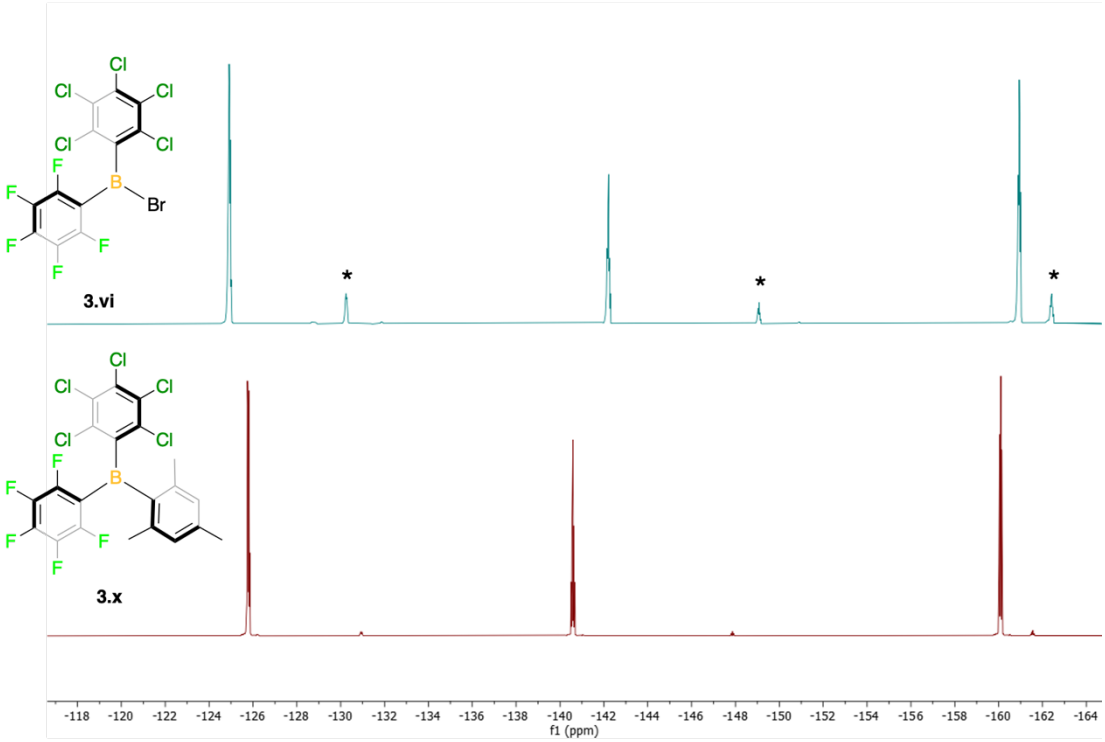

*Figure 3.14 – ^{19}F NMR spectra of bromoborane **3.vi** and corresponding mesityl borane **3.x**. Asterisks denote residual methoxyborane precursor **3.iv** seen in spectra of **3.vi**.*

The ^{19}F NMR resonances shift from -125.8, -140.6 and -160.1 ppm for **3.vi** to -129.4, -146.5 and -160.9 ppm for **3.x**. The ^{11}B signal shifts from 60.0 to 63.5 ppm. By ^{19}F NMR, the mesityl substituted borane is almost identical to the analogous *bis* pentafluoro species $MesB(C_6F_5)_2$ which gives rise to resonances at -129.6, -145.3 and -161.2 in the same solvent (C_6D_6).[19]

The boron shift (in deuterated toluene) of *bis* pentafluoromesityl borane is somewhat higher at 69.7 – compared to the corresponding bromoborane which is 61.6 in protio hexane, echoing the downfield shift of this signal in **3.x** compared to **3.vi**.[20] Due to the lack of literature on perchlorinated analogues of these boranes, a comparison akin to that with the perfluorinated systems cannot be made.

The borane $BrBC_6F_4NMe_2/C_6Cl_5$ (**3.xii**) can be synthesised in an analogous fashion by reaction of an excess of mesityl lithium with **3.ix**, which proceeds overnight at room temperature, or in 2h at 80 °C (**Figure 3.15**).

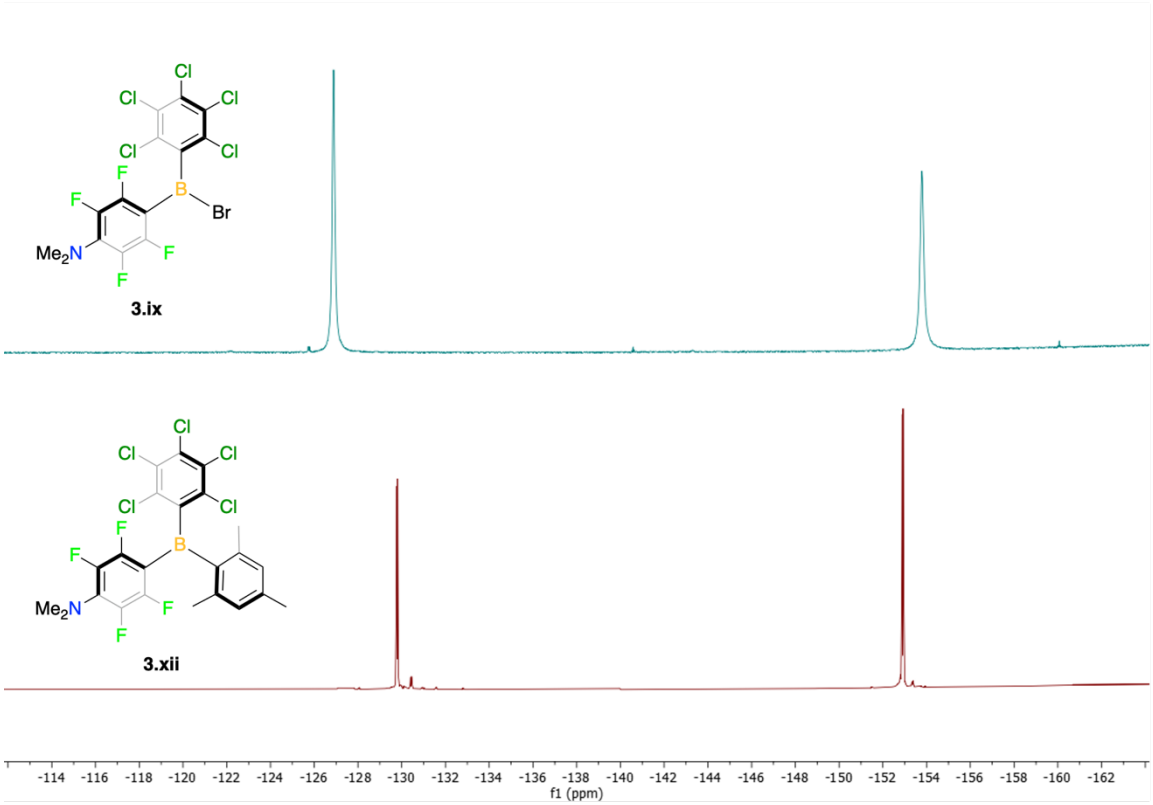

*Figure 3.15 – ^{19}F NMR spectra of bromoborane **3.ix** and the corresponding mesityl borane **3.xii**.*

The ^{11}B resonance shifts from 57.4 in **3.ix** to 69.5 ppm in **3.xii**; the separation between the *ortho*- and *meta*- ^{19}F resonances shift from -126.9 and -153.8 ppm to -130.0 and -153.0 ppm. By contrast, salt metathesis using Ar^F_6/C_6Cl_5 species **3.viii** to yield **3.xi** is slow and progress can be tracked over several days (**Figure 3.16**).

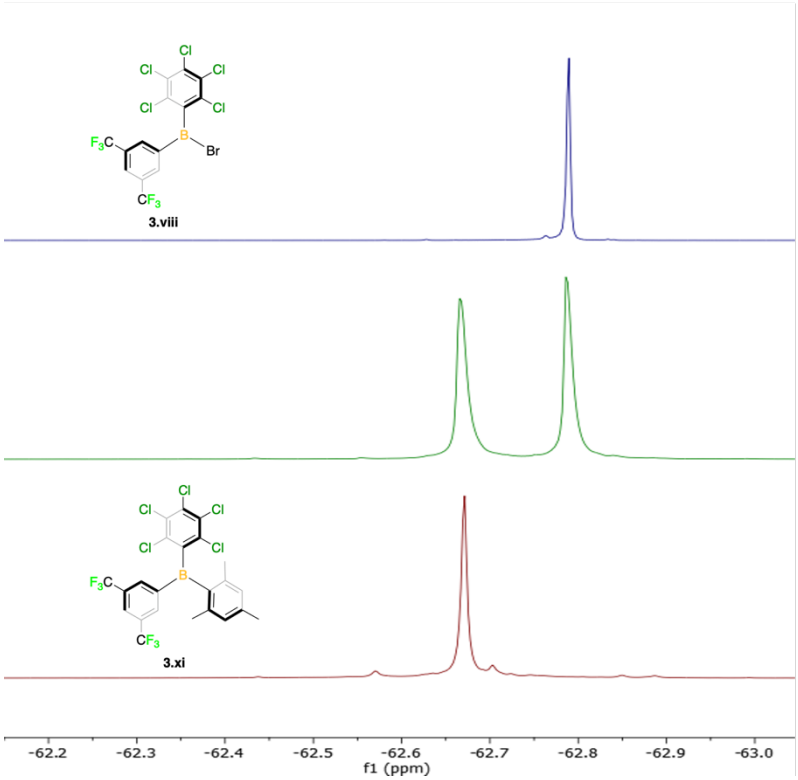

*Figure 3.16 – ^{19}F NMR spectra of bromoborane **3.vii** and the corresponding mesityl borane **3.xi**.*

This synthesis also requires an additional step to yield a spectroscopically pure product – sublimation (150 °C at $3x10^{-2}$ mbar) removes a mesityl-containing impurity but significantly depresses yield.

In all cases, these compounds (**3.x** – **3.xii**) exist as oils which makes their structural characterisation challenging. Therefore, crystallinity was sought through the synthesis of adducts, to confirm connectivity. Reaction at NMR scale with donors such as DMAP, MeCN and NaOMe, although giving the corresponding four-co-ordinate products, did not yield species amenable to characterisation through X-ray crystallography.

These results would appear to suggest that if the final substituent to be added is sufficiently bulky, heteroleptic triaryl boranes furnished with three groups functionalised by lithiation are synthetically attainable. Furthermore, it was envisaged that the precursor bromoboranes might

prove to be useful precursors for FLPs in combination with lithiated xanthene reagents. This hypothesis is explored in the next chapter.

3.4 Conclusions

The work described herein on the synthesis of heteroleptic triarylboranes establishes a number of design principles:

1) The first substituent to be added must be amenable to safe transport from one vessel to another, to allow for the initial hydro-borane precursor to be present in excess. In our hands, this appears to decisively exclude pentafluorophenyl C_6F_5.
2) A functionalised aryl ring can only be added if it is tolerant to *in-situ* lithiation.
3) The final group, if an aryl ring, must possess sufficient steric shielding in the *ortho*-positions, as demonstrated by the lack of success in adding phenyl, anisole, or dimethylaniline rings to encumbered boranes. However, adding a small substituent sooner in the synthetic scheme remains somewhat unexplored. It might be expected that following first addition of a reasonably large aryl group, a diaryl methoxyborane featuring, for example, a phenyl ring could be attained. These could then be employed as precursors for boranes possessing a third group with some *ortho*- functionality.

There is good spectroscopic evidence for the synthesis of heteroleptic triaryl boranes furnished with two bulky electron withdrawing groups and one mesityl substituent, although the properties of these species have not been probed to any appraisable extent. Further characterisation (spectroscopic and computational Lewis acidity quantification) is necessary. Having laid this synthetic groundwork, there are several directions in which this work could be taken. One route could look at the existing species and explore their reduction over a group

one metal to see if this generates a radical anion capable of hydrogen activation, with or without the assistance of a Lewis base.

It is worth considering the influence of a cationic group in the *para*- position in terms of acidity enhancement. Further synthetic work on the borane $MesB(C_6F_4NMe_2)(C_6Cl_5)$ **3.xii** should look at methylation of the amine, and the reactivity of the resultant cation.

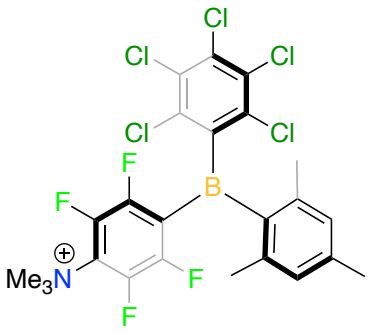

Figure 3.17 – Exemplar potential cationic tris heteroleptic borane.

Another route would involve using this method to make new boranes. For example, **3.vi** – **3.ix** can be used as precursors for tris aryl species bearing three different substituents. If the only requirement for the third aryl group is that it has *ortho* substituents greater than or equal to the size of methyl, the other positions on the ring in theory can be decorated differently. For example, future work might mimic the results of Gabbai mentioned in **Section 3.3.1** in making a series of boranes with an anilium group in the place of the mesityl substituent.

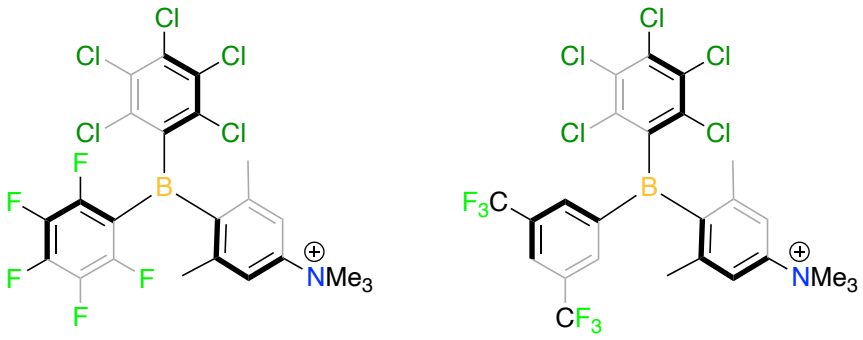

Figure 3.18 – Exemplar potential cationic tris heteroleoptic boranes.

An alternate project might employ a leaving group such as bromine at the *para* position of an aryl ring.[9] Once appended to the boron centre, one potential reaction could be to attach a pendant aryl group to the *para* position – this might confer crystallinity through π stacking which would be useful in the context of definitive structural characterisation. Additionally, this could be exploited in anchoring to a surface support to explore the heterogeneous catalytic potential of these boranes; although the impact of a surface upon acidity would perhaps be best explored with a siloxy mimic first.

It might also be interesting to look at alternate bulky functional groups on the boron centre. For example, ferrocenyl-substituted boranes have attracted attention as Lewis superacids which have been used in C—F and S—F bond activation.[21] This behaviour can be realised by their oxidation. If this route were to exploit the lithiation of ferrocene, it would likely involve significant synthetic investigation, and consideration of substituent addition order, considering that mono-lithiated ferrocene is generally made *in-situ* prior to quenching.[22] Unless it is isolable, this would necessitate it being the second substituent added – and thus stable to reaction with boron tribromide.

There is clearly strong potential to extend investigations into these boranes in multiple directions to yield new species with diverse properties such as tuneable acidity and fluorescence with applications in, for example, chemical sensing.

3.5 Synthetic Procedures and Spectroscopic Data for New Compounds

3.i – *Bis*pentafluorophenyl methoxyborane

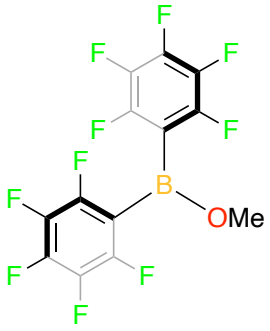

3.i

^{n}BuLi (15.6 mL of a 1.6 M solution in hexanes, 25 mmol, 1 equiv.) was added dropwise to a solution of C_6F_5Br (8 mL, 25 mmol, 1 equiv.) in Et_2O (50 mL) at -78 °C. A solution of $BH_3.SMe_2$ (2.37 mL, 25 mmol, 1 equiv.) in Et_2O (20 mL) was then added and the reaction mixture warmed to room temperature. Me_3SiCl (3.17 mL, 25 mmol, 1 equiv.) was added, followed by C_6F_5Br (8 mL, 25 mmol, 1 equiv). The reaction mixture was cooled again to -78 °C. and ^{n}BuLi (15.6 mL of a 1.6 M solution in hexanes, 25 mmol, 1 equiv.) added dropwise. The resulting suspension was warmed to room temperature and Me_3SiCl (3.17 mL, 25 mmol, 1 equiv.) added, then dry MeOH slowly (aprox. 3.2 mL, 75 mmol, 3 equiv.), causing rapid gas evolution. After stirring for 16 h, volatiles were removed *in vacuo* and the product extracted into pentane. Removal of the solvent and dissolution in dichloromethane, then cooling to -30 °C yielded colourless, X-ray quality crystals of **3.i** almost instantaneously. Yield: 12.83 g, 54%. Anal calcd for: $C_{13}H_3BF_{10}O$ C 41.53, H 0.80. Found: C 41.80, H 1.05. ^{1}H NMR (500 MHz, C_6D_6) δ 3.35 (s, 3H, OMe*CH*$_3$). ^{11}B{^{1}H} NMR (160 MHz, C_6D_6) δ 40.6. ^{13}C{^{1}H} NMR (126

MHz, C_6D_6) δ 148.8, 146.9, 144.4 – 144.2 (m), 142.4 – 142.1 (m), 138.7 (ddd, *J* = 18.2, 12.4, 5.1 Hz), 136.7 (ddd, *J* = 18.1, 12.4, 5.3 Hz) Ar*C*. 57.0 (OMe*C*). $^{19}F\{^1H\}$ NMR (377 MHz, C_6D_6) δ -132.7 (dd, *J* = 23.2, 10.9 Hz, *o*-C_6F_5), -149.1 (t, *J* = 21.1 Hz, *p*-C_6F_5), -161.2 (br. s, *m*-C_6F_5)

3.ii – Pentafluorophenyl-3,5-bis(trifluoromethyl)phenyl methoxyborane

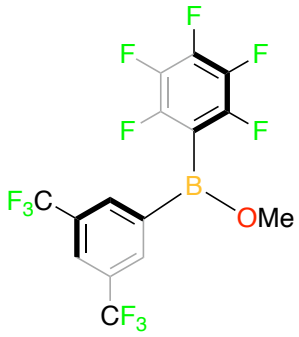

3.ii

^{n}BuLi (15.6 mL of a 1.6 M solution in hexanes, 25 mmol, 1 equiv.) was added dropwise to a solution of $BrC_6H_3(CF_3)_2$-3,5 (5.8 mL, 25 mmol, 1 equiv.) in Et_2O (50 mL) at -78 °C and the reaction mixture stirred until an amber solution was observed (ca. 4 h). This mixture was added rapidly to a solution of $BH_3.SMe_2$ (2.37 mL, 25 mmol, 1 equiv.) in Et_2O (20 mL) at -78 °C and warmed to room temperature. After stirring for 30 min, Me_3SiCl (3.17 mL, 25 mmol, 1 equiv.) was added, followed by C_6F_5Br (8 mL, 25 mmol, 1 equiv). The reaction mixture was cooled again to -78 °C, and ^{n}BuLi (15.6 mL of a 1.6 M solution in hexanes, 25 mmol, 1 equiv.) added dropwise. The resulting suspension was warmed to room temperature and Me_3SiCl (3.17 mL, 25 mmol, 1 equiv.) added, then dry MeOH slowly (aprox. 3.2 mL, 75 mmol, 3 equiv.), causing rapid gas evolution. After stirring for 16 h, volatiles were removed *in vacuo* and the product extracted into pentane. Removal of the solvent and dissolution in dichloromethane, then cooling to -30 °C yielded colourless, X-ray quality crystals of **3.ii** almost instantaneously.

Two further crystallisations yielded additional spectroscopically pure material. Yield: 6.31 g, 60%. Anal calcd for $C_{13}H_{3B}F_{10}O$ C: 41.53, H: 0.80. Found C: 41.50 H: 0.76. ^{1}H NMR (500 MHz, C_6D_6) δ 8.13 (d, *J* = 1.8 Hz, 1H, Ar*H*), 7.84 (s, 2H, Ar*H*), 3.23 (d, *J* = 3.1 Hz, 3H, OMe*CH*$_3$). ^{11}B{^{1}H} NMR (160 MHz, C_6D_6) δ 42.1.^{13}C{^{1}H} NMR (126 MHz, C_6D_6) δ 147.3, 145.4, 143.7, 141.6, 138.7, 136.7, 134.9, 132.1 – 131.3 (m), 127.2, 126.2, 125.0, 122.8, 120.7 (Ar*C*), 56.6 (OMe*C*). ^{19}F{^{1}H} NMR (470 MHz, C_6D_6) δ -62.5 to -63.3 (m), -131.5 (dd, *J* = 23.8, 10.7 Hz, *o*-C_6F_5), -148.4 to -148.7 (m, *p*-C_6F_5), -159.3 (ddtt, *J* = 30.2, 22.1, 14.6, 6.3 Hz, *m*-C_6F_5).

3.iii – Pentachlorophenyl-3,5-bis(trifluoromethyl)phenyl methoxyborane

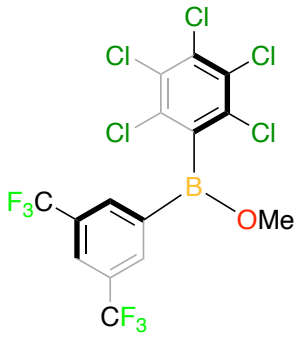

3.iii

C_6Cl_6 (7.1 g, 25 mmol, 1 equiv.) was slurried in Et_2O (80 mL) and cooled to -78 °C. ^{n}BuLi (15.6 mL of a 1.6 M solution in hexanes, 25 mmol, 1 equiv.) was added dropwise and the reaction mixture stirred until an amber solution was observed (ca. 4 h). This mixture was added rapidly to a solution of $BH_3.SMe_2$ (2.37 mL, 25 mmol, 1 equiv.) in Et_2O (20 mL) at -78 °C and then warmed to room temperature. After stirring for 30 min, Me_3SiCl (3.17 mL, 25 mmol, 1 equiv.) was added, followed by $BrC_6H_3(CF_3)_2$-3,5 (5.8 mL, 25 mmol, 1 equiv.). The reaction mixture was cooled again to -78 °C, and ^{n}BuLi (15.6 mL of a 1.6 M solution in hexanes, 25 mmol, 1 equiv.) added dropwise. The resulting suspension was warmed to room temperature and Me_3SiCl (3.17 mL, 25 mmol, 1 equiv.) added, then dry MeOH slowly (aprox. 3.2 mL, 75

mmol, 3 equiv.), causing rapid gas evolution. After stirring for 16 h, volatiles were removed *in vacuo* and the product extracted into pentane. Removal of the solvent and dissolution in dichloromethane, then cooling to -30 °C yielded colourless, X-ray quality crystals of **3.iii** almost instantaneously. Two further crystallisations yielded additional spectroscopically pure material. Yield: 10.56 g, 84% Anal calcd for $C_{15}H_6BCl_5F_6O$: C 35.70, H: 1.19. Found: C 35.53, H 1.12. ^{1}H NMR (500 MHz, C_6D_6) δ 8.26 (d, J = 1.8 Hz, 2H, Ar*H*), 7.84 (s, 1H, Ar*H*), 3.18 (s, 3H, OMe*CH*$_3$). $^{11}B\{^{1}H\}$ NMR (160 MHz, C_6D_6) δ 42.3. $^{13}C\{^{1}H\}$ NMR (126 MHz, C_6D_6) δ 135.6 (*i*-C_6Cl_5), 134.7 (*i*-Ar^F_6), 132.9 (*p*-C_6Cl_5), 132.5 (*o*-C_6Cl_5), 132.1 (*o*-C_6Cl_5), 131.8 (*o*-Ar^F_6), 131.5 (*o*-Ar^F_6), 127.2 (*m*-C_6Cl_5), 126.1 (*m*-C_6Cl_5), 126.0 (both *m*-Ar^F_6), 125.0 (*m*-CF_3), 122.8 (*m*-CF_3), 120.7 (*p*-Ar^F_6), 55.7 (OMe*C*). $^{19}F\{^{1}H\}$ NMR (470 MHz, C_6D_6) δ -62.7.

3.iv – Pentachlorophenyl-pentafluorophenyl methoxyborane

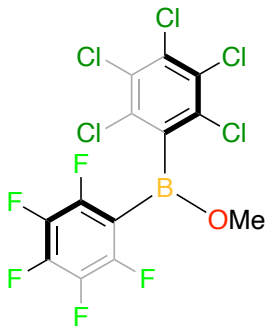

3.iv

C_6Cl_6 (7.1 g, 25 mmol, 1 equiv.) was slurried in Et_2O (80 mL) and cooled to -78 °C. ^{n}BuLi (15.6 mL of a 1.6 M solution in hexanes, 25 mmol, 1 equiv.) was added dropwise and the reaction mixture stirred until an amber solution was observed (ca. 4 h). This mixture was added rapidly to a solution of $BH_3.SMe_2$ (2.37 mL, 25 mmol, 1 equiv.) in Et_2O (20 mL) at -78 °C and then warmed to room temperature. After stirring for 30 min, Me_3SiCl (3.17 mL, 1 equiv.) was added, followed by C_6F_5Br (8 mL, 25 mmol, 1 equiv). The reaction was cooled again to -

78 °C, and ^{n}BuLi (15.6 mL of a 1.6 M solution in hexanes, 25 mmol, 1 equiv.) added dropwise. The resulting suspension was warmed to room temperature and Me_3SiCl (3.17 mL, 25 mmol, 1 equiv.) added, then dry MeOH slowly (aprox. 3.2 mL, 75 mmol, 3 equiv.), causing rapid gas evolution. After stirring for 16 h, volatiles were removed *in vacuo* and the product extracted into pentane. Removal of the solvent and dissolution in dichloromethane, then cooling to -30 °C. yielded colourless, X-ray quality crystals of **3.iv** almost instantaneously. Two further crystallisations yielded additional spectroscopically pure material. Yield: 9.25 g, 81%. Anal calcd for $C_{13}H_3BCl_5F_5$: C: 35.70, H: 1.20. Found: C: 35.64, H: 1.18. ^{1}H NMR (500 MHz, C_6D_6) δ 3.27 (s, 3H, OMe*CH*$_3$). ^{11}B{^{1}H} NMR (160 MHz, C_6D_6) δ 40.0. ^{13}C{^{1}H} NMR (126 MHz, C_6D_6) δ 150.9 (*o*-C_6F_5), 148.9 (*p*-C_6F_5), 144.7 (*i*-C_6Cl_5), 144.6 (*m*-C_6F_5), 138.5 (*p*-C_6Cl_5), 136.5 (*o*-C_6Cl_5), 135.2 (residual co-crystallised C_6Cl_6), 132.6 (*m*-C_6Cl_5), 132.2 (*i*-C_6F_5), 55.8 (OMe*C*). ^{19}F{^{1}H} NMR (470 MHz, C_6D_6) δ -130.9 (dq, J = 21.0, 5.7 Hz, *o*-C_6F_5), -147.9 (tt, J = 20.9, 5.5 Hz, *p*-C_6F_5), -161.5 to -161.7 (m, *m*-C_6F_5).

3.v – Pentachloro-4-*N*,*N*-dimethylamino-2,3,5,6 tetrafluorophenyl methoxyborane

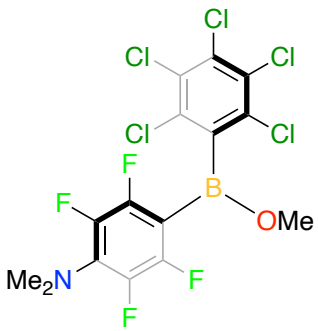

3.v

C_6Cl_6 (7.1 g, 25 mmol, 1 equiv.) was slurried in Et_2O (80 mL) and cooled to -78 °C. ^{n}BuLi (15.6 mL of a 1.6 M solution in hexanes, 25 mmol, 1 equiv.) was added dropwise and the

reaction mixture stirred until an amber solution was observed (ca. 4 h). This mixture was added rapidly to a solution of $BH_3.SMe_2$ (2.37 mL, 25 mmol, 1 equiv.) in Et_2O (20 mL) at -78 °C and warmed to room temperature. After stirring for 30 min, Me_3SiCl (3.17 mL, 25 mmol, 1 equiv.) was added, followed by $IC_6F_4NMe_2$ (8 g, 25 mmol, 1 equiv.). The reaction mixture was cooled again to -78 °C. and ^nBuLi (15.6 mL of a 1.6 M solution in hexanes, 25 mmol, 1 equiv.) added dropwise. The suspension was warmed to room temperature and Me_3SiCl (3.17 mL, 25 mmol, 1 equiv.) added, then dry MeOH slowly (aprox. 3.2 mL, 75 mmol, 3 equiv.), causing rapid gas evolution. After stirring for 16 h, volatiles were removed *in vacuo* and the product extracted into pentane. Removal of the solvent and dissolution in dichloromethane, then cooling to -30 °C yielded colourless, X-ray quality crystals of **3.v**. Yield: 3.56 g, 30 %. Anal calcd for $C_{15}H_9BCl_5F_4NO$: C: 37.28, H: 1.88. Found: C: 37.30, H: 1.81. ^1H NMR (400 MHz, C_6D_6) δ 3.34 (s, 3H, OMeCH_3), 2.43 (t, J = 2.6 Hz, 6H, NMe_2CH_3). $^{11}B\{^1H\}$ NMR (128 MHz, C_6D_6) δ 40.3. $^{13}C\{^1H\}$ NMR (101 MHz, C_6D_6) δ 152.9 (br. s, Ar$C_6F_4NMe_2$), 150.3 (br. s, Ar$C_6F_4NMe_2$), 141.9 (br. s, Ar$C_6F_4NMe_2$), 139.5 (ArC_6Cl_5), 135.3 (residual co-crystallised C_6Cl_6), 134.6 (ArC_6Cl_5), 132.8 (ArC_6Cl_5), 132.1 (ArC_6Cl_5), 55.5 (s, OMe*C*), 42.4 (t, J = 4.9 Hz, NMe_2C). $^{19}F\ \{^1H\}$ NMR (377 MHz, C_6D_6) δ -132.7 to -132.9 (m, *o*-C_6F_5), -152.9 to -153.1 (m, *m*-C_6F_5).

General procedure for bromination of methoxyboranes

Methoxyborane **3.ii** – **3.v** (1.1 mmol, 1 equiv.) was dissolved in of hexane (30 mL), and BBr_3 (0.3 mL, 3.3 mmol, 3 equiv.) added rapidly. The reaction was sealed in a Teflon capped ampoule and heated at 80 °C overnight. The product was cooled to room temperature and all volatiles removed *in vacuo*.

3.vi – Pentachlorophenyl-pentafluorophenyl bromoborane

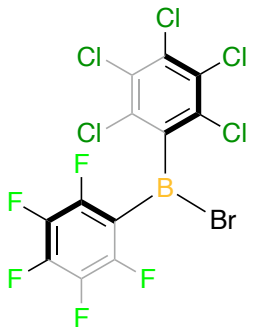

3.vi

Compound **3.vi** was not isolated, but conversion was confirmed by $^{11}B\{^1H\}$ and $^{19}F\{^1H\}$ NMR spectroscopy. It is a brown oil which was used for further chemistry assuming quantitative conversion and without further purification. The presence of residual precursor (ca. 5 %) does not appear to impact the onwards reactivity. $^{11}B\{^1H\}$ NMR (128 MHz, C_6D_6) δ 60.0. $^{19}F\{^1H\}$ NMR (377 MHz, C_6D_6) δ -125.7 to -125.9 (m, *o*-C_6F_5), -140.6 (tt, J = 21.4, 9.3 Hz, *p*-C_6F_5), -160.0 to -160.2 (m, *m*-C_6F_5).

3.vii – Pentafluorophenyl-3,5-bis(trifluoromethyl)phenyl bromoborane

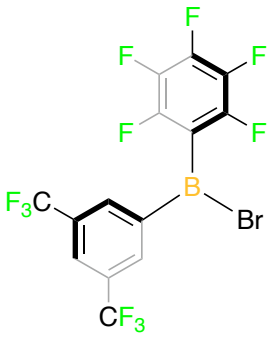

3.vii

Compound **3.vii** was not isolated but conversion was confirmed by ^1H, $^{11}B\{^1H\}$ and $^{19}F\{^1H\}$ NMR spectroscopy. It is a brown oil which was used for further chemistry assuming

quantitative conversion and without further purification. ^{1}H NMR (400 MHz, C_6D_6) δ 8.20 (s, 2H), 7.82 (s, 1H). ^{11}B{^{1}H} NMR (128 MHz, C_6D_6) δ 65.8. ^{19}F{^{1}H} NMR (377 MHz, C_6D_6) δ -62.8 (s), -128.8 to -129.2 (m, *o*-C_6F_5), -145.6 to -145.9 (m, *p*-C_6F_5), -159.4 to -159.9 (m, *m*-C_6F_5).

This reaction was stirred over Cu powder to remove the HBr by-product which hinders onward reactivity.

3.viii – Pentachlorophenyl-3,5-bis(trifluoromethyl)phenyl bromoborane

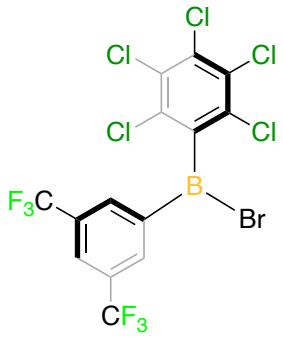

3.viii

Compound **3.viii** was isolated as a fine, off-white powder and used for subsequent chemistry without further purification. Yield: 750 mg, 81%. Anal calcd for $C_{14}H_3BBrCl_5F_6$: C 30.40, H 0.55. Found: C 30.75, H 0.62. ^{1}H NMR (500 MHz, C_6D_6) δ 8.40 (d, *J* = 1.8 Hz, 2H Ar*H*), 7.48 (s, 1H Ar*H*). ^{11}B{^{1}H} NMR (160 MHz, C_6D_6) δ 64.0. ^{13}C{^{1}H} NMR (126 MHz, C_6D_6) δ 139.4, 138.4, 137.1, 137.0, 133.0, 132.9, 132.7, 132.5, 132.3, 132.2, 130.7, 128.8, 128.6, 128.4, 128.2, 126.6, 124.4, 122.3, 120.1 (Ar*C*). ^{19}F{^{1}H} NMR (470 MHz, C_6D_6) δ -62.8.

3.ix – Pentachloro-4-N,N-dimethylamino-2,3,5,6 tetrafluorophenyl bromoborane

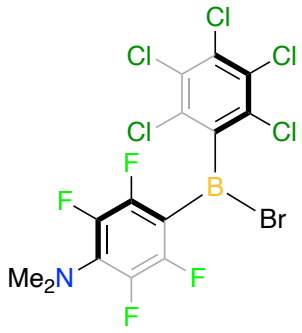

3.ix

Compound **3.ix** was isolated as a fine, off-white powder and used for subsequent chemistry without further purification. Yield: 427 mg, 73%. Anal calcd for $C_{14}H_6BBrCl_5F_4N$: C 31.60, H: 1.14. Found: C 31.95, H 1.85. ^{1}H NMR (500 MHz, C_6D_6) δ 2.32 (t, J = 3.0 Hz, 6H, NMe_2CH_3). ^{11}B{^{1}H} NMR (160 MHz, C_6D_6) δ 57.4. ^{13}C{^{1}H} NMR (126 MHz, C_6D_6) δ 153.5 (br.s, Ar$C_6F_4NMe_2$), 151.4 (br.s, Ar$C_6F_4NMe_2$), 143.8 (br.s, Ar$C_6F_4NMe_2$), 140.0 (d, J = 20.0 Hz, Ar$C_6F_4NMe_2$), 138.1 (d, J = 13.6 Hz, Ar$C_6F_4NMe_2$) 134.3 (ArC_6Cl_5), 132.3 (ArC_6Cl_5), 130.4 (ArC_6Cl_5), 42.7 (NMe_2C). ^{19}F{^{1}H} NMR (470 MHz, C_6D_6) δ -126.9 (br.s, *o*-C_6F_5), -153.8 (br.s, *m*-C_6F_5).

General procedure for attempted syntheses of Ph, $MeOC_6H_4$, $NMe_2C_6H_4$ boranes described in Section 3.3.4

PhLi, *p*-$MeOC_6H_4Li$ or *p*-$NMe_2C_6H_4Li$ (1 equiv.) was slurried in toluene (20 mL) and cooled to -78 °C. A solution of bromoborane **3.vi**, **3.viii** or **3.ix** (1 equiv.) was dissolved in toluene (20 mL) and added dropwise to the aryllithium solution. The reaction mixture was allowed to warm slowly to room temperature. In all cases this yielded 4 co-ordinate products, as confirmed by sharp resonances around 0 in the respective ^{11}B NMR spectra.

General procedure for syntheses of mesityl boranes

MesLi (2 equiv.) was slurried in toluene (20 mL) and cooled to -78 °C. A solution of bromoborane **3.vi**, **3.viii** or **3.ix** (1 equiv.) was dissolved in toluene (20 mL) and added dropwise. The reaction mixture was allowed to warm to room temperature slowly. Reactions were heated to 80 °C and monitored by ^{19}F NMR spectroscopy to determine completion. In all cases these compounds are oils and were used assuming quantitative conversion.

3.x – 2,4,6-trimethylphenyl-pentachlorophenyl-pentafluorophenyl borane

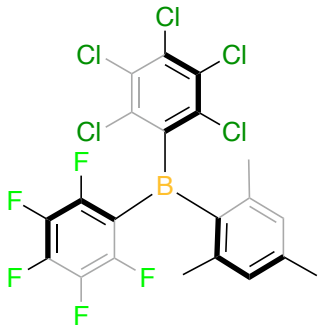

3.x

Yield: 1.1 mL, 35 %. ^{1}H NMR (400 MHz, C_6D_6) δ 6.61 (s, 2H, MesAr*H*), 2.04 (s, 9H, MesAlk*H*). ^{11}B{^{1}H} NMR (128 MHz, C_6D_6) 63.5. ^{13}C{^{1}H} NMR (101 MHz, C_6D_6) δ 148.4 (br. s), 145.9 (br. s), 143.0, 138.4 (br. s), 134.8, 132.7, 132.4, 129.5 (Ar*C*), 21.0 (Mes*CH*$_3$). ^{19}F{^{1}H} NMR (377 MHz, C_6D_6) δ -129.3 to -129.5 (m, *o*-C_6F_5), -146.5 (tt, *J* = 20.8, 4.6 Hz, *p*-C_6F_5), -160.6 to -161.3 (m, *m*-C_6F_5).

3.xi – 2,4,6-trimethylphenyl-pentachlorophenyl-3,5-bis(trifluoromethyl)phenyl borane

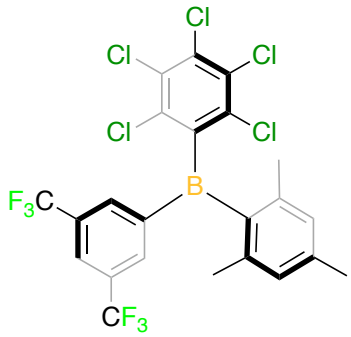

3.xi

Yield: 0.5 mL, 10 %. ^{1}H NMR (400 MHz, C_6D_6) δ 8.16 (d, J = 1.8 Hz, 2H, $Ar^{F}{}_6ArH$), 7.90 (s, 1H, $Ar^{F}{}_6ArH$), 6.65 (d, J = 14.2 Hz, 2H, MesAr*H*), 2.05 (s, 3H, MesAlk*H*), 1.92 (s, 6H, MesAlk*H*). ^{11}B{^{1}H} NMR (160 MHz, C_6D_6) δ 68.2. ^{13}C{^{1}H} NMR (101 MHz, C_6D_6) δ 142.7, 141.9, 137.2, 135.7, 133.4, 132.6, 132.0, 131.7, 129.4, 128.8 – 128.2 (m), 125.2 – 124.4 (m) (Ar*C*), 23.6, 20.9, 20.1 (dt, J = 38.4, 19.1 Hz) (Alk*C*). ^{19}F{^{1}H} NMR (377 MHz, C_6D_6) δ -62.7.

3.xii – 2,4,6-trimethylphenyl-pentachloro-4-N,N-dimethylamino-2,3,5,6 tetrafluorophenyl borane

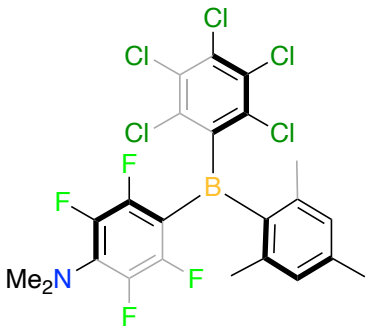

3.xii

Yield: 0.95 mL, 41 %. ^{1}H NMR (400 MHz, C_6D_6) δ 6.70 (s, 2H, MesAr*H*), 2.42 (t, J = 2.8 Hz, 6H, NMe_2CH_3), 2.26 (s, 6H, MesAlk*H*), 2.09 (s, 3H, MesAlk*H*). ^{11}B{^{1}H} NMR (128 MHz, C_6D_6) δ 69.5. ^{19}F{^{1}H} NMR (377 MHz, C_6D_6) δ -129.7 to -130.0 (m, *o*-C_6F_5), -152.8 to -153.1 (m, *m*-C_6F_5).

3.5 References

1 Z. Huang, S. Wang, R. D. Dewhurst, N. V. Ignat'ev, M. Finze and H. Braunschweig, *Angew. Chemie - Int. Ed.*, 2020, **59**, 8800–8816.

2 I. B. Sivaev and V. I. Bregadze, *Coord. Chem. Rev.*, 2014, **270**–**271**, 75–88.

3 T. J. Herrington, A. J. W. Thom, A. J. P. White and A. E. Ashley, *Dalt. Trans.*, 2012, **41**, 9019–9022.

4 J. L. Carden, L. J. Gierlichs, D. F. Wass, D. L. Browne and R. L. Melen, *Chem. Commun.*, 2019, **55**, 318–321.

5 A. G. Massey and A. J. Park, *J. Organomet. Chem.*, 1966, **5**, 218–225.

6 S. Keess, A. Simonneau and M. Oestreich, *Organometallics*, 2015, **34**, 790–799.

7 A. E. Ashley, T. J. Herrington, G. G. Wildgoose, H. Zaher, A. L. Thompson, N. H. Rees, T. Krämer and D. O'Hare, *J. Am. Chem. Soc.*, 2011, **133**, 14727–14740.

8 R. J. Blagg, T. R. Simmons, G. R. Hatton, J. M. Courtney, E. L. Bennett, E. J. Lawrence and G. G. Wildgoose, *Dalt. Trans.*, 2016, **45**, 6032–6043.

9 M. Ferger, S. M. Berger, F. Rauch, M. Schönitz, J. Rühe, J. Krebs, A. Friedrich and T. B. Marder, *Chem. – A Eur. J.*, 2021, **27**, 9094–9101.

10 D. Turnbull and M.-A. Légaré, *Chem. Sci.*, 2023, **14**, 14256–14261.

11 S. M. Berger, M. Ferger and T. B. Marder, *Chem. – A Eur. J.*, 2021, **27**, 7043–7058.

12 A. Simonneau and M. Oestreich, *Nat. Chem.*, 2015, **7**, 816–22.

13 Q. Yin, Y. Soltani, R. L. Melen and M. Oestreich, *Organometallics*, 2017, **36**, 2381–2384.

14 Q. Yin, S. Kemper, H. F. T. Klare and M. Oestreich, *Chemistry*, 2016, **22**, 13840–13844.

15 R. J. Blagg and G. G. Wildgoose, *RSC Adv.*, 2016, **6**, 42421–42427.

16 C. Gardner Swain, E. C. Lupton, D. H. McDaniel, H. C. Brown, J. Org Chem, H. van Bekkum, P. E. Verkade, B. M. Wepster, R. Trav, R. Knowles, R. O. C Norman, G. K. Radda, J. Chem Soc, D. A. Brimacombe and P. D. Ralph, *J. Am. Chem. Soc.*, 1968, **90**, 4328–4337.

17 C. W. Chiu, Y. Kim and P. F. Gabbaï, *J. Am. Chem. Soc.*, 2009, **131**, 60–61.

18 K. Samigullin, M. Bolte, H. W. Lerner and M. Wagner, *Organometallics*, 2014, **33**, 3564–3569.

19 Z. Niu, W. Zhang, P. C. Lan, B. Aguila and S. Ma, *Angew. Chemie Int. Ed.*, 2019, **58**, 7420–7424.

20 V. V. Bardin, S. A. Prikhod'ko, M. M. Shmakov, A. Y. Shabalin and N. Y. Adonin, *Russ. J. Gen. Chem.*, 2020, **90**, 50–61.

21 L. Köring, A. Stepen, B. Birenheide, S. Barth, M. Leskov, R. Schoch, F. Krämer, F. Breher and J. Paradies, *Angew. Chemie Int. Ed.*, 2023, **62**, e202216959.

22 R. Sanders and U. T. Mueller-Westerhoff, *J. Organomet. Chem.*, 1996, **512**, 219–224.

Chapter 4 – Synthesis and Unusual Dihydrogen Activation with Perchlorinated FLPs

4.1 Introduction

Few molecular species dominate a field as decisively as *tris*(pentafluorophenyl)borane $B(C_6F_5)_3$ (**1.14**) does as the choice of acid in Frustrated Lewis Pair chemistry.[1–3] The pentafluoro rings are both effective shrouds for the coordinatively unsaturated trivalent boron centre and highly electron withdrawing.[4] When looking to expand the scope of boranes in this capacity, alternative halogenated molecules are a natural investigative extension. Species such as *tris*pentachlorophenylborane $B(C_6Cl_5)_3$ (**3.7**) and *tris*{3,5-*bis*(trifluoromethyl)phenyl}borane $B\{C_6H_3(CF_3)_2\text{-}3,5\}_3$ ($BAr^F{}_{18}$) (**4.1**) possess the requisite large substituents which also act as effective electron sinks (**Figure 4.1**).

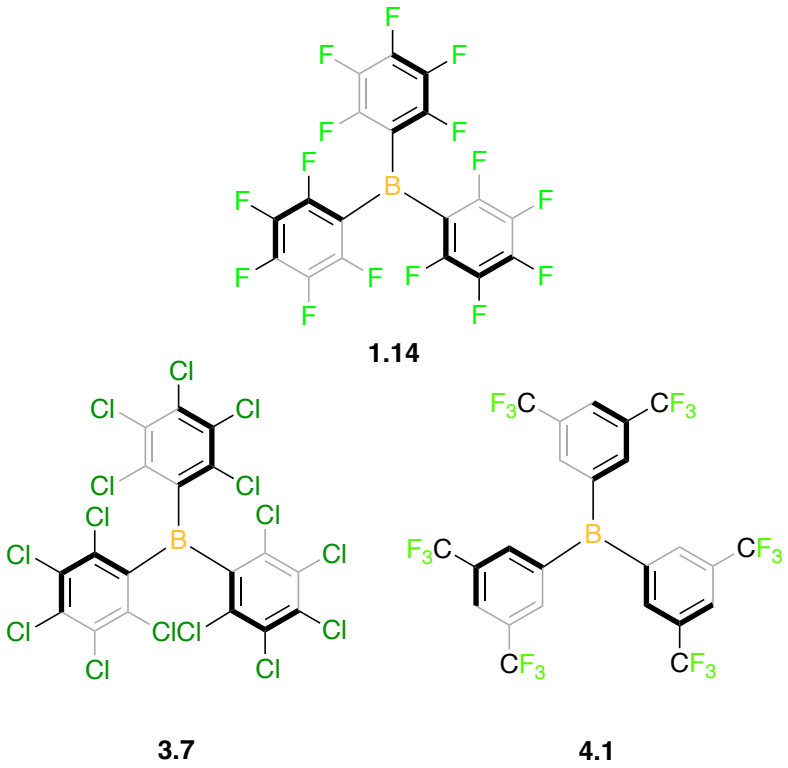

Figure 4.1 – Trispentafluorophenylborane $B(C_6F_5)_3$, trispentachlorophenylborane $B(C_6Cl_5)_3$ and tris{3,5-bis(trifluoromethyl)phenyl}borane $BAr^F{}_{18}$.

4.1.1 Measuring Acidity

The ability to predict acidity is a valuable tool and multiple methods exist for quantification. Spectroscopically, the Gutmann Beckett method employs triethyl phosphine oxide (Et_3PO) as a probe molecule. Co-ordination to an acid *via* the oxygen atom perturbs the ^{31}P chemical shift, and the extent thereof can be measured and compared to other species. The reported shift difference ($\Delta\delta$/ppm) for $BAr^F{}_{18}$ is 28.2, while for $B(C_6F_5)_3$ it is 26.6, suggesting greater Lewis acid strength for the former. However, under comparable conditions $BAr^F{}_{18}$ binds water and diethyl ether more reversibly than $B(C_6F_5)_3$ – implying lower Lewis acid strength.[5] This ordering of acidity is further reinforced by the hydrogen activation ability of xanthene-based pairs **1.54** (Mo *et al.*) and **4.2** (unpublished results, Aldridge group). Irreversible cleavage of

the H—H bond is mediated by the former species at 1 atm. pressure, whilst the latter requires 4 atm. of hydrogen for comparable bond activation (**Scheme 4.1**).

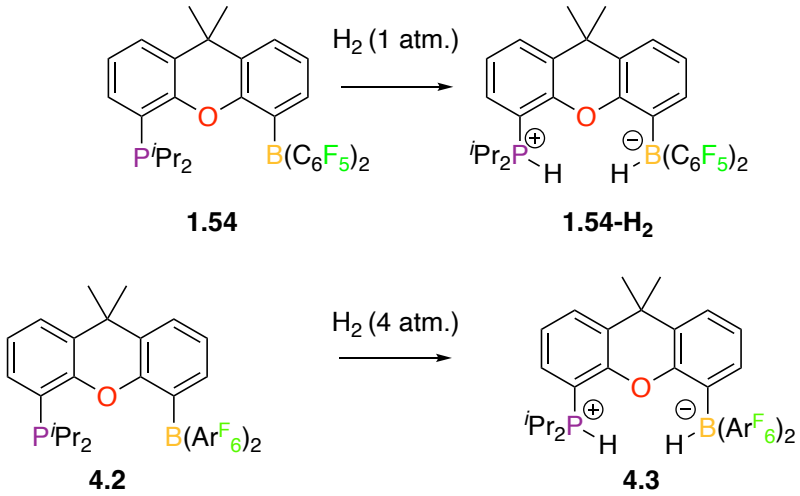

Scheme 4.1 – Impact of modulated acidity on the facility for hydrogen activation.

The predictive utility of the Gutmann Beckett method can also be limited by congestion about the borane, which can render the acidic centre inaccessible. This was informatively demonstrated by Ashley and co-workers in the case of $B(C_6Cl_5)_3$, for which a $Et_3PO \rightarrow LA$ complex cannot be formed (see **Section 3.1.1**).[6] When electronics alone are considered, perchlorinated boranes would be expected to act as stronger acids than their fluorinated congeners ($o_pCl = 0.23$ *versus* $o_pF = 0.06$). This is due to the more efficient orbital overlap, and thus donation of electron density, from the lone pairs of fluorine into the aromatic π system. Electrochemical measurements reinforce this hypothesis, indicating a more electron deficient boron centre when C_6F_5 rings are formally replaced by C_6Cl_5 groups in *tris*pentahaloboranes. The converse is suggested by spectroscopic measurements, which indicate diminishing Lewis acidity with the introduction of more C_6Cl_5 groups (less significant chemical shift perturbation). Conflicting conclusions from different experiments suggest that the subtle interplay of sterics and electronics is decisive in determining experimental properties.

Additionally, the result is influenced by the nature of the probe molecule is considered – measuring acidity *via* the Childs method does not necessarily give the same outcome as the Gutmann Beckett. Therefore, an alternative benchmarking (such as dihydrogen activation ability) within otherwise identical FLPs might provide a more accurate quantitative description of usable acidity.

4.2 Aims

In pursuit of FLPs which are electronically tuneable at the acidic component, a series of bulky Lewis acids was studied as a means of developing a systematic understanding of substituent effects. This analysis was also extended to potential surface supported FLPs. The synthesis of the target FLPs will be discussed herein, followed by a separate analysis of hydrogen activation.

4.3 Results and Discussion

4.3.1 Synthesis of *bis*(pentachlorophenyl)borane containing FLPs

While many FLPs adorned with fluorinated Lewis acids are reported in the literature, perchlorinated species are comparatively unexplored. The haloborane $ClB(C_6Cl_5)_2$ **3.5** has been previously reported, and its synthesis is facile. It was therefore used as the acidic precursor in the first instance. The 5-lithio xanthene phosphine precursors used in the synthesis of these FLPs were prepared as shown in **Scheme 4.2**. They were chosen because they are isolable at scale (ca. 10 g) and reliably give spectroscopic data in agreement with previous reports.[7]

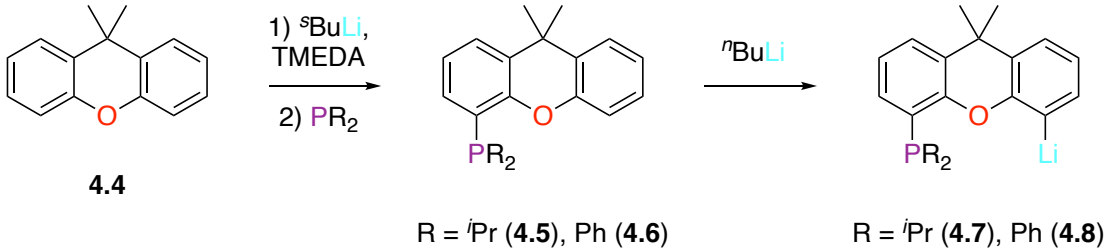

*Scheme 4.2 – Synthesis of xanthene phosphine lithiates **4.7** and **4.8**.*

As such, $ClB(C_6Cl_5)_2$ was synthesised according to the literature procedure and used in the synthesis of FLPs **4.i** and **4.ii** (**Scheme 4.3**).[6]

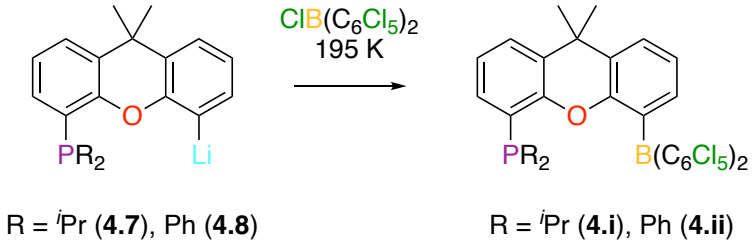

*Scheme 4.3 – Synthesis of perchlorinated FLPs **4.i** and **4.ii**.*

The ^{31}P NMR spectra of the products **4.i** and **4.ii** are particularly diagnostic and correspond well to those measured for the analogous perfluorinated FLPs; a single signal at -15.0 ppm is seen for **4.i** and one at -17.6 ppm is observed for **4.ii**. Bright yellow single crystals suitable for X-ray crystallography were attained for both **4.i** and **4.ii** by cooling saturated solutions in toluene to -30 °C (**Figure 4.2** and **Figure 4.3**).

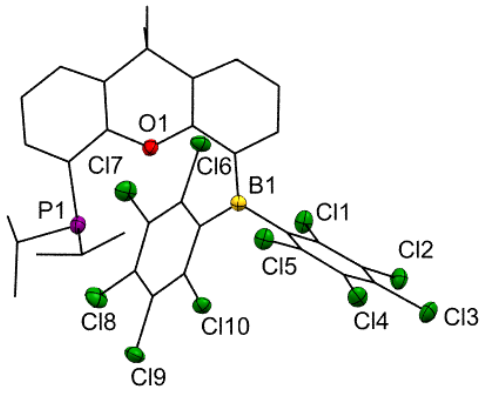

*Figure 4.2 – Molecular structure of **4.i** as determined by X-ray crystallography. Ellipsoids are shown at 50% probability, carbon atoms are shown in wireframe format and hydrogen atoms are omitted for clarity. The P···B distance is 4.532(1) Å. The coplanar angle between the two xanthene aryl rings is 153.6°.*

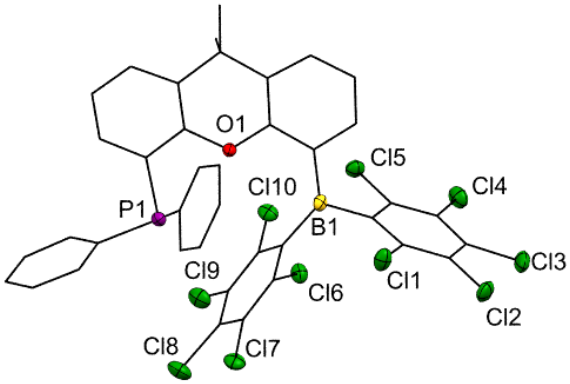

*Figure 4.3 – Molecular structure of **4.ii** as determined by X-ray crystallography. Ellipsoids are shown at 50% probability, carbon atoms are shown in wireframe format and hydrogen atoms are omitted for clarity. The P···B distance is 4.553(2) Å. The coplanar angle between the two xanthene aryl rings in 176.5°.*

4.3.2 Structural Analyses of 4.i and 4.ii

4.i and **4.ii** are variants of literature compounds and comparison of key structural parameters of these systems with the corresponding fluoroaryl FLPs is presented in **Table 4.1**.

	Distance / Å		Angle / °	
FLP	P···B	P···Aryl	C_{phenyl}—B—$C_{phenyl'}$	Coplanar ϕ
1.54	4.487(3)	3.604	120.0(4)	151.2
1.57	4.070(2)	-	120.0(4)	138.9
4.i	4.526(2)	3.507	119.9(6)	161.5
4.ii	4.552(1)	3.343	119.1(4)	176.5

*Table 4.1 – Summary of relevant structural parameters for **1.54**, **1.59**, **4.i** and **4.ii**. Coplanar angle defined in **Section 1.4.3**.*

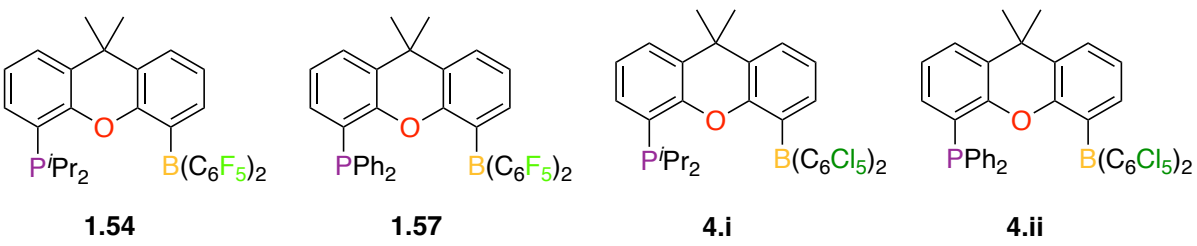

1.54 **1.57** **4.i** **4.ii**

*Figure 4.4 – Perfluorinated FLPs **1.54** and **1.57**, and their novel perchlorinated analogues **4.i** and **4.ii**.*

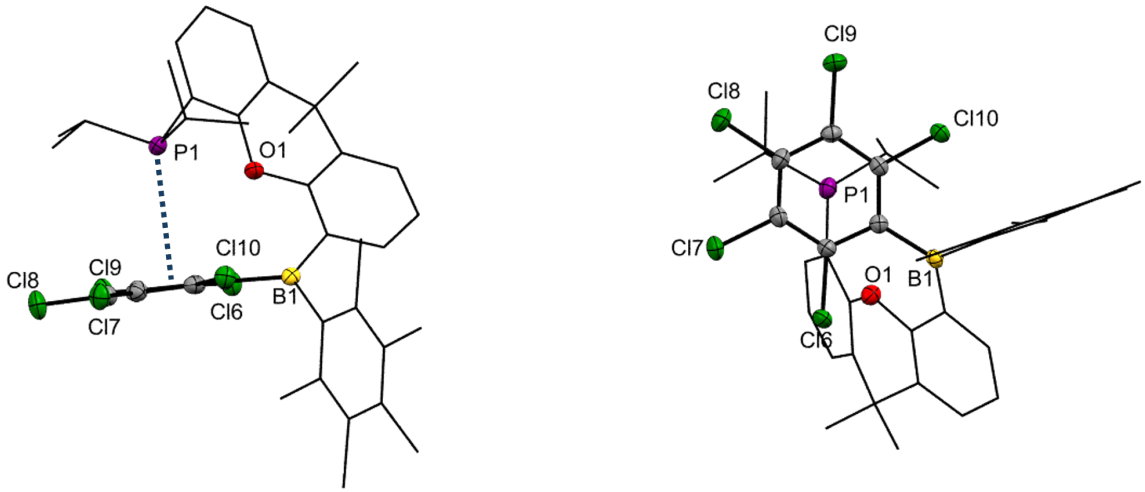

*Figure 4.5 – Illustration of the on phosphorus lone pair pointing towards electron deficient aryl ring bonded to boron on exemplar X-ray structure of **4.i**. Ellipsoids are shown at 50% probability, most carbon atoms are shown in wireframe format and hydrogen atoms are omitted for clarity.*

The P···B separation in **1.57** is significantly shorter than that determined for each of **1.54**, **4.i** and **4.ii**, likely because the backbone is very puckered. The coplanar angle between aryl rings, ϕ, is 138.9 °. In contrast, the perchlorinated analogue **4.ii** possesses the greatest P···B separation of the four compounds and a relatively flat backbone scaffold (ϕ = 176.5°). The *iso*propyl systems both have similarly puckered backbones (ϕ =151.2°, 153.6° for **1.54** and **4.i**, respectively) and in all cases the angles about the boron centre are almost equal to eachother, and 120°. Looking at the solid-state structures, the lone pair on phosphorus points towards the centre of one of the borane aryl substituents in all cases except **1.57**, giving rise to the possibility of an intramolecular interaction between the phosphorus lone pair and the electron deficient aryl substituent on boron. Comparing the phosphine to aryl distances with anion-π interactions with fluoroarenes, they are slightly longer than most reported.[8] For example, anion-hexafluorobenzene interactions have been computed in a range of 2.57 – 3.20 Å, and within sandwich complexes of fluoroaryl rings, aryl to anion distances up to 3.446 Å have been calculated. This could be source of **1.57**'s puckered backbone. If, in all cases except **1.57**, there is a non-covalent interaction between the lone pair of the phosphorus centre and the electron deficient aryl ring of the borane, this could be enforcing a more planar xanthene scaffold. The relevance of non-covalent interactions in the context of dihydrogen activation will be explored later in this chapter.

4.3.3 Synthesis of FLPs featuring unsymmetrical Lewis Acids

Given that the synthetic routes to the brominated precursors for heteroleptic triaryl boranes have been established in **Section 3.3.3**, these seemed to be viable reagents for the formation of a series of FLPs featuring unsymmetrical borane functions (**Figure 4.6**). The envisaged synthetic route towards such FLPs is shown in **Scheme 4.4.**

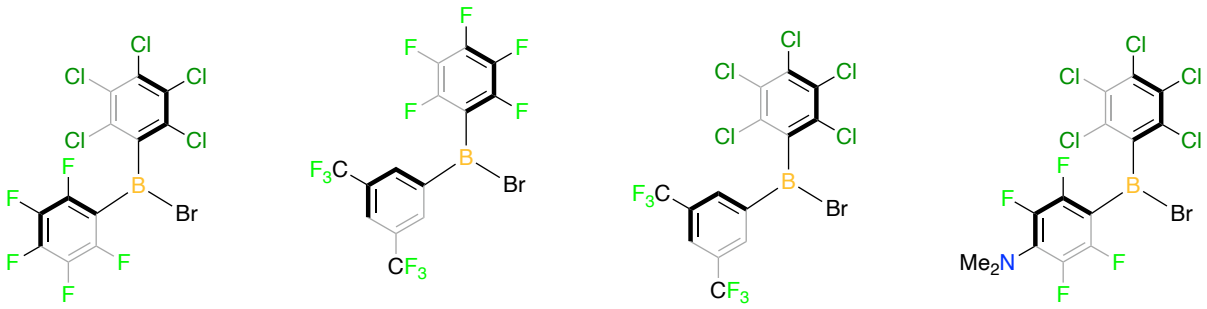

Figure 4.6 – Bromoboranes used in this work.

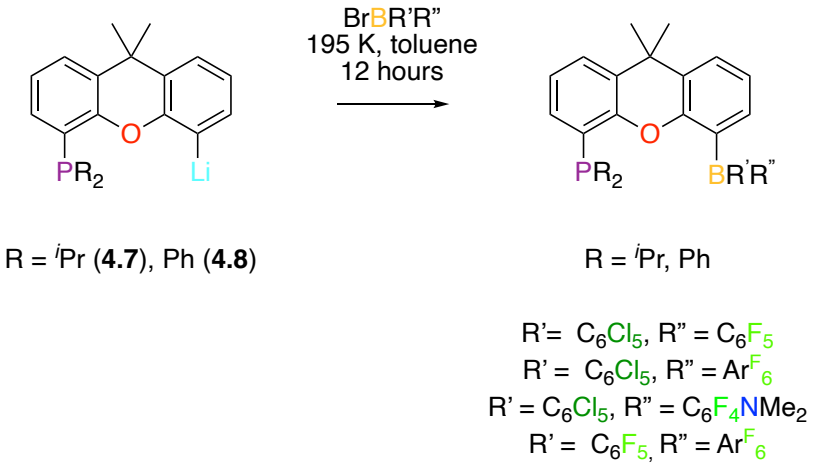

Scheme 4.4 – Envisaged synthetic route for these FLPs.

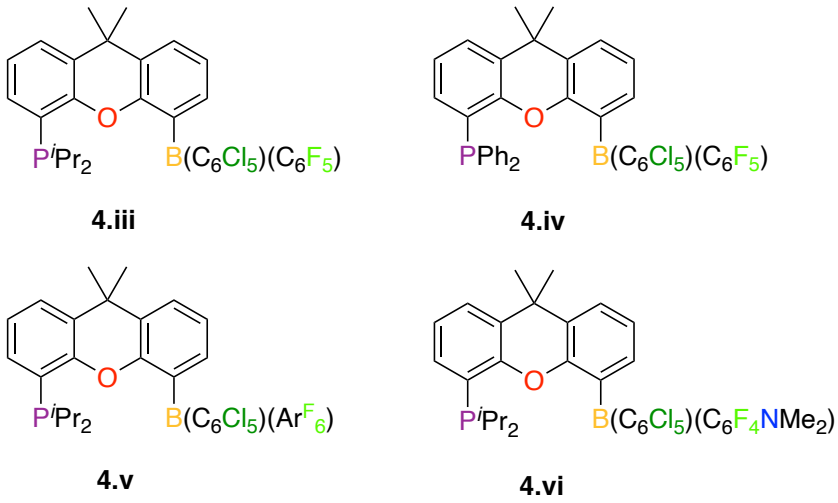

*Figure 4.7 – FLPs **4.iii** – **4.vi** synthesised via Scheme 4.4.*

This method, using lithiated xanthene phosphine **4.7** and bromoborane **3.vi** was successfully applied for the synthesis of the mixed C_6Cl_5/C_6F_5 system **4.iii**. The ^{31}P NMR spectrum of the

product contains a singlet at -11.0 ppm and the ^{19}F NMR spectrum features three multiplets at -129.1, - 148.8 and -163.3 ppm. A signal corresponding to the product cannot be seen in the ^{11}B NMR spectrum presumably because it is too broad. Single crystals of **4.iii** were obtained from a toluene solution cooled to -30 °C (**Figure 4.8**).

Similarly, the reaction of **4.8** with bromoborane **3.vi** yields the related diphenylphosphine substituted FLP **4.iv**. The product is characterised by three multiplets at -127.9, -146.6, -162.6 ppm in the ^{19}F NMR spectrum and a singlet at -16.9 ppm in the ^{31}P NMR spectrum. Once again, no signal that can be assigned to the product could be observed in the ^{11}B NMR spectrum. However, X-ray quality crystals of **4.iv** could be obtained from a saturated solution in hexane at room temperature (**Figure 4.9**).

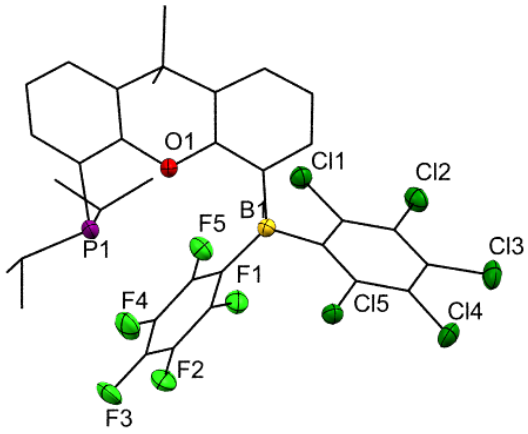

*Figure 4.8 – Molecular structure of **4.iii** as determined by X-ray crystallography. Ellipsoids are shown at 50% probability, carbon atoms are shown in wireframe format and hydrogen atoms are omitted for clarity. The P···B distance is 4.526(2) Å. The coplanar angle between the two xanthene aryl rings is 161.5°.*

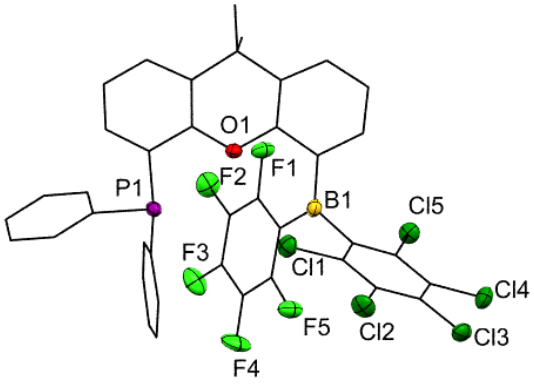

*Figure 4.9 – Molecular structure of **4.iv** as determined by X-ray crystallography. Ellipsoids are shown at 50% probability, carbon atoms have been shown in wireframe format and hydrogen atoms are omitted for clarity. The P···B distance is 4.470(10) Å and the coplanar angle between the two xanthene aryl rings is 175.1°.*

In a similar fashion, the mixed $C_6Cl_5/Ar^F{}_6$ system **4.v** was synthesised from **4.7** and **3.8**, following the route shown in **Scheme 4.4**. The ^{31}P and ^{19}F NMR spectra of the product both show the expected singlet resonances (at -12.8 ppm and -62.4 ppm respectively). No signal that can be attributed to the product was observed in the ^{11}B NMR spectrum. Crystals of **4.v** suitable for X-ray crystallography were obtained from a toluene solution cooled to -30 °C (**Figure 4.10**).

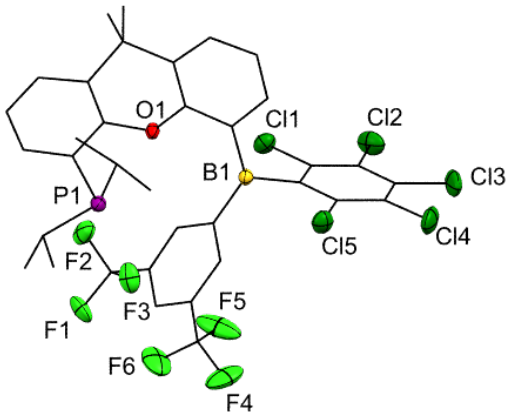

*Figure 4.10 – Molecular structure of **4.v** as determined by X-ray crystallography. Ellipsoids are shown at 50% probability, carbon atoms are shown in wireframe format and hydrogen atoms are omitted for clarity. The P···B distance is 4.520(2) and the coplanar angle between the two xanthene aryl rings is 162.5°.*

To target the synthesis of FLPs tethered to a surface through the Lewis acidic moiety, it was proposed that a functionality amenable to modification to facilitate surface attachment might be introduced at a remote position to the boron atom. Separating the tether away from a borane moiety is also preferable to making a direct boron to surface bond, as the potency of the acidic site is easily dampened by co-ordination to an electronegative attachment site such as nitrogen or oxygen.[9] Within this rationale, **4.7** and **3.ix** were combined in an attempt to form FLP **4.vi** which features a *para*-NMe_2 function appended to one of the B-bound aryl groups. Although not crystallographically characterised, the successful synthesis of **4.vi** can be inferred from multinuclear NMR spectroscopy. However, an impurity which proved impossible to separate is present in approximately 30 % quantity (on the basis of ^{1}H NMR spectroscopy). Within the ^{1}H NMR spectrum, a distinct resonance corresponding to the impurity is a triplet (J = 3.1 Hz) at 2.34 ppm. For comparison, there is a triplet signal at 2.64 ppm (J = 2.6 Hz) corresponding to the methyl protons of the $C_6F_4NMe_2$ substituent in **4.vi** – suggesting the protons resonating at 2.34 ppm are also from a dimethylaniline group. The splitting pattern is also seen in the

precursor **3.ix**. A doublet (J = 143 Hz) at -14.9 is observed in both the proton coupled and decoupled ^{11}B NMR spectrum, which could indicate the boron atom is unexpectedly coupling to an aryl fluorine. There are two additional multiplets in the ^{19}F NMR spectrum at similar chemical shifts to those for **4.vi**, at -126.9 and -154.1. This unknown impurity is pervasive, despite efforts to remove it through washing, sublimation and fractional crystallisation and could explain the lack of success in obtaining crystals suitable for X-ray diffraction. The synthesis of **4.vi** is also unreliable, with apparently identical reaction conditions failing to yield identical results. This is disappointing given the incorporation of the dimethylaniline functionality, which was envisaged in the context of a group for surface attachment.

The presence of the desired product is suggested by the single resonance in the ^{31}P NMR spectrum at -10.3 ppm. In the ^{11}B NMR spectrum, a broad singlet corresponding to compound **4.vi** is seen at 53.7 ppm and in the ^{19}F NMR spectrum there are multiplets at -129.4 and -154.7 ppm.

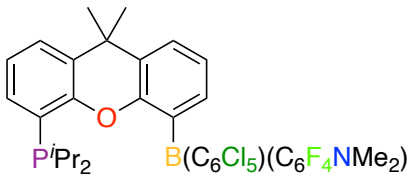

4.vi

*Figure 4.11 – Proposed structure of FLP **4.vi**.*

4.3.4 Structural Analysis of 4.iii, 4.iv and 4.v

The solid-state structures of these FLPs featuring a *tris* heteroleptic Lewis acid were compared (**Table 4.2**).

	Distance / Å		Angle / °	
FLP	P···B	P···Aryl	C_{phenyl}—B—$C_{phenyl'}$	Coplanar ϕ
4.iii	4.526(4)	3.372	119.6(4)	161.5
4.iv	4.470(10)	3.471	120.0(7)	175.1
4.v	4.520(2)	3.671*	119.9(5)	162.5

*Table 4.2 – Summary of relevant structural parameters for FLPs **4.iii - 4.v**.*Average taken of two distances due to two molecules in the asymmetric unit.*

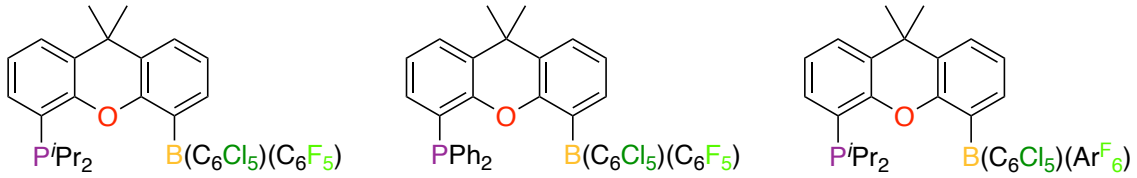

4.iii **4.iv** **4.v**

*Figure 4.12 – FLPs **4.iii - 4.v**.*

In all cases, the lone pair on the phosphine points toward the perfluorinated aryl ring, potentially based on a steric preference of the larger perchlorinated substituent. The P···Aryl distances of FLPs **4.iii** – **4.v** are in the same region as those in **4.i** and **4.ii** (**Table 4.1**) and the phosphine to borane distances of all five FLPs are within 0.082 Å of each other. Compounds **4.iii** and **4.v** are almost identical by the metrics other than the phosphine to aryl distance, with slightly bowed backbones compared to the flatter scaffold seen in **4.iv**.

4.3.5 Syntheses of *Tetra*-substituted Borates

The synthetic route outlined in **Scheme 4.4** was also applied in attempts to make an FLP featuring boron bound C_6F_5 and Ar^F_6 groups, using precursors **4.7** and **3.vii**. In this case the bromoborane precursor (**3.vii**) was generated *in situ* from **3.ii** and used assuming quantitative conversion (by ^{1}H NMR spectroscopy). Notably, generation of the bromoborane precursor **3.vii** in the first place is less facile than other heteroleptic diaryl bromoboranes **3.vi**, **3.viii** and **3.ix**. Stirring over copper powder is required to yield **3.vii** from **3.ii** without undesirable side reactions arising due to the formation of HBr, such as the formation of a tetra co-ordinate bromoborane.

Rather than yielding the expected FLP however, the product obtained from **4.7** and **3.vii** is instead a four co-ordinate *bis*xanthene borane **4.vii** Li[$(C_6F_5)(Ar^F_6)$B(4-xanth-P^{i}Pr)$_2$] (**Figure 4.13**). Compound **4.vii** was characterised by ^{11}B NMR spectroscopy, which features a singlet resonance at -8.2 ppm. In the ^{19}F NMR spectrum, resonances are observed at -62.5 corresponding to the six fluorine atoms in the Ar^F_6 substituent, and at -126.3, -148.0 and -161.9 ppm due to the C_6F_5 ring. The structure of **4.vii** was confirmed by X-ray crystallography, with crystals obtained from a hexane solution cooled to 4 °C.

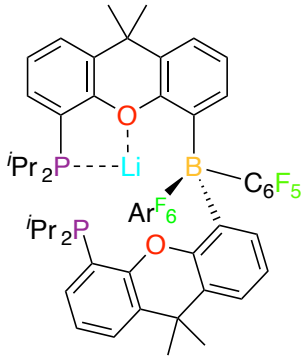

4.vii

*Figure 4.13 – Bisxanthene borate **4.vii**.*

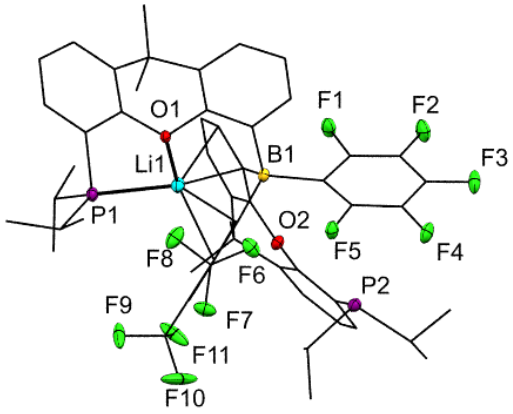

*Figure 4.14 – Molecular structure of **4.vii** as determined by X-ray crystallography. Ellipsoids are shown at 50% probability, carbon atoms are shown in wireframe format and hydrogen atoms are omitted for clarity.*

Potentially, this compound arises as the formation of **3.vii** is not quantitative from its methoxyborane precursor, and the lithiated xanthene phosphine **4.7** is therefore present in excess, allowing for the formation of a *bis*xanthene borate. The target FLP is also the least sterically congested system examined, due to the lack of halogens at the *ortho* positions of the Ar^F_6 ring, and the relatively small fluorine atoms on the pentafluoro ring (compared to the pentachlorinated analogue). To avoid this undesirable reaction, inverse addition of half an equivalent of lithiated xanthene phosphine **4.7** to **3.vii** was attempted (**Scheme 4.5**). However, rather than the desired product, the formation of $^{i}Pr_2PH$-(xanth)-$BBr(C_6F_5)(Ar^F_6)$, **4.viii** was observed. The ^{11}B NMR spectrum is, surprisingly, too broad for interpretation. Signals in the ^{19}F NMR spectrum of the product are found at -61.9 (Ar^F_6), -159.2 and -164.7 ppm in a 4:1:2 ratio by integration. The latter two resonances were perplexing as three resonances in similar positions to those in **4.vii** were expected. It is unlikely there are overlapping peaks in the spectrum, as it is well resolved with a flat baseline. The structure of this species was determined by X-ray crystallography (**Figure 4.15**), with crystals of **4.viii** obtained from a hexane solution at 4 °C. The HBr potentially arises during the formation of the precursor **3.vii** and is not fully

removed by the copper powder added to the reaction vessel. These *tetra*-substituted products **4.vii** and **4.viii**, demonstrate the requirement for steric protection both adjacent to, and remote from, the boron centre to prevent the uptake of four substituents. This reaction was probed no further.

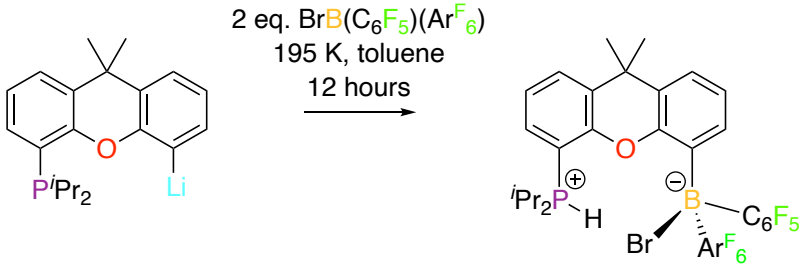

4.7 **4.viii**

*Scheme 4.5 – Attempted synthesis of $^{i}Pr_2$(xanth)B(C_6F_5)(Ar^F_6) from **4.7** and **3.vii**.*

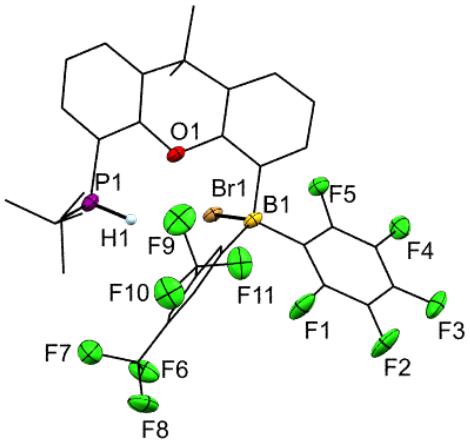

*Figure 4.15 – Molecular structure of **4.viii** as determined by X-ray crystallography. Ellipsoids are shown at 50% probability, carbon atoms are shown in wireframe format and most hydrogen atoms have been omitted for clarity. The P···B distance is 4.562(5) Å.*

4.3.6 Spectroscopic Measurement of the Lewis Acidity

The acidity of FLPs **4.i** – **4.iv** was probed by monitoring co-ordination of triethyl phosphine oxide. Unfortunately, this approach met with limited success, as in all but one case (**4.v**) an adduct does not form, presumably on the basis of the prohibitive steric bulk about the borane.

This echoes the limitations of the Gutmann Beckett method observed by Ashley *et al.* (**Section 4.1.1**).[6] The ^{31}P spectral data is summarised in **Table 4.3** and compared to the perfluorinated equivalent reported by Mo *et al.* in 2015.

FLP	^{31}P NMR shift of Et_3PO / ppm	Δδ / ppm	Acceptor Number
1.54	73.7	27.2	72.5
4.v	61.9	15.4	46.3

Table 4.3 – Summary of successful spectroscopic acidity measurements. Acceptor number = (δ (sample)- 41.0) × {100/(86.14 - 41.0)}[10]

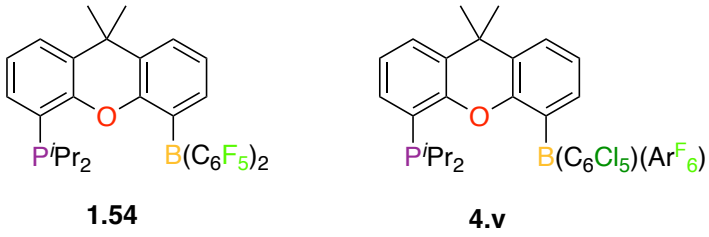

1.54 **4.v**

*Figure 4.16 – Diisopropylphosphine FLPs **1.45** and **4.v** which form a complex with triethyl phosphine oxide.*

From this data, the borane moiety in FLP **4.v** appears to be less acidic than that in **1.54**.[11] In the context of the pentachlorophenyl group being a documented hindrance to Et_3PO complexation, it is difficult to say how much this depression in acidity of **4.v** compared to **1.54** is down to the inferior electron withdrawing properties of the Ar^F_6 group and how much is down to the steric shrouding effect of the C_6Cl_5 substituent.

4.3.7 Substitution of the Lewis Acid Substituent

While FLP anchoring through a *para* functionalised arene was not attained here, a serendipitous result suggested a potential new direction for the pursuit of surface supported FLPs based on the xanthene molecular architecture. Excess methanol or water reacts with both

4.i and **4.iii** to form the same product **4.ix** (**Scheme 4.6**) the identity of which was determined in both cases by X-ray crystallography as $^{i}Pr_2P(xanth)B(C_6Cl_5)(OH)$ (**Figure 4.17**)

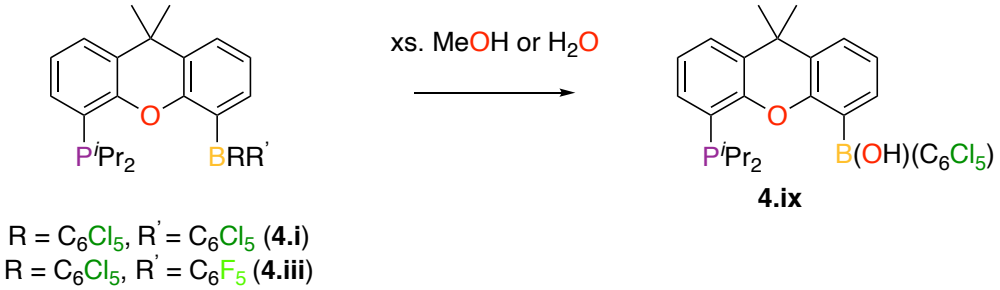

R = C_6Cl_5, R' = C_6Cl_5 (**4.i**)
R = C_6Cl_5, R' = C_6F_5 (**4.iii**)

*Scheme 4.6 – Formation of **4.ix** from **4.i** or **4.ii** in the presence of methanol or water.*

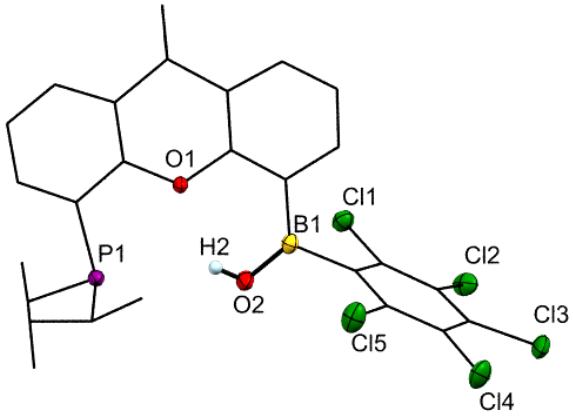

*Figure 4.17 – Molecular structure of **4.ix** as determined by X-ray crystallography. Ellipsoids are shown at 50% probability, carbon atoms are shown in wireframe format and most hydrogen atoms are omitted for clarity. The P···B distance is 4.363(2) Å.*

The reaction in the case of the mixed C_6Cl_5/C_6F_5 system **4.iii** suggests that C_6F_5 is a superior leaving group to C_6Cl_5. This approach might therefore be leveraged in the synthesis of surface supported FLPs reminiscent of the reports by O'Hare and co-workers discussed in **Section 1.5**, in which a C_6F_5 ring on trispentafluorophenyl borane is displaced by a silica source. Unfortunately, the yield of this reaction is very low – only producing trace amounts of product from a 200 mg scale reaction. Using silica as an alternate source of the hydroxyl group, to

synthesise a surface supported FLP was unsuccessful, as suggested by the lack of change in the solid-state ^{31}P NMR spectra between **4.ix** and the product of the reaction with silica.

4.3.8 Reactivity of FLPs with Hydrogen

Given the established reactivity of similar perfluoroaryl species with dihydrogen, we sought to investigate whether heterolytic hydrogen splitting would be observed with the FLPs reported above. Compound **4.i** demonstrates reversible dihydrogen activation at room temperature under 1 atm. of H_2 at room temperature (**Scheme 4.7**). The product, **4i-H$_2$**, is characterised by a signal in the ^{31}P NMR spectrum at 14.6 ppm ($^1J_{PH}$ = 518 Hz) and a resonance in the ^{11}B NMR spectrum at -9.9 ppm, with $^1J_{BH}$ = 65 Hz. Colourless single crystals of the zwitterionic species **4.i-H$_2$** were obtained from a toluene solution on standing for 30 d at room temperature (**Figure 4.18**).

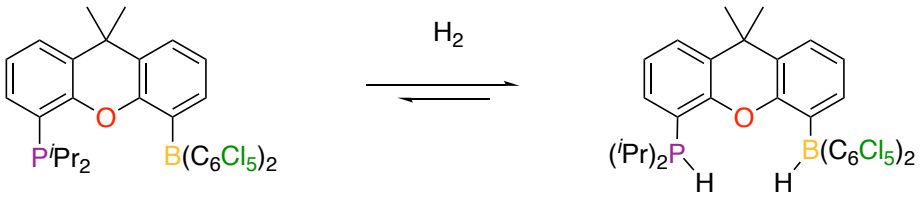

4.i **4.i-H$_2$**

*Scheme 4.7 – Reversible room temperature dihydrogen splitting by FLP **4.i**.*

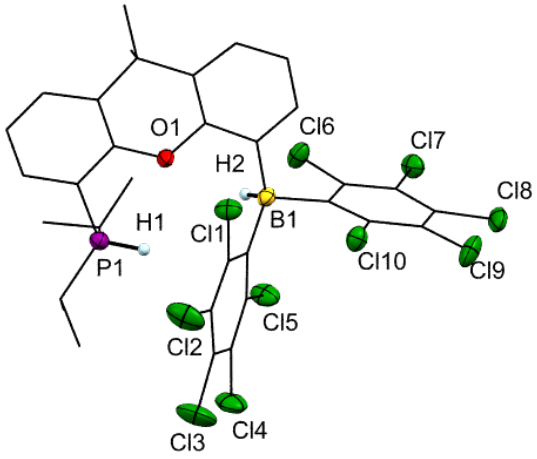

*Figure 4.18 – Molecular structure of **4.i-H$_2$** as determined by X-ray crystallography. Ellipsoids are shown at 50% probability, carbon atoms are shown in wireframe format, toluene solvent molecule, and most hydrogen atoms are omitted for clarity. The P···B distance is 4.394(2) Å.*

Notwithstanding the difficulties in locating hydrogen atoms by X-ray crystallography, the structure of **4.i-H$_2$** is suggested by the significant change in geometry around the borane fragmoent. The average C_{phenyl}—B—C_{phenyl}, bond angle in **4.i** is 119.1(1)° whereas it narrows to 113.1(1)° in **4.i-H$_2$**, due to quaternisation at B(1). Hydrogen atoms bound to phosphorus and boron could also be located in the Fourier difference map. The reversibility in dihydrogen activation by **4.i**, is inferred from monitoring from this equilibrium by variable temperature NMR studies. This implies lower cumulative acid/base strength than the corresponding fluorinated pair **1.54**, which irreversibly forms the hydrogenated product **1.54-H$_2$** when exposed to hydrogen under similar conditions.

By contrast, reactivity with dihydrogen was not observed for the diphenylphosphine system **4.ii** at pressures up to 4 atm. at room temperature. Using the spectroscopic techniques employed in this work, no evidence for the corresponding reaction between FLP **4.iv**, which also features a -PPh_2 unit, and H_2 was found.

Under 1 atm. of hydrogen pressure, **4.iii** reversibly activates dihydrogen at room temperature to give **4.iii-H$_2$**. (**Scheme 4.8**) As in the case of **4i-H$_2$**, the product could be spectroscopically characterised. A second singlet is seen in the $^{31}P\{^{1}H\}$ NMR spectrum at 14.1 ppm. In the ^{31}P spectrum a doublet is observed ($^{1}J_{PH}$ = 188 Hz) and a peak at -9.7 in the ^{11}B NMR spectrum. The latter decoupled spectrum is too broad for the expected doublet to be deconvoluted. Single crystals of **4.iii-H$_2$** suitable for confirmation of connectivity by X-ray crystallography were obtained from a toluene solution at room temperature on standing for 7 days (**Figure 4.19**).

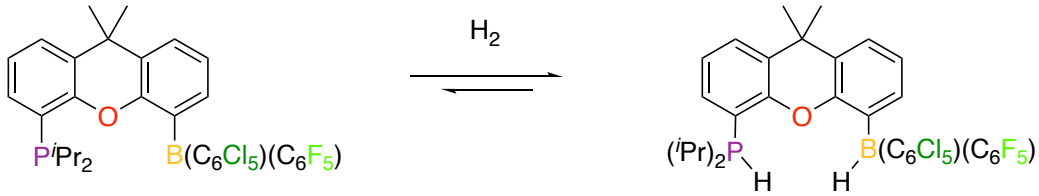

4.iii **4.iii-H$_2$**

*Scheme 4.8 – Reversible room temperature dihydrogen splitting by FLP **4.iii**.*

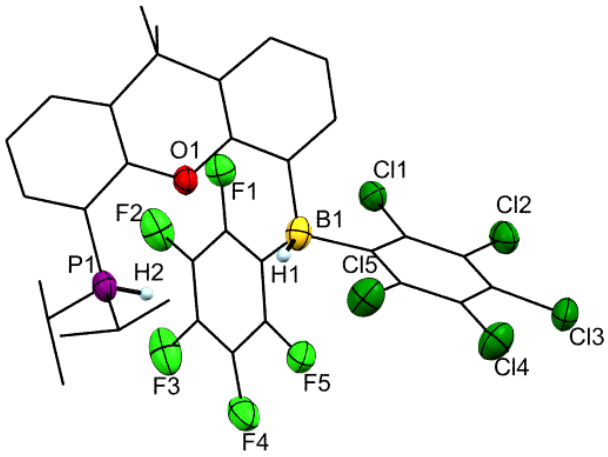

*Figure 4.19 – Molecular structure of **4.iii-H$_2$** as determined by X-ray crystallography. Ellipsoids are shown at 30% probability, carbon atoms are shown in wireframe format, toluene solvent molecule and most hydrogen atoms are omitted for clarity.*

While the mixed system $C_6Cl_5/Ar^F{}_6$ **4.v** is unreactive to 1 atm. of dihydrogen at room temperature, cooling of a sample in deuterated toluene revealed additional resonances in the

^{31}P and ^{11}B NMR spectra attributed to the hydrogenated species **4.v-H$_2$** (**Scheme 4.9**). The signal in the ^{31}P NMR spectrum resonates at 16.2 ppm and the new signal in the ^{11}B NMR spectrum is at -11.4 ppm.

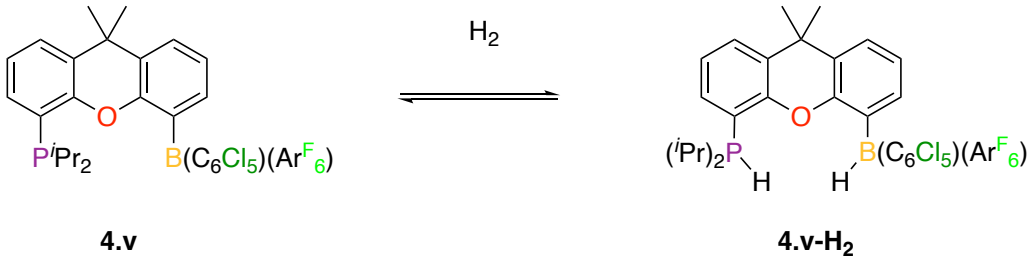

4.v **4.v-H$_2$**

*Scheme 4.9 – Reversible dihydrogen splitting by FLP **4.v**.*

4.3.9 Variable Temperature NMR Spectroscopy

The three -P^{i}Pr$_2$ FLPs amenable to dihydrogen activation (**4.i**, **4.iii** and **4.v**) were probed by variable temperature NMR spectroscopy in an attempt to obtain the thermodynamic parameters for these reactions. The relative integrals of the signals in the ^{31}P NMR spectra corresponding to the parent FLP and the corresponding hydrogen activation product were compared. An inverse-gated pulse sequence was used, as is standard in quantitative NMR spectroscopy experiments since it minimises the influence of the Nuclear Overhauser effect (NOE). The NOE changes the relative intensity of a signal *via* the transfer of nuclear spin polarization between spin-active nuclei.

By means of reference, the previously reported xanthene-based FLP **1.55** (which also demonstrates reversible hydrogen splitting – **Scheme 4.10**) has been investigated in the range 363 to 298 K. As expected for an entropically unfavourable reaction, the proportion of **1.55-H$_2$** increases relative to "free" **1.55** at lower temperatures.

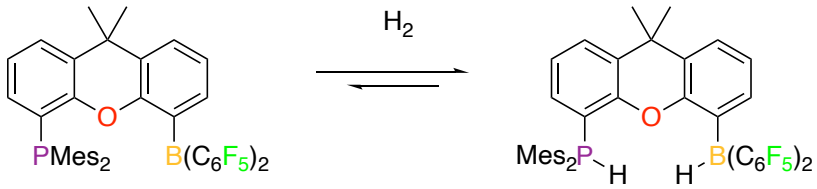

1.55 **1.55-H_2**

*Scheme 4.10 – Reversible dihydrogen splitting by FLP **1.55**.*

This can be represented by a van't Hoff plot (LnK vs 1/T) corresponding to the loss of hydrogen from **1.55-H_2** *i.e.* for the reaction $[1.55 - H_2] \rightleftharpoons 1.55 + H_2$. The plot has a negative slope of -ΔH°/R, and an intercept ΔS°/R from which values for ΔH° and ΔS° of 38 kJ mol^{-1} and 102 J mol^{-1} K^{-1} can be determined. Loss of H_2 is an endothermic reaction and the entropy change is positive, consistent with other reports of (reversible) dihydrogen activation by intramolecular FLPs. We therefore expected to observe a similar trend and derive entropic and enthalpic terms for **4.i**, **4.ii** and **4.v** in a similar manner.

Considering first the *bis*(perchlorophenyl) system **4.i**, as the temperature was lowered from 293 to 263 K in five degree increments, the expected behaviour (based on **1.55**) held true. A ΔH° value of 29 kJ mol^{-1} and ΔS° of 106 J mol^{-1} K^{-1} could be extracted from the van't Hoff plot (R^2 = 0.945). Below 263 K, and down to 223 K however the regime changes. A second, inverted, linear regime is observed from which values of ΔH° = -26 kJ mol^{-1} and ΔS° = -106 J mol^{-1} K^{-1} (R^2 = 0.949) could be derived (**Graph 4.1**).

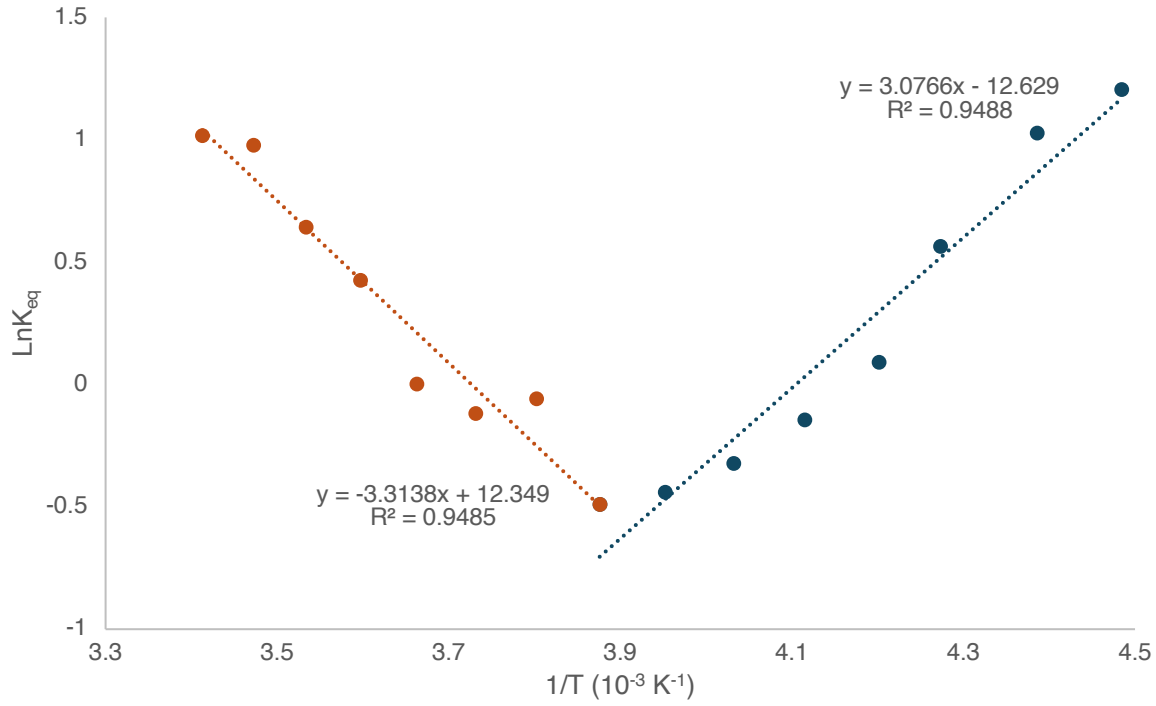

*Graph 4.1 – Van't Hoff plot for dihydrogen activation by FLP **4.i** as probed by variable temperature ^{31}P NMR spectroscopy.*

These results imply that as the temperature of the sample is decreased, the reaction first moves in the direction of the hydrogenated product (as per conventional FLP behaviour) before moving in the opposite sense below a certain critical temperature – in this case around 258 K. This result held under all conditions trialled: extending the pulse delay to ensure complete relaxation, holding the samples at each temperature for 30 minutes to allow equilibration, centring the spectra midway between the two furthest points, integrating the ^{31}P NMR resonances relative to an internal standard of known concentration (Ph_3PO). The unusual results exemplified by **Graph 4.1** are reproducibly observed.

Turning to the compound **4.iii**, the analogous equilibrium was also probed by variable temperature ^{31}P NMR spectroscopy. From 298 down to 268 K the expected trend of growth in the proportion of the hydrogenated product **4.iii-H_2** also holds. From this region of **Graph 4.2**,

a ΔH° value of 19 kJ mol^{-1} and ΔS° of 72 J mol^{-1} K^{-1} could be obtained (R^2 = 0.965). These values, somewhat smaller than those for **4.i**, imply that the uptake of hydrogen is less favourable for **4.iii** and its release occurs with a smaller entropic gain. Enthalpy wise, presumably this relates to a lower cumulative Lewis acidity/basicity of the system, and entropically perhaps a more rigid parent FLP structure. Below 268 K, once more there appears to be a reversal in the equilibrium. The low temperature data from 268 down to 223 K give a linear plot of LnK_{eq} versus 1/T from which values of ΔH° = -8 kJ mol^{-1} and ΔS° = -28 J mol^{-1} K^{-1} (R^2 = 0.983) can be obtained. Notably, both the gradient and the y-intercept of this van't Hoff plot are halved as well as of opposite sign to the high temperature values, whereas for **4.i** they are exactly inverted about the minimum.

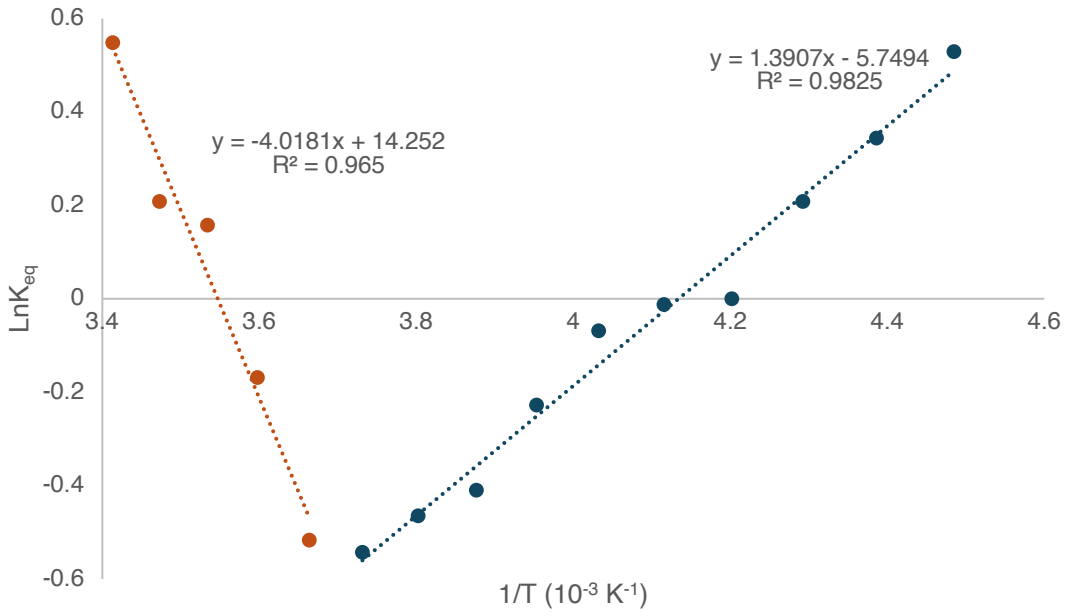

*Graph 4.2 – Van't Hoff plot for dihydrogen activation by FLP **4.iii** as probed by variable temperature ^{31}P NMR spectroscopy.*

The hydrogenation of **4.v**, the third -P^{i}Pr$_2$ containing FLP, was also probed. The dihydrogen activation complex **4.v-H$_2$** is observed both in small quantities at low temperatures (ca. 16 - 30 % compared to **4.v** by ^{31}P NMR integration) and does not yield reliable data for a linear van't

Hoff plot. As such, this does not allow for quantitative evaluation of any trend in analogous fashion to **4-i** and **4-iii**.

4.3.10 Quantum Chemical Calculations

Spectroscopic evidence appears to indicate that the equilibrium moves first toward, then away from the hydrogenated product. This might be due to another process which becomes competitive with hydrogenation at lower temperature, such as aggregation of the FLPs in solution, preventing reactivity. This process must be both entropically unfavourable (so that it becomes relevant at lower temperatures) and enthalpically favourable, with values of ΔS° and ΔH° which render it competitive with dihydrogen activation. The factors underpinning regime inversion have been probed by quantum chemical calculations carried out by Agamemnon Crumpton.

Head to tail dimerization due to the formation of intermolecular donor/acceptor interactions between the phosphine and borane on adjacent molecules (**Figure 4.20**) appears to be a feasible aggregation pattern and thus was investigated first.

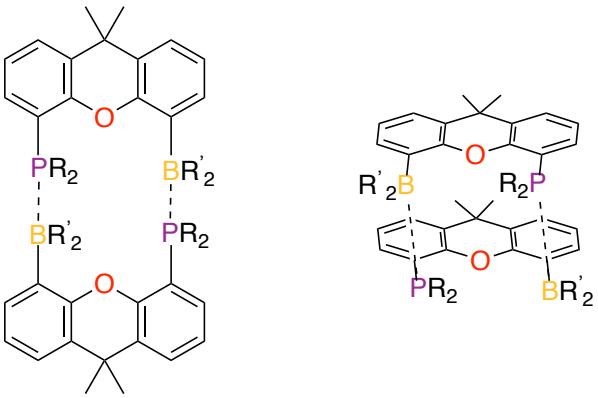

Figure 4.20 – End and side on aggregation of FLPs.

However, the FLPs are too congested for this type of aggregation and no local minima could be located computationally featuring a P→B interaction of this sort. In addition, no resonances corresponding to P→B interactions are seen in the spectroscopic data. Returning to the

evidence in hand *i.e.* NMR spectroscopy supported by X-ray crystal structures, we wondered whether the explanation might lie in the solid state structures. Observationally, a key similarity in these structures is the presence of an electron deficient aryl substituent on the borane. The lone pair on the phosphine (as shown earlier in **Figure 4.5**) is oriented towards the centroid of the electron deficient aryl ring. Conceivably, the strength of a lone pair/electron poor region interaction could become competitive with hydrogen activation at lower temperatures, in effect conformationally locking the FLP in an orientation where hydrogenation cannot occur due to intramolecular non-covalent interactions. However, both the relative weakness (enthalpically) and minor entropic effect of such an intramolecular interaction rule this out as a possible explanation for the low temperature behaviour of **4.i** and **4.iii** in the presence of H_2. However, these structural observations led us to consider alternative, non-covalent interactions as the basis for aggregation of these FLPs at low temperatures. For example, it might be informative that these unusual trends are seen in perchlorinated FLPs. These FLPs are very amenable to crystallisation, potentially due to facile π-stacking of the chloroaryl rings, so the competitive aggregation could instead be based on oligomerisation due to this.

Looking first at **4.i**, there are a plethora of possible orientations for two associated FLP molecules to exist in if they are held together by non-covalent interactions. Semi-empirical methods and molecular modelling were therefore used to rapidly evaluate potential oligomeric structures, and from this the lowest energy geometry was derived (**Figure 4.21**). The dimeric structure is held together by van der Waals interactions (ca. 30 kcal mol^{-1}) between the xanthene backbones and pentachlorophenyl rings on adjacent molecules.

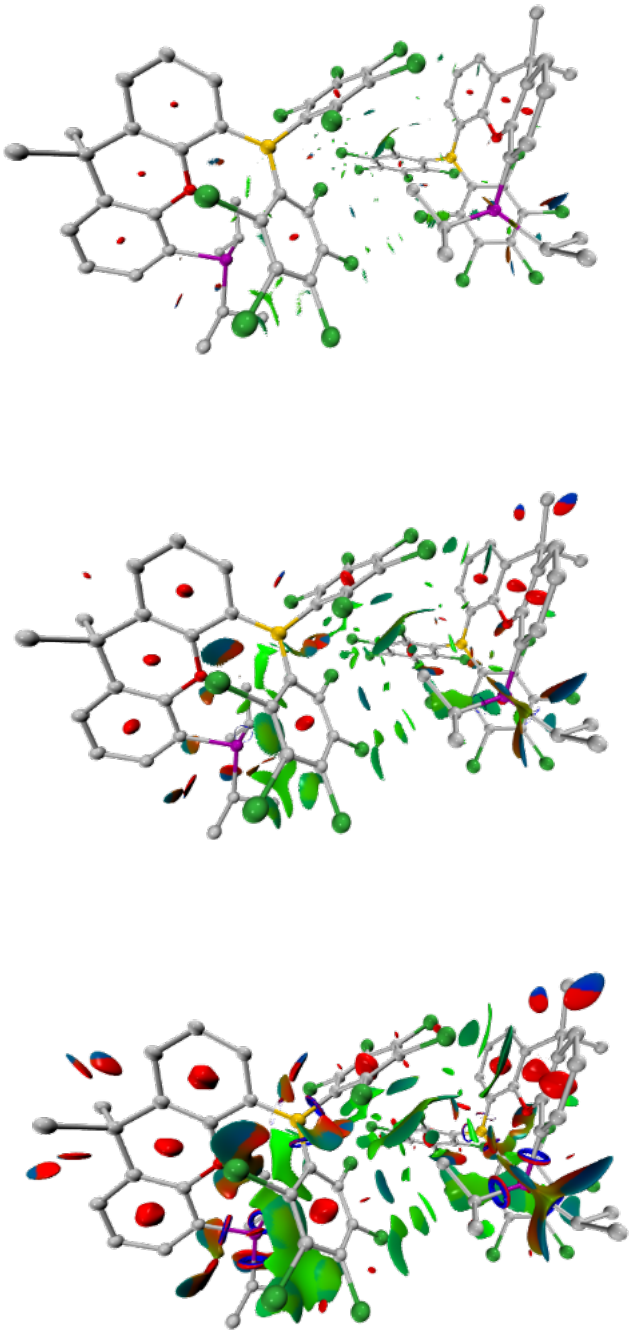

Figure 4.21 - Visualisation of non-covalent interactions between adjacent molecules of ***4.i****, denoted* $(\mathbf{4.i})_2$*. Most relevant interactions only are seen in the top image and progressively weaker ones in the two lower pictures.*

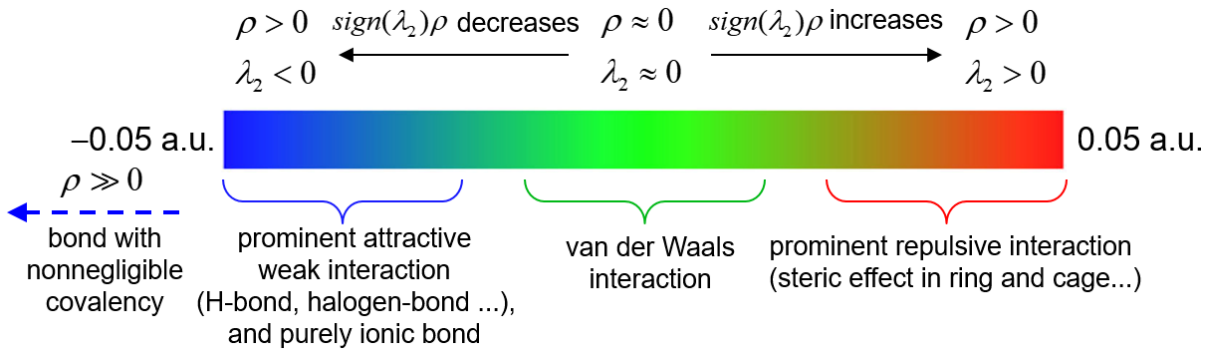

Figure 4.22 – Key to describe relative interaction strength displayed in images generated from quantum chemical calculations.

The Gibbs energy of oligomerisation, like hydrogenation, is temperature dependent, reflecting the unfavourable entropy of aggregation (**Graph 4.3**). Crucially, the two become competitive around 250 K, within 10 K of the experimentally observed regime switch. Above this temperature, dihydrogen activation is a lower energy pathway whereas below it is oligomerisation, consistent with experimental observations.

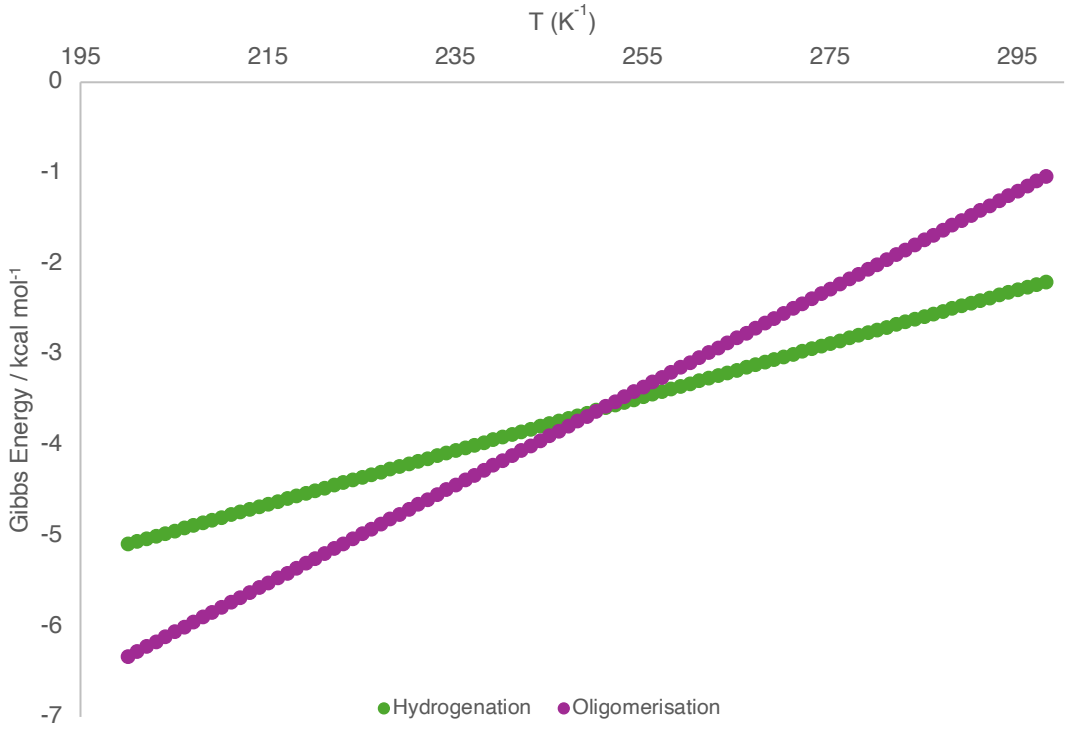

Graph 4.3 – Energies of oligomerisation and hydrogenation as a function of temperature.

This process might be summarised by the equation $\mathbf{4.i} + H_2 \rightleftharpoons [\mathbf{4.i} - H_2] \rightleftharpoons ½\ (\mathbf{4.i})_2 + H_2$. If now the Gibbs energy of hydrogenation for FLP **4.iii** is plotted as a function of temperature, and compared to oligomerisation energy (**Graph 4.4**), a similar observation can be made. Between 200 and 275 K, it is energetically favourable for the FLPs to aggregate, however above this inflection point, dihydrogen activation is a lower energy process, again, consistent with experimental observations. It appears that these interactions can be observed due to two factors: the pentachlorophenyl group is highly amenable to facilitating strong van der Waals interactions, and these FLPs activate hydrogen so slightly that it can be visualised on the same energy scale as intermolecular forces.

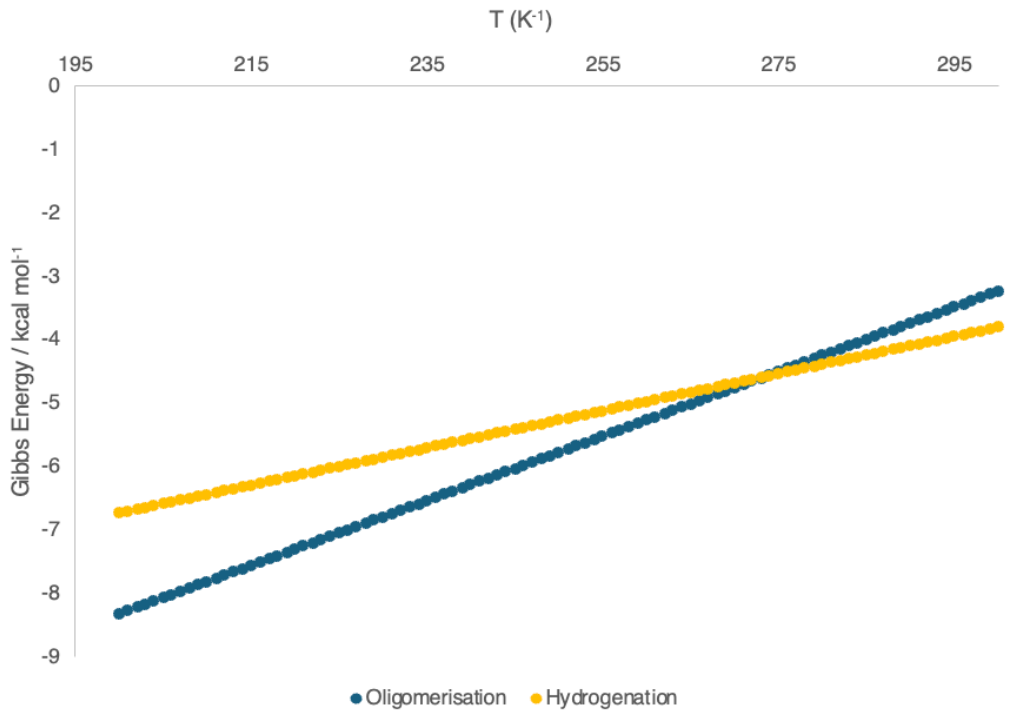

Graph 4.4 – Energies of oligomerisation and hydrogenation as a function of temperature.

Considering, once more, a visual representation of the intermolecular forces contributing to dimerization, a similar picture can be derived for **4.iii** as **4.i** (**Figure 4.23**), and the pathway described as $\mathbf{4.iii} + H_2 \rightleftharpoons [\mathbf{4.iii} - H_2] \rightleftharpoons ½\ (\mathbf{4.iii})_2 + H_2$.

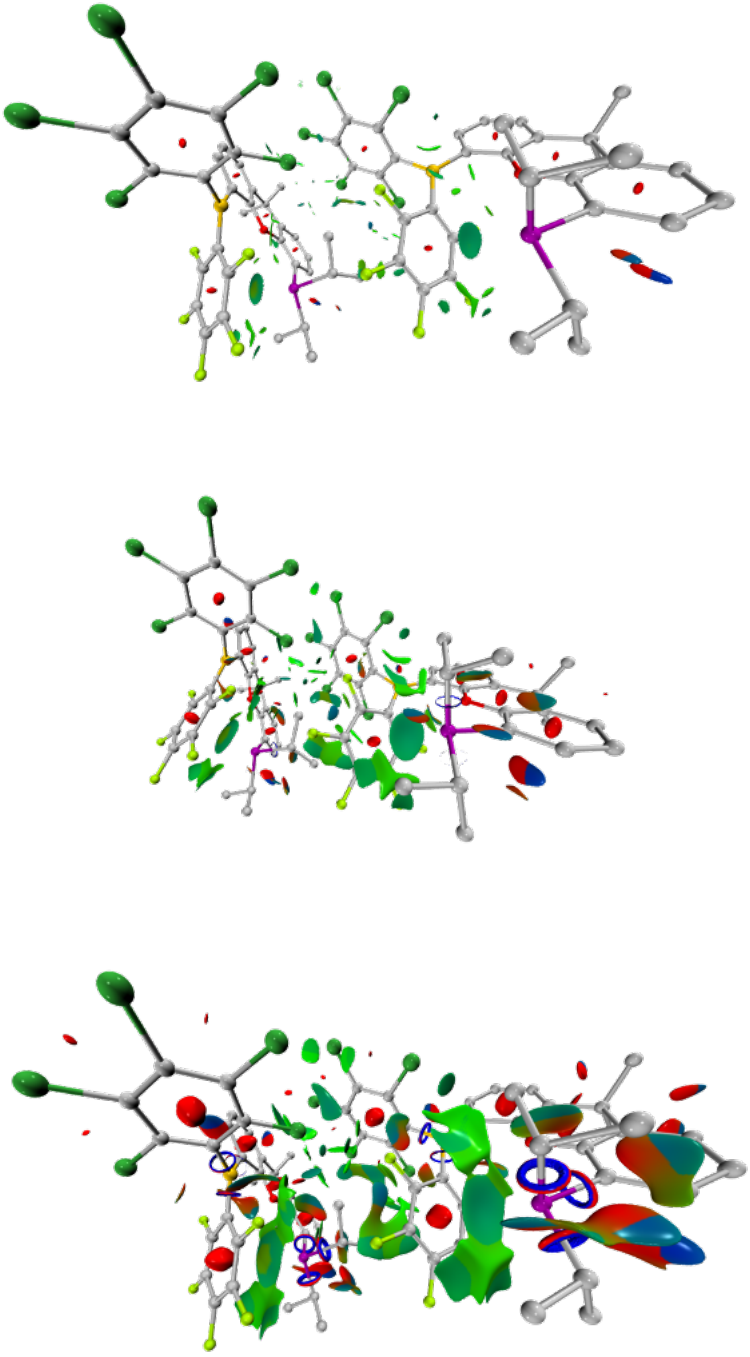

Figure 4.23 – Visualisation of non-covalent interactions between adjacent molecules of ***4.iii****, denoted* ***(4.iii)***$_2$*. Most relevant interactions only are seen in the top image and progressively weaker ones in the two lower pictures.*

4.4 Conclusions

This chapter has looked at the synthesis, characterisation, and dihydrogen reactivity of a family of Frustrated Lewis Pairs featuring pechloroaryl substituted boranes. The C_6Cl_5 group appears to modulate reactivity in directly comparable pairs *i.e.* **1.54** and **4.i**, possibly due to the steric imposition of the flanking *ortho*- chlorine atoms onto the boron active site. This has also been observed by other researchers observing attenuated acidity due to impeded access to the boron centre (**Section 4.1.1**). The size of this group can be viewed as advantageous when looking to synthesise a compound featuring a three co-ordinate boron centre, as observed in the facile synthesis of **4.iii** and **4.vi** compared to the unexpected reaction products **4.vii** and **4.viii** observed with less sterically demanding aryl groups (**Figure 4.24**).

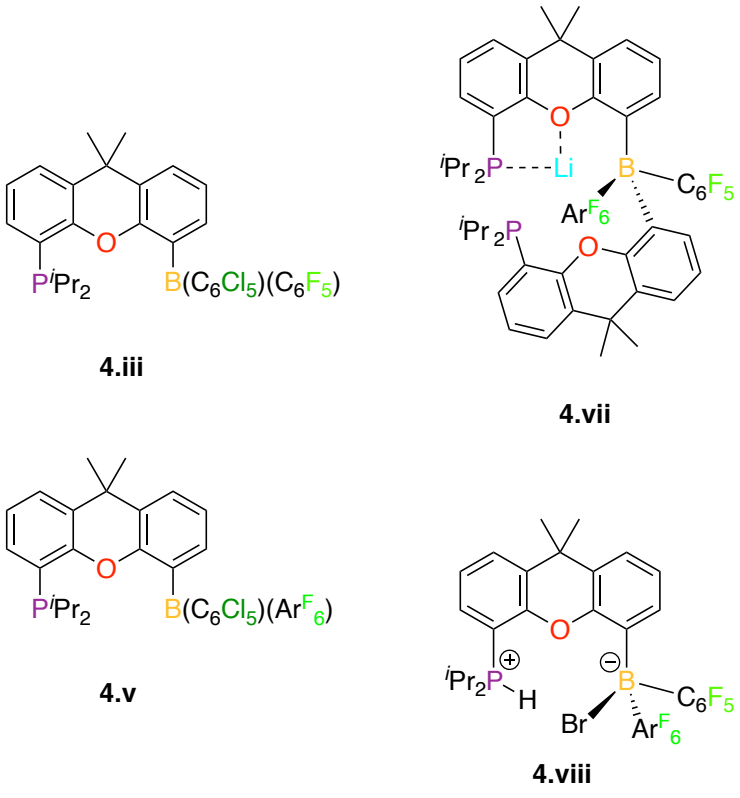

Figure 4.24 – Perchlorinated borane FLPs compared with attempted syntheses of perfluorinated borane FLPs.

A hypothesis has been presented to explain the surprising spectroscopic observations of two FLPs (**4.i** and **4.iii)** which facilitate hydrogen splitting in counter-intuitive manner as a function of temperature. These observations are due to the thermodynamically marginal nature of H_2 activation, meaning that dimerization of the FLPs *via* non-covalent interactions becomes relevant to reactivity. In light of these observations, it would be interesting to investigate other FLPs with pentachlorophenyl substituents on the Lewis acid, to see whether π stacking of adjacent molecules, and its ensuing interference with reactivity, is more widely observed, and can be potentially exploited in terms of rationalising dihydrogen activation pathways or reactivity trends more widely.

4.5 Synthetic Procedures and Spectroscopic Data for New Compounds

4.i – *Bis*(pentachlorophenyl)boryl-9,9,-dimethyl-xanthen-4-yl-di*iso*propylphosphine

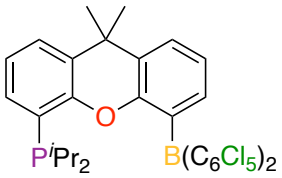

4.i

$ClB(C_6Cl_5)_2$ (500 mg, 0.92 mmol, 1 equiv.) was dissolved in toluene (20 mL) and added to a slurry of **4.7** (305 mg, 0.92 mmol, 1 equiv.), also in toluene (20 mL), at -78 °C. The reaction mixture was immediately warmed to room temperature and stirred for 16 h before filtration. Removal of volatiles yielded **4.i** as a bright yellow powder which was recrystallised from a concentrated hexane solution at -30 °C. Yield: 510 mg, 67%. Anal calcd for $C_{33}H_{26}BCl_{10}OP$ C: 47.43; H: 3.15. Found: C: 47.03, H: 2.95. ^{1}H NMR (500 MHz, C_6D_6) δ 7.28 (dd, *J* = 7.7, 1.8 Hz, 1H, Ar*H*), 7.15 – 6.99 (m, 3H, Ar*H*), 6.90 (t, *J* = 7.6 Hz, 1H, Ar*H*), 6.82 (t, *J* = 7.6 Hz,

1H, Ar*H*), 1.80 (*J* = 7.0 Hz, 2H, ^{i}Pr*CH*), 1.36 (br s, 6H, XAN*CH*$_3$), 1.03 (dd, *J* = 14.6, 6.9 Hz, 6H, ^{i}Pr*CH*$_3$), 0.77 (dd, *J* = 10.8, 6.8 Hz, 6H, ^{i}Pr*CH*$_3$). ^{13}C {^{1}H} NMR (126 MHz, C_6D_6) δ 156.8, 154.0, 153.9, 137.2, 134.6, 133.7, 131.3, 129.8, 129.8, 129.0, 128.0, 127.9 126.3, 123.6, 123.3, 123.1, 30.0 (s XAN*CH*$_3$) 20.4 (^{i}Pr*CH*$_3$), 18.3 (s ^{i}Pr*CH*$_3$). ^{31}P{^{1}H} NMR (202 MHz, C_6D_6) δ -14.4. No signals attributable to the tertiary carbon of the ^{i}Pr groups or quaternary XAN*C* carbon are observed. No signals attributable to the product were found in the ^{11}B spectrum.

4.ii – *Bis*(pentachlorophenyl)boryl-9,9,-dimethyl-xanthen-4-yl-diphenylphosphine

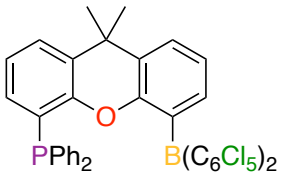

4.ii

$ClB(C_6Cl_5)_2$ (500 mg, 0.92 mmol, 1 equiv.) was dissolved in toluene (20 mL) and added to a slurry of **4.8** (375 mg, 0.92 mmol, 1 equiv.), also in toluene (20 mL), at -78 °C. The reaction mixture was immediately warmed to room temperature and stirred for 16 h before filtration. Removal of volatiles yielded **4.ii** as a bright yellow powder which was recrystallised from a concentrated toluene solution at -30 °C overnight. Yield: 453 mg, 55 %. Anal calcd for $C_{39}H_{22}BCl_{10}OP$ C: 51.83 H: 2.44. Found C: 51.66 H: 2.39. ^{1}H NMR (500 MHz, C_6D_6) δ 7.4 – 7.2 (m, 4H, Ar*H*), 7.1 – 7.0 (m, 9H, Ar*H*), 6.9 – 6.7 (m, 2H Ar*H*), 6.7 (t, *J* = 7.6 Hz, 1H Ar*H*), 1.4 (s, 6H, XAN*CH*$_3$). ^{13}C{^{1}H} NMR (126 MHz, C_6D_6) δ 156.8, 152.8, 136.7, 133.7, 133.3, 130.4, 129.9, 129.9, 128.7, 128.4, 127.4, 125.6, 125.5, 124.6, 124.2 (Ar*C*), 34.3 (XAN*CH*$_3$). No signals attributable to the quaternary XANC carbon are observed. ^{31}P{^{1}H} NMR (202 MHz, C_6D_6) δ -17.6. No signals attributable to the product were found in the ^{11}B{^{1}H} spectrum.

4.iii – (Pentachlorophenyl)(pentafluorophenyl)boryl-9,9,-dimethyl-xanthen-4-yl-di*iso*propylphosphine

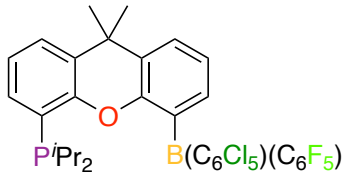

4.iii

3.iv (504 mg, 1.1 mmol, 1 equiv.) was dissolved in hexane (20 mL), and BBr_3 (0.3 mL, 3 equiv.) added rapidly. The reaction mixture was sealed in a Teflon capped ampoule and heated at 80 °C overnight. The resulting mixture was cooled to room temperature and volatiles removed *in vacuo* to yield **3.vi** as a brown oil which was used assuming quantitative conversion. This sample of **3.vi** was redissolved in toluene (20 mL) and added dropwise to a solution of **4.7** (440 mg, 1.1 mmol, 1 equiv.), also in toluene (20 mL), at -78 °C. The reaction mixture was warmed to room temperature and stirred for 16 h prior to filtration. Bright yellow crystals of **4.iii** were obtained from a concentrated benzene solution at room temperature. Yield: 364 mg, 44%. Anal calcd for $C_{33}H_{26}BCl_5F_5OP$: C: 52.62; H: 3.49. Found: C: 52.29, H: 3.73. ^{1}H NMR (500 MHz, C_6D_6) δ 7.28 – 7.22 (m, 2H, Ar*H*) 7.09 (dd, *J* = 7.7, 1.6 Hz, 1H, Ar*H*), 7.01 (dt, *J* = 7.6, 1.9 Hz, 1H, Ar*H*), 6.90 (t, *J* = 7.6 Hz, 1H, Ar*H*), 6.81 (t, *J* = 7.5 Hz, 1H Ar*H*), 1.69 (sept, *J* = 6.9 Hz, 2H, ^{i}Pr*CH*), 1.32 (s, 6H, XAN*CH*$_3$), 0.95 (dd, *J* = 14.6, 6.9 Hz, 6H, ^{i}Pr*CH*$_3$), 0.76 (dd, *J* = 11.7, 6.9 Hz, 6H, ^{i}Pr*CH*$_3$). ^{11}B{^{1}H} NMR (160 MHz, C_6D_6) δ 59.3. ^{13}C{^{1}H}NMR (126 MHz, C_6D_6) δ 156.8, 153.5 (*J* = 15.4 Hz), 136.7, 134.0, 133.7, 132.2, 131.9, 131.3, 131.2 130.0, 129.8, 128.0, 126.6, 123.6, 123.4, 123.1, 123.0, 33.4 (XAN*C*), 31.9 (XAN*CH*$_3$), 23.1 (*J* = 15.5 Hz, ^{i}Pr*CH*), 19.6 (*J* = 19.1 Hz, ^{i}Pr*CH*$_3$), 18.7 (*J* = 11.3 Hz, ^{i}Pr*CH*$_3$). ^{19}F{^{1}H} NMR (470 MHz, C_6D_6) δ -129.0 to 129.2 (m, *o*-C_6F_5), -148.7 to -148.9 (m, *p*-C_6F_5), -163.3 (td, *J* = 22.9, 8.9 Hz, *m*-C_6F_5). ^{31}P{^{1}H} NMR (202 MHz, C_6D_6) δ -11.0.

4.iv – (Pentachlorophenyl)(pentafluorophenyl)boryl-9,9,-dimethyl-xanthen-4-yl-diphenylphosphine

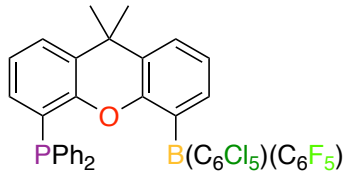

4.iv

3.iv (504 mg, 1.1 mmol, 1 equiv.) was dissolved in hexane (20 mL), and BBr_3 (0.3 mL, 3 equiv.) added rapidly. The reaction mixture was sealed in a Teflon capped ampoule and heated at 80 °C overnight. The resulting mixture was cooled to room temperature and volatiles removed *in vacuo* to yield **3.vi** as a brown oil which was used assuming quantitative conversion. This sample of **3.vii** was redissolved in toluene (20 mL) and added dropwise to a solution of **4.8** (440 mg, 1.1 mmol, 1 equiv.), also in toluene (20 mL), at -78 °C. The reaction mixture was warmed to room temperature and stirred for 16 h prior to filtration. Bright yellow crystals of **4.iv** were obtained from a concentrated benzene solution at room temperature. Yield: 364 mg, 44%. Anal calcd for $C_{33}H_{26}BCl_5F_5OP$: C: 52.62; H: 3.49. Found: C: 52.29, H: 3.73. ^{1}H NMR (500 MHz, C_6D_6) δ 7.28 – 7.22 (m, 2H, Ar*H*) 7.09 (dd, *J* = 7.7, 1.6 Hz, 1H, Ar*H*), 7.01 (dt, *J* = 7.6, 1.9 Hz, 1H, Ar*H*), 6.90 (t, *J* = 7.6 Hz, 1H, Ar*H*), 6.81 (t, *J* = 7.5 Hz, 1H Ar*H*), 1.69 (sept, *J* = 6.9 Hz, 2H, ^{i}Pr*CH*), 1.32 (s, 6H, XAN*CH*$_3$), 0.95 (dd, *J* = 14.6, 6.9 Hz, 6H, ^{i}Pr*CH*$_3$), 0.76 (dd, *J* = 11.7, 6.9 Hz, 6H, ^{i}Pr*CH*$_3$). ^{11}B{^{1}H} NMR (160 MHz, C_6D_6) δ 59.3. ^{13}C{^{1}H}NMR (126 MHz, C_6D_6) δ 156.8, 153.5 (*J* = 15.4 Hz), 136.7, 134.0, 133.7, 132.2, 131.9, 131.3, 131.2 130.0, 129.8, 128.0, 126.6, 123.6, 123.4, 123.1, 123.0, 33.4 (XAN*C*), 31.9 (XAN*CH*$_3$), 23.1 (*J*= 15.5 Hz, ^{i}Pr*CH*), 19.6 (*J* = 19.1 Hz, ^{i}Pr*CH*$_3$), 18.7 (*J* = 11.3 Hz, ^{i}Pr*CH*$_3$). ^{19}F{^{1}H} NMR (470 MHz, C_6D_6) δ -129.0 to 129.2 (m, *o*-C_6F_5), -148.7 –to -148.9 (m, *p*-C_6F_5), -163.3 (td, *J* = 22.9, 8.9 Hz, *m*-C_6F_5). ^{31}P{^{1}H} NMR (202 MHz, C_6D_6) δ -11.0.

4.v – (Pentachlorophenyl)-(3,5-bis(trifluoromethyl)phenyl)boryl-9,9,-dimethyl-xanthen-4-yl-di*iso*propylphosphine

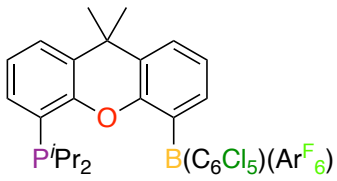

4.v

3.viii (879 mg, 1.1 mmol, 1 equiv.) was dissolved in toluene, and added dropwise to a solution of **4.7**, also in toluene, at -78 °C. Reaction was warmed to room temperature and stirred for 16 h prior to filtration. Bright yellow crystals of **4.v** were grown out of a concentrated toluene solution at room temperature. Yield: 336 mg, 42 % Anal calcd for $C_{35}H_{29}BCl_5F_6OP$: C: 52.59; H: 3.67. Found: C: 52.35, H: 3.81. ^{1}H NMR (500 MHz, C_6D_6) δ 8.42 (d, *J* = 1.8 Hz, 2H, Ar*H*), 7.98 (s, 1H, Ar*H*), 7.32 – 7.25 (m, 2H, Ar*H*), 7.11 (dd, *J* = 7.6, 1.6 Hz, 1H, Ar*H*), 7.01 (dt, *J* = 7.7, 1.8 Hz, 1H, Ar*H*), 6.90 (q, *J* = 7.8 Hz, 2H, Ar*H*), 1.65 (hept, *J* = 6.9 Hz, 2H, ^{i}Pr*CH*), 1.39 (s, 6H (XAN*CH*$_3$), 0.84 (dd, *J* = 13.7, 6.8 Hz, 6H, ^{i}Pr*CH*$_3$), 0.72 (dd, *J* = 12.2, 7.0 Hz, 6H, ^{i}Pr*CH*$_3$). ^{13}C {^{1}H} NMR (126 MHz, C_6D_6) δ 156.6, 154.5, 154.3, 137.4, 135.9, 134.7, 132.5, 132.4, 132.1, 132.0, 131.8, 131.7, 131.6, 131.4, 130.7, 130.7, 126.2, 126.1, 125.2, 125.1, 124.9, 123.7, 123.5, 123.1, 34.7 (XAN*C*), 31.0 (XAN*CH*$_3$), 24.0 (d, *J* = 15.2 Hz, ^{i}Pr*CH*$_3$), 19.8 (^{i}Pr*CH*), 19.7 (d, *J* = 7.2 Hz, ^{i}Pr*CH*$_3$) ^{31}P{^{1}H} NMR (202 MHz, C_6D_6) δ -11.9. ^{19}F{^{1}H} NMR (470 MHz, C_6D_6) δ -62.4. No signals attributable to the product were found in the ^{11}B spectrum.

4.vi – (Pentachlorophenyl)(4-*N*,*N*-dimethylamino-2,3,5,6 tetrafluorophenyl)boryl-9,9,-dimethyl-xanthen-4-yl-di*iso*propylphosphine

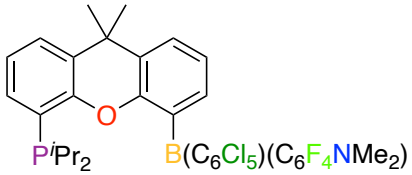

4.vi

3.ix (585 mg, 1.1 mmol, 1 equiv.) was dissolved in toluene (20 mL), and added dropwise to a solution of **4.7**, also in toluene (20 mL), at -78 °C. The reaction mixture was warmed to room temperature and stirred for 16 h prior to filtration. **4.vi** was isolated as a bright yellow powder. Yield: 150 mg, 18 %. Anal calcd for $C_{35}H_{32}BCl_5F_4NOP$: C: 54.06; H: 4.15; N: 1.80. Found C: 53.97, H: 4.20, N: 1.73. ^{1}H NMR (400 MHz, Tol) δ 7.26 (ddd, J = 15.0, 7.6, 1.7 Hz, 2H, Ar*H*), 7.13 (dd, *J* = 7.7, 1.6 Hz, ^{1}H, Ar*H*), 7.06 (t, *J* = 1.9 Hz, ^{1}H, Ar*H*), 6.93 (t, *J* = 7.6 Hz, 1H, Ar*H*), 6.83 (t, *J* = 7.6 Hz, ^{1}H, Ar*H*), 2.64 (t, *J* = 2.6 Hz, 6H, NMe$_2$*CH$_3$*), 1.77 (sept, *J* = 7.0 Hz, 2H, ^{i}Pr*CH*), 1.38 (s, 6H, XAN*CH$_3$*), 0.99 (dd, *J* = 13.9, 6.9 Hz, 6H, ^{i}Pr*CH$_3$*), 0.83 (dd, *J* = 12.0, 7.0 Hz, 6H, ^{i}Pr*CH$_3$*). ^{11}B{^{1}H} NMR (128 MHz, Tol) δ 53.7. ^{13}C{^{1}H} NMR (101 MHz, Tol) δ 154.9, 134.9, 132.0, 131.3, 123.1, 42.7, 34.6, 31.5, 24.0. ^{19}F{^{1}H} NMR (377 MHz, Tol) δ -129.4 (dt, *J* = 19.3, 6.5 Hz), -154.6 to -154.8 (m).

4.vii – Lithio(pentachlorophenyl)(3,5-bis(trifluoromethyl)phenyl)(9,9,-dimethyl-xanthen-4-yl-di*iso*propylphosphine)borate-9,9,-dimethyl-xanthen-4-yl-di*iso*propylphosphine

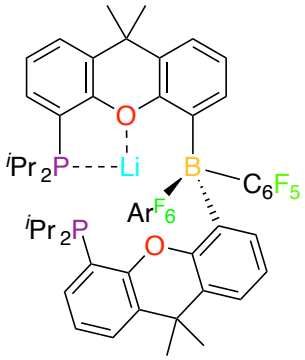

4.vii

3.ii (464 mg, 1.1 mmol, 1 equiv.) was dissolved in hexane (20 mL) and stirred over Cu powder, and BBr_3 (0.3 mL, 3.3 mmol, 3 equiv.) added rapidly. The reaction mixture was sealed in a Teflon capped ampoule and heated at 80 °C overnight. The resulting mixture was cooled to room temperature and volatiles removed *in vacuo* to yield **3.vii** as a greyish brown oil which was used assuming quantitative conversion. This sample of **3.vii** was redissolved in toluene (20 mL) and added dropwise to a solution of **4.8** (440 mg, 1.1 mmol, 1 equiv.), also in toluene (20 mL), at -78 °C. The reaction mixture was warmed to room temperature and stirred for 16 h prior to filtration. Bright yellow crystals of **4.vii** were obtained from a concentrated hexane solution at 4 °C. Yield: 868 mg, 71 %. ^{1}H NMR (400 MHz, C_6D_6) δ 8.26 (s, 3H), 7.98 (s, 1H), 7.74 (s, 1H), 7.67 (s, 1H), 7.34 – 7.27 (m, 2H), 7.08 (q, J = 10.2 Hz, 1H), 7.02 – 6.84 (m, 7H), 6.80 (d, J = 8.1 Hz, 1H), 6.64 (s, 1H), 2.11 (s, 1H), 1.65 (d, J = 6.6 Hz, 2H), 1.57 (s, 1H), 1.47 (dd, J = 28.7, 5.3 Hz, 4H), 1.37 (s, 6H), 1.34 – 1.18 (m, 10H), 1.11 – 1.02 (m, 1H), 1.02 – 0.94 (m, 2H), 0.98 – 0.77 (m, 7H), 0.77 – 0.53 (m, 6H). ^{11}B{^{1}H} NMR (128 MHz, C_6D_6) δ -8.2. ^{19}F{^{1}H} NMR (377 MHz, C_6D_6) δ -62.5, -126.2 – -126.3 (m), -148.0 (t, J = 21.5 Hz), -161.9 (q, J = 11.6 Hz). ^{31}P{^{1}H} NMR (162 MHz, C_6D_6) δ -10.6 (dd, J = 13.9, 5.5 Hz).

4.viii – (Pentachlorophenyl)-3,5-bis(trifluoromethyl)phenyl)bromoboryl-9,9,-dimethyl-xanthen-4-yl-di*iso*propylphosphonium bromide

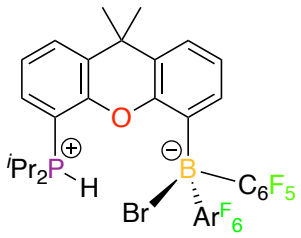

4.viii

3.ii (464 mg, 1.1 mmol, 1 equiv.) was dissolved in hexane (20 mL) and stirred over Cu powder, and BBr_3 (0.3 mL, 3.3 mmol, 3 equiv.) added rapidly. The reaction mixture was sealed in a Teflon capped ampoule and heated at 80 °C overnight. The resulting mixture was cooled to

room temperature and volatiles removed *in vacuo* to yield **3.vii** as a greyish brown oil which was used assuming quantitative conversion. This sample of **3.vii** was redissolved in toluene (20 mL) and a solution of **4.8** (880 mg, 2.2 mmol, 2 equiv.), also in toluene (20 mL), was added at -78 °C. The reaction mixture was warmed to room temperature and stirred for 16 h prior to filtration. Bright yellow crystals of **4.viii** were grown out a concentrated hexane solution at 4 °C. No clean ^{1}H NMR spectroscopic data can be obtained for a crystalline sample. ^{19}F{^{1}H} NMR (377 MHz, C_6D_6) δ -61.9, -159.2 (t, J = 21.1 Hz), -164.6 to -164.8 (m). ^{31}P{^{1}H} NMR (162 MHz, C_6D_6) δ 8.8

4.ix – (Pentachlorophenyl)hydroxyboryl-9,9,-dimethyl-xanthen-4-yl-di*iso*propylphosphine

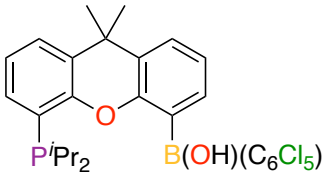

4.ix

An excess of methanol or water (ca. 0.1 mL) was added to a solution of **4.i** or **4.iii** (200 mg, 0.24 mmol (**4.i**) or 0.27 mmol (**4.iii**)) in hexane (20 mL) at room temperature. **4.ix** crystallised in fractional quantities at 4 °C and no robust spectroscopic data could be obtained for this compound.

General procedure for the hydrogenation of FLPs 4.i, 4.iii and 4.v

Approx. 6 mg of each compound was dissolved in 0.6 mL of deuterated toluene and added to a high-pressure NMR tube through a syringe filter. A sealed capillary containing a solution of Ph_3PO in deuterated toluene (540 mmol concentration) was added to the tube as an internal standard. The resulting solution was degassed by three freeze-pump-thaw cycles and 1 atm. H_2 was added. Samples were held in a cold bath (-78 °C) to ensure that no precipitation was

observed. For variable temperature measurements, samples were held at each temperature for 30 mins prior to spectra being measured. For ^{31}P measurements, spectra were centred midway between the two furthest peaks, the relaxation delay was extended to 30 s and the pulse sequence was altered to inverse gated coupling to allow for quantitative comparison by integration of phosphorous signals. Hydrogenated products were not isolated; however X-ray quality crystals were obtained of **4.i-H$_2$** and **4.iii-H$_2$** from an NMR tube containing both the hydrogenation products and the parent FLPs.

Chemical Shifts of ^{31}P Signals Attributed to Hydrogenated Products at 293 K (ppm)

FLP-H$_2$	**^{31}P**
4.i	14.6
4.iii	14.1
4.v*	16.2

*Spectrum measured at 248 K (the highest temperature at which FLP-H$_2$ was observed).

4.6 References

1 E. A. Patrick and W. E. Piers, *Chem. Commun.*, 2020, **56**, 841–853.

2 T. A. Gazis, D. Willcox and R. L. Melen, in *Frustrated Lewis Pairs*, eds. J. Chris Slootweg and A. R. Jupp, Springer International Publishing, Cham, 2021, pp. 209–235.

3 D. W. Stephan, *Science (80-.).*, 2016, 354.

4 G. Erker, *Dalt. Trans.*, 2005, **0**, 1883–1890.

5 T. J. Herrington, A. J. W. Thom, A. J. P. White and A. E. Ashley, *Dalt. Trans.*, 2012, **41**, 9019–9022.

6 A. E. Ashley, T. J. Herrington, G. G. Wildgoose, H. Zaher, A. L. Thompson, N. H. Rees, T. Krämer and D. O'Hare, *J. Am. Chem. Soc.*, 2011, **133**, 14727–14740.

7 I. Zulkifly, University of Oxford, 2020.

8 M. Giese, M. Albrecht and K. Rissanen, *Chem. Rev.*, 2015, **115**, 8867–8895.

9 I. B. Sivaev and V. I. Bregadze, *Coord. Chem. Rev.*, 2014, **270**–**271**, 75–88.

10 M. A. Beckett, G. C. Strickland, J. R. Holland and K. S. Varma, *Polymer (Guildf).*, 1996, **37**, 4629–4631.

11 R. J. Mayer, N. Hampel and A. R. Ofial, *Chem. – A Eur. J.*, 2021, **27**, 4070–4080.

Chapter 5 – In Pursuit of a Tethered Phosphine Frustrated Lewis Pair

5.1 Introduction

Derivatives of 9H-xanthene have found widespread use as organic dyes, with applications in biological research and human medicine.[1,2] In addition, due to its rigidity and the abundance of methods for its modular functionalisation, xanthene has been used a building block for a large range of multidentate ligands. These xanthene-based ligands have been complexed to elements from across the *s*-, *p*-, *d*- and *f*-blocks of the Periodic Table.[3–5] Aside from their application as ligands, phosphine-substituted xanthene derivatives have been used as the basis for geminal P/B Frustrated Lewis Pairs.[6]

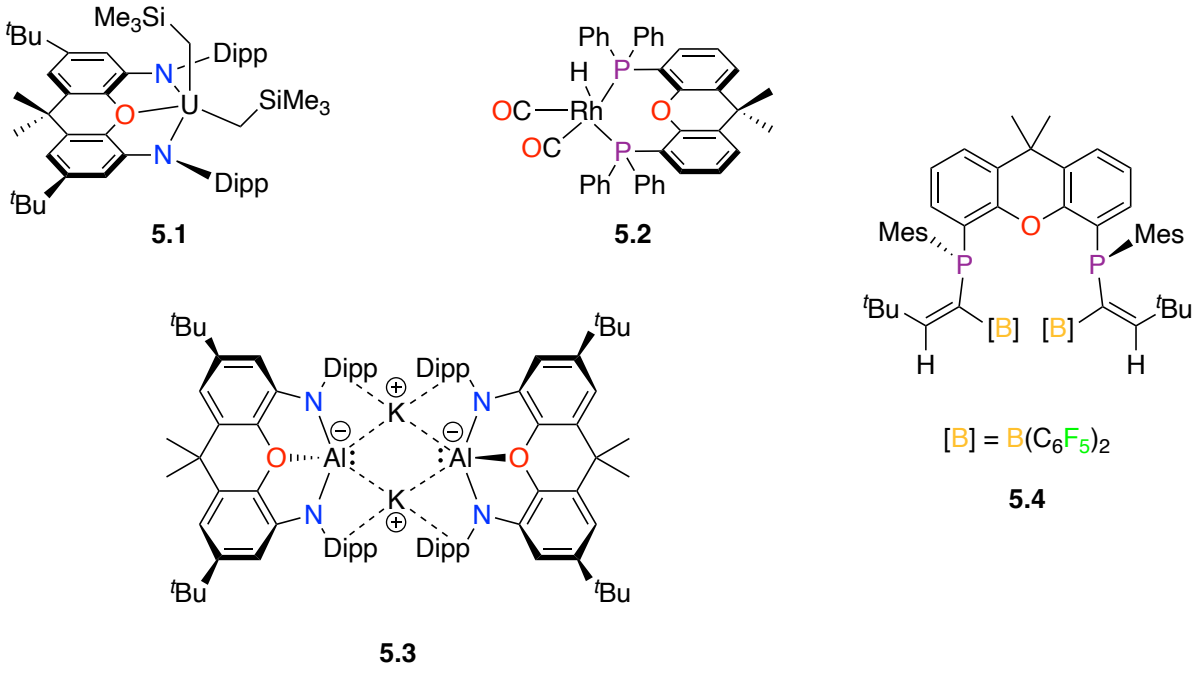

Figure 5.1 – Uranium, rhodium, and aluminium complexes of xanthene ligands and a geminal xanthene-based FLP .

Unsymmetrical substitution of xanthene is also possible (**Scheme 5.1**) and has been used in the FLP chemistry described in this section, as well as Chapters 1 and 4. This is accomplished by stepwise metalation and electrophilic quenching steps. First the 4-position is lithiated before addition of a chlorophosphine base, then the 5-position is lithiated followed by reaction with a haloborane.

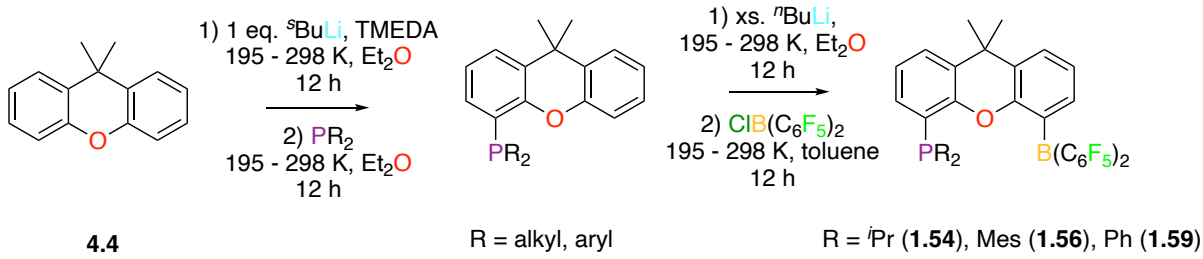

Scheme 5.1 – General synthesis of xanthene backbone FLPs via stepwise metalation and quenching.

Several xanthene based FLPs of this type have been reported, featuring a range of dialkyl and diaryl phosphine units.[7–9] The structural diversity in these pairs, and a wide array of potential substituents, is encouraging in terms of the potential to incorporate a surface linker at the phosphine. This might be envisaged either by leveraging a labile P—X bond (direct phosphorus to surface linkage) or a phosphine bonded to a substituent such as an aryl group featuring a linking group (indirect attachment) as shown in **Figure 5.2**.

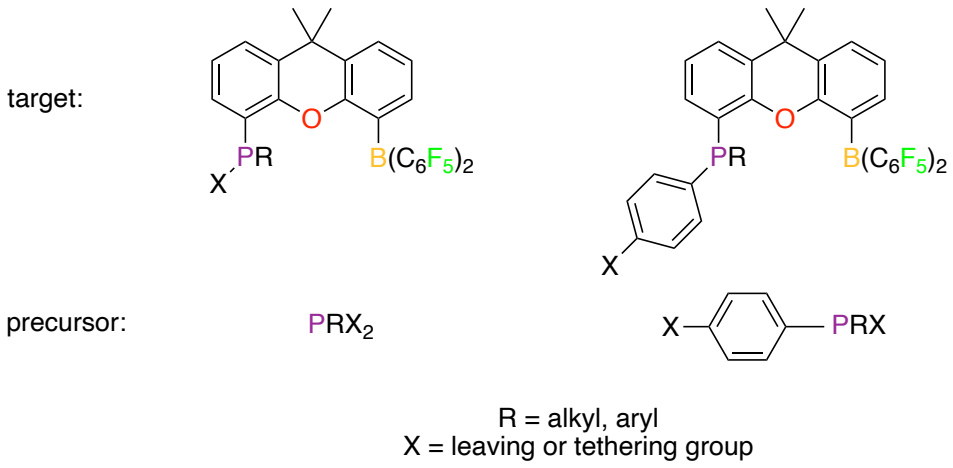

Figure 5.2 – General structures of potential precursors to surface-supported FLPs.

The synthesis of unsymmetrical chlorophosphines featuring one alkyl and one aryl group is well established, *via* the reactions of a Grignard with a dihalo-aryl or -alkyl phosphine.[10–12] Diaryl chlorophopshines featuring two different organic substituents, where one is phenyl, can also be prepared from diethylaminophosphines (**Scheme 5.2**).

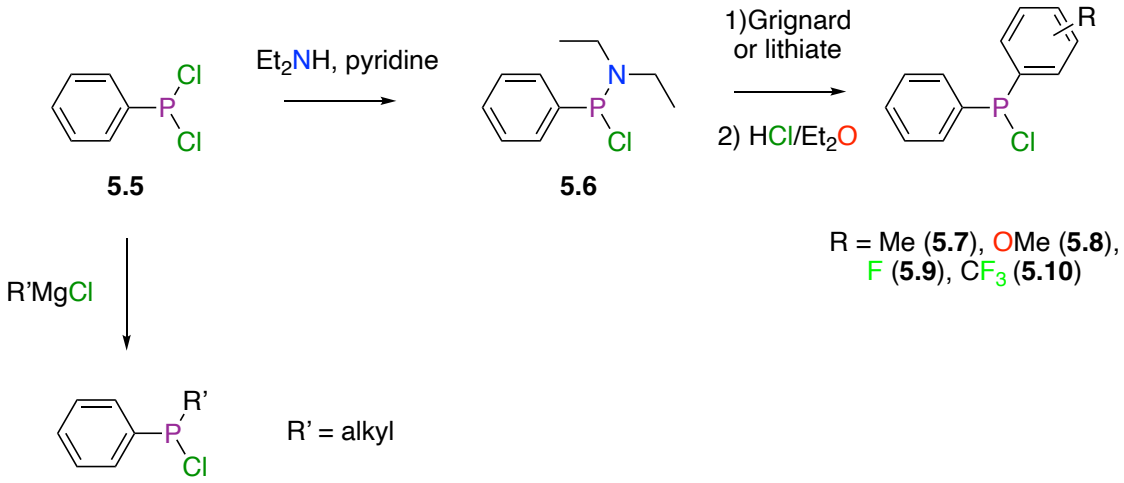

Scheme 5.2 – General synthesis of chlorophosphines with two different organic substituents.

A report by Lee and co-workers details examples of phosphines furnished with either methyl, methoxy, fluoro or trifloromethyl groups in the *ortho*, *meta* and *para* positions of the second aromatic ring in systems of the type PCl(Ph)Ar *i.e.* **5.7** – **5.10**, **Scheme 5.2**.[13] These molecules are also P-chiral, as is typical of ligands used in enantioselective catalysis.[14]

In terms of a molecular linker to a surface, a hydroxyl group emerges as a logical covalent bridge, as demonstrated by Taoufik and co-workers (**Section 1.5**).[15] Given the inherent acidity of alcoholic protons, a protecting group which is tolerant to lithiation *and* whose deprotection conditions do not impact the borane function would be required. Potential examples of these are methoxy methyl ethers and benzyl groups, although the latter is removed by catalytic hydrogenation which somewhat negates the use of *p*- over *d*- block elements.[16]

5.2 Aims

At the outset of this project, to our knowledge there were no xanthene-backbone FLPs featuring a phosphine bearing three different substituents. Therefore, a synthetic route towards systems with the general structure of the targets shown in **Figure 5.2** was sought. The first aim was the synthesis and characterisation of xanthene-phosphine precursors with a tethering group either directly or remotely bound to the phosphorus centre. Tethers based on aryl groups were targeted as the plethora of functionalised arenes in the literature gives broad scope to this protocol as a means of attachment to a surface. With the tethered phosphines in hand, subsequent work would focus on the construction of FLPs and an examination of their reactivity with industrially relevant small molecules such as dihydrogen and CO_2. Hydrogen activation was targeted with a view towards using these systems as hydrogenation catalysts. Due to the exploratory nature of all of the synthetic steps, surface attachment of the FLP systems was an additional parallel project.

5.3 Results and Discussion

5.3.1 Synthesis of Xanthene-derivatised Chlorophosphines

Initial investigations examined xanthene-phosphines with a leaving group at the phosphorus centre, prepared by reacting a dichlorophosphine directly with lithio-xanthene (**Scheme 5.3**). A substituent featuring a protected surface linking group would subsequently be incorporated through salt metathesis between the resulting dichloro(xanthene)phosphine and a metalated tether.

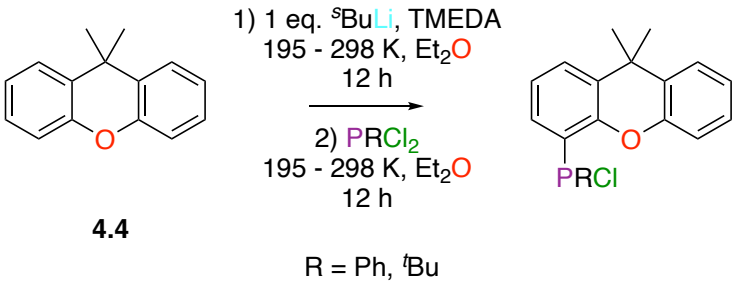

Scheme 5.3 – Envisaged synthesis of xanthene chlorophosphines.

Access to the desired structural motif is highly contingent on the size of the organic group at phosphorus. Reaction of 4-lithio-9,9-dimethylxanthene with dichlorophenylphosphine ($PPhCl_2$) preferentially generates the *bis*-xanthene phosphine $(xanth)_2PPh$, **5.i** in 43 % yield, as indicated both by a single resonance in the ^{31}P NMR spectrum at -22.8 ppm and by X-ray crystallography (**Figure 5.3**). **5.i** is formed even when an excess of phosphine is used, and when inverse addition of the lithio-xanthene precursor to the chlorophosphine is attempted.

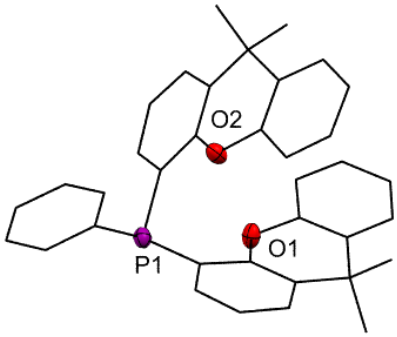

*Figure 5.3 – Molecular structure of **5.i** as determined by X-ray crystallography. Ellipsoids are shown at 50% probability. Carbon atoms are shown in wireframe format and hydrogen atoms are omitted for clarity.*

In the ^1H NMR spectrum of **5.i**, the two signals at 1.40 and 1.37 ppm, corresponding to the methyl protons appended to the methyl groups at the 9- position on the xanthene backbone are observed. This is because the conformation adopted renders the molecule chiral at phosphorus, as such the methyl groups on each xanthene ligand are diastereotopic.

Formation of a singly substituted xanthene chlorophosphine as shown in **Scheme 5.3** was preferred when the sterically more demanding dichloro*tert*butylphosphine (P^tBuCl_2) was employed. Conversion to **5.ii** was evidenced by a characteristic peak at 104.0 ppm in the ^{31}P NMR spectrum and further by the growth of single crystals suitable for X-ray diffraction (**Figure 5.4**). The crystalline yield of **5.ii** (32 %) is reduced by its tendency to sublime during work-up.

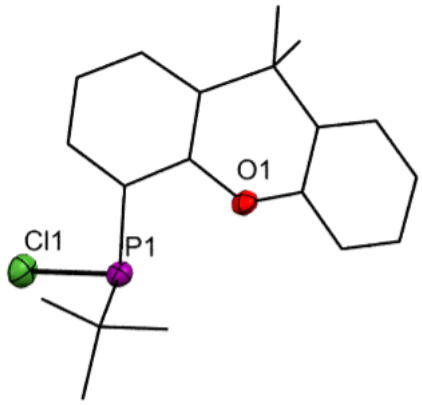

*Figure 5.4 – Molecular structure of **5.ii** as determined by X-ray crystallography. Ellipsoids are shown at 50% probability. Carbon atoms are shown in wireframe format and hydrogen atoms are omitted for clarity.*

The ^1H NMR resonance corresponding to the *tert*butyl group is observed at 1.13 ppm ($^3J_{PH}$ = 13.1 Hz). Resonances attributed to the protons of the diastereotopic methyl groups in the 9-position of the xanthene backbone are found at 1.35 and 1.31 ppm. The *tert*butyl group is a strongly electron donating substituent which elevates the basicity of the phosphine. It might therefore compensate for a more weakly donating tethering group, such as one based around an aryl substituent. This is critical because the Lewis basicity of the phosphine component of a P/B FLP is relevant to the function of these systems in small molecule binding/activation. For example, as it was envisaged that these systems would be used for dihydrogen activation, it should be noted that a xanthene based FLP system with a diphenylphosphine base is not

known to activate H_2 upon the application of 1 atm. of pressure (although it does so at high pressure).

5.3.2 Synthesis of Directly Tethered Phosphines

Making a direct covalent phosphorus to surface attachment could involve the construction of a P—O bond. This route was investigated using benzyl protected 1,4 diphenol, allowing for convenient probing by solution-phase analytical techniques (*i.e.* NMR spectroscopy). Xanthene-based FLPs reported in the literature have all been characterised and their reactivity tested by these means so this would provide a useful point of comparison. Facility for attachment could be first probed by bonding to an aryloxy functionalised arene, before employing more specialised, less accessible surface-characterisation techniques such as FT-IR and solid state NMR.

The motivation for the use of a diphenol tether is two-fold: the P—O—C linker is a mimic of a surface itself, and it informs whether aryloxy phosphines can be employed in remotely tethered species. A benzyl protecting group was selected as it was envisaged that the conditions required for its deprotection (hydrogenation) would be unlikely to interfere with any other reactive moiety within the molecule. 4-Benzyloxyphenol was therefore deprotonated with sodium hydride prior to its reaction with chlorophosphine **5.ii** to form **5.iii** in 78 % yield (**Scheme 5.4**). The resulting tethered phosphine **5.iii** was crystallographically characterised, providing proof of the successful implementation of this synthetic strategy (**Figure 5.5**).

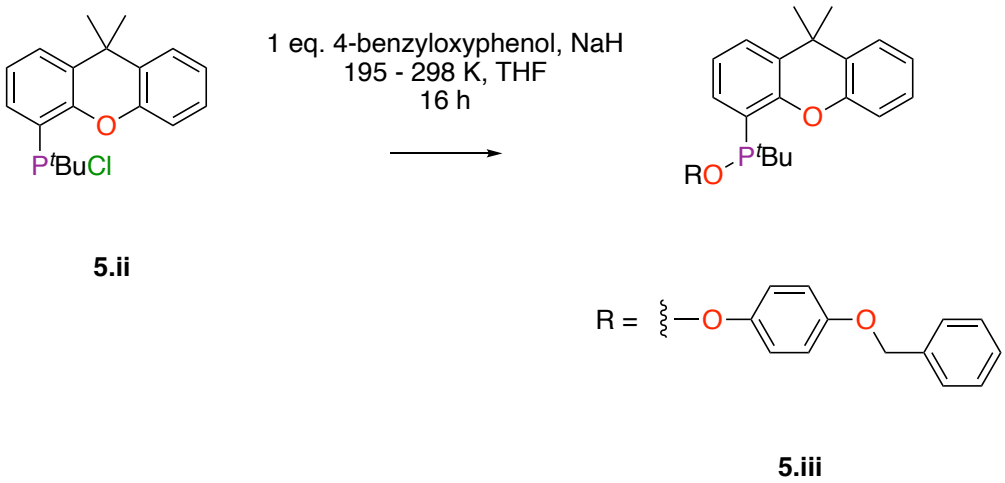

5.ii

5.iii

*Scheme 5.4 – Synthesis of model tethered phosphine **5.iii**.*

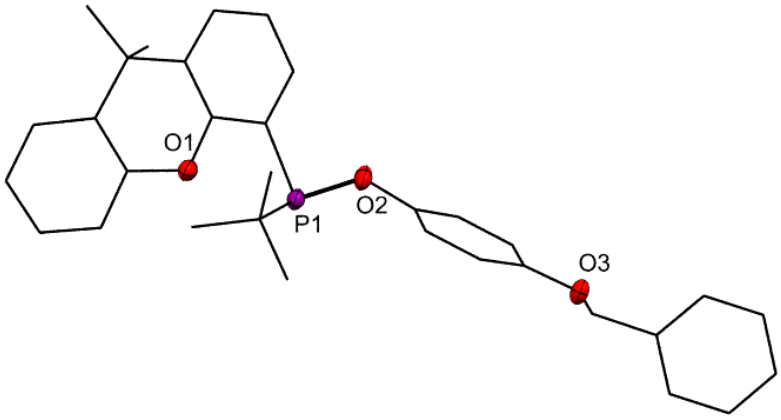

*Figure 5.5 – Molecular structure of **5.iii** as determined by X-ray crystallography. Ellipsoids are shown at 50% probability. Carbon atoms are shown in wireframe format and hydrogen atoms are omitted for clarity.*

Substitution of one of the chloride substituents at the phosphorus centre of complex **5.ii** with an aryloxy group shifts the ^{31}P NMR resonance from 104.0 to 121.5 ppm in **5.iii**. In the ^{1}H NMR spectrum of **5.iii**, the benzyl aliphatic protons give rise to a signal at 4.61 ppm. The xanthene backbone methyl groups are found at 1.41 and 1.39 ppm, and the phosphine *tert*butyl protons give rise to a doublet at 1.28 ppm ($^{3}J_{PH}$ = 12.5 Hz) *i.e.* slightly more shielded than in **5.ii**. Unfortunately, **5.iii** proved not to be amenable to subsequent metalation at the 5-position,

potentially due to the lability of its P—O bond (typical bond enthalpy = 335 kJ mol^{-1} compared to 513 kJ mol^{-1} for P—C).[17] Attempting to prepare an analogous phosphine with a halogen rather than a proton at the 5- position in order to leverage the weaker C—Br bond did not yield the desired compound **5.iii'** (**Figure 5.6**). It should also be noted that the acidic protons at the benzyl position of the aryloxy group might be prone to deprotonation by organolithium reagents.

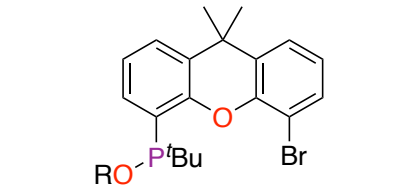

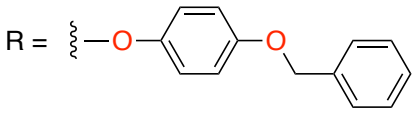

5.iii'

*Figure 5.6 – Desired structure of tethered phosphine **5.iii'**.*

5.3.3 Anisole Tethered Phosphines

Next, systems that resemble remotely tethered supported FLPs were investigated. 4-Lithioanisole was chosen to introduce a model tether, as the methoxy group can be thought of as a simple molecular mimic of a surface positioned remotely from the phosphine. The two routes by which phosphine **5.v** was prepared are summarised in **Scheme 5.5**. The ^{31}P chemical shift is of the product **5.v** is at 3.4 ppm. Within the ^{1}H NMR spectrum, a singlet corresponding to the three methoxy protons is seen at 3.23 ppm. A doublet due to the phosphine *tert*butyl group arises at 1.37 ppm and the protons of the methyl groups in the 9- position on the xanthene backbone give rise to a broad singlet at 1.34 ppm. Spectra of this compound are not well

resolved. The 4-methoxy phenyl group can be incorporated by direct addition of lithioanisole to xanthene chlorophosphine **5.ii** (Method A). This involves lithiation of 4-bromoanisole prior to reaction with **5.ii**. Alternatively, the phosphine PCl(*t*Bu)(C_6H_4OMe) **5.iv** can be constructed prior to reaction with lithiated xanthene (Method B), in a route analogous to **Scheme 5.3**. Method B introduces synthetic challenges associated with the rapid decomposition of **5.iv**, which is an oil highly prone to oxidation. However, the range of possible preparable phosphines of the type **5.iv** from the corresponding dichloroalkyl precursors and *para* functionalised aryls could give rise to a greater range of resultant systems.

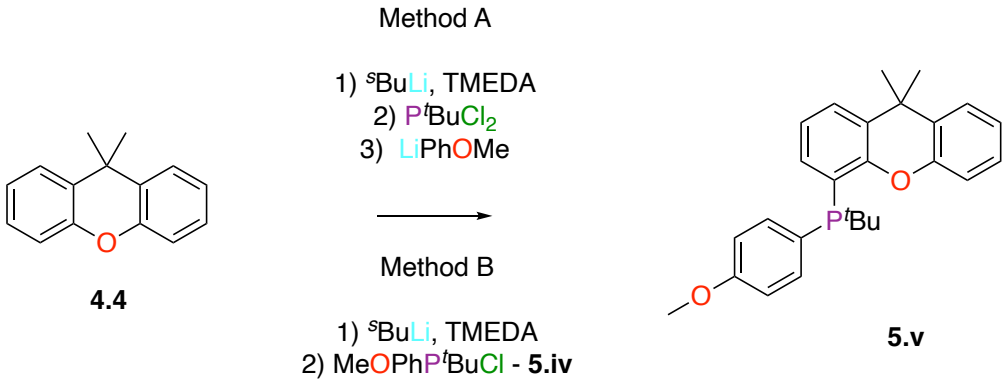

*Scheme 5.5 – Synthesis of methoxyphenol xanthene phosphine **5.v**.*

Lithiation of **5.v** at the 5 position was attempted with *tert*butyllithium. However, no change was observed in the ^{31}P spectrum of this reaction mixture, suggesting that incorporation of the anisole group yields a species which is not amenable to metalation with this reagent. This observation is in keeping with previous work in the Aldridge group, wherein the facility for xanthene-phosphine lithiation is not always predictable. For example, di*iso*propyl and diphenyl phosphine xanthene derivatives lithiates **4.7** and **4.8** are isolable at multi gram scale from protio precursors **4.5** and **4.6**, while the corresponding di*tert*butyl and dimesityl lithiates **5.13** and **5.14** are only attainable from brominated precursors **5.11** or **5.12** and are not isolated but are used *in-situ* for onward chemistry (**Scheme 5.7**).

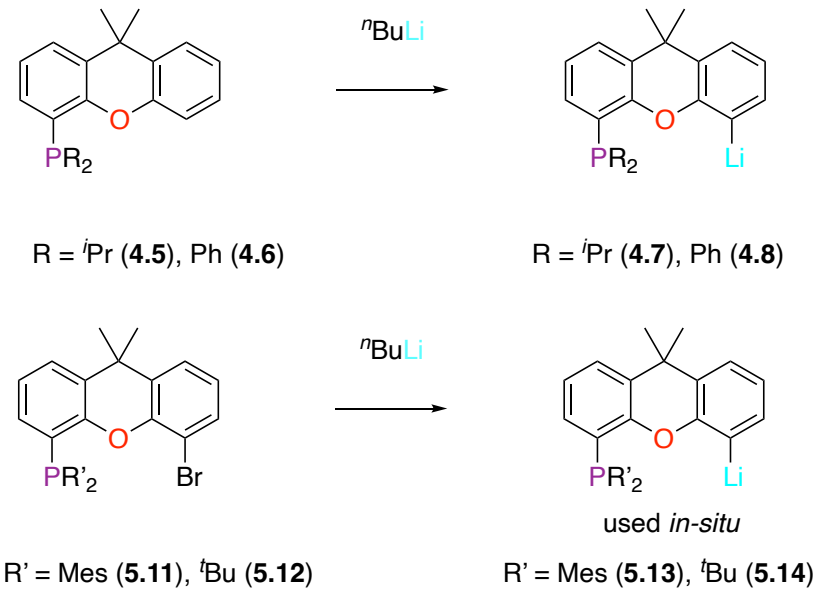

Scheme 5.6 – Isolable and in-situ generated lithiated xanthene phosphines.

The presence or absence of an isolable xanthene phosphine lithiate, such as **4.7** or **4.8**, does not appear to correlate with electron donating ability, but rather more with the steric profile of the substituents at the phosphine. Given the aggregated nature of organolithium reagents, it might be expected that employing an additive, or donor solvent to yield a lower order species would favour the desired lithiation chemistry by allowing the reagent the physical space to react. Moving to reaction conditions that favour lower order butyllithium aggregates e.g. addition of TMEDA, use of THF solvent does not, however, lead to metalation and neither does using a Schlosser's base.

The factors underpinning the relative ease or difficulty of proton/lithium exchange appear non-trivial and exploring routes such as transition metal catalysed C—H activation is outside the remit of this work. It is also difficult to use this approach to introduce electron deficient bulky *bis*aryl boranes to xanthene precursors. Rather, metalation of a weaker bond was sought. The brominated precursors 4,5-dibromo-9,9-dimethylxanthene and 4,5-dibromo-2,7-di*tert*butyl-9,9-dimethylxanthene were prepared *via* literature procedures and employed to prepare

xanthene chlorophosphines **5.vi** and **5.vii** featuring a bromine atom in the 5- position **(Scheme 5.7**).[18] Compound **5.vi** gives rise to a resonance at 103.2 ppm in the ^{31}P NMR spectrum, characteristic of a phosphine bonded to one each of aryl, alkyl and halide substituents.[19–22] X-ray crystallography also confirmed its structure, based on single crystals obtained from sublimation at room temperature under atmospheric pressure of nitrogen (**Figure 5.7**).

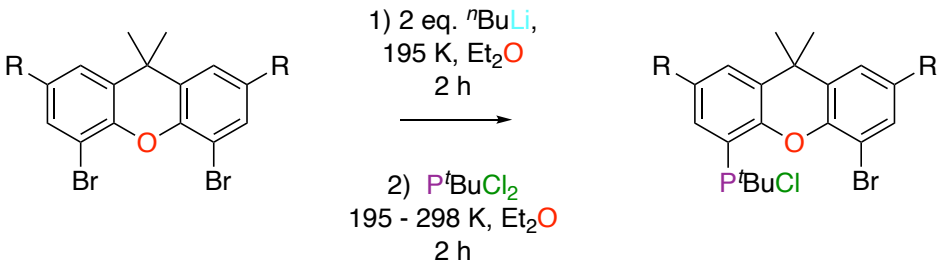

R = H (**5.15**), ^{t}Bu (**5.16**)

R = H (**5.vi** 64 %), ^{t}Bu (**5.vii** 35 %)

*Scheme 5.7 – General synthesis of brominated xanthene chlorophosphine **5.vi** and **5.vii**.*

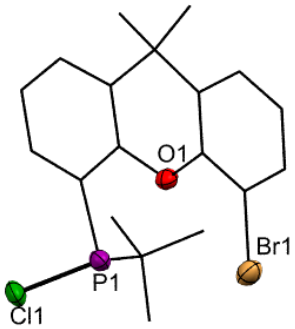

*Figure 5.7 – Molecular structure of **5.vi** as determined by X-ray crystallography. Ellipsoids are shown at 50% probability. Carbon atoms are shown in wireframe format and hydrogen atoms are omitted for clarity.*

The corresponding system **5.vii** featuring tert-butyl groups in the 2- and 7- positions, possesses an essentially identical ^{31}P spectroscopic signature to **5.vi**, and was similarly characterised by X-ray crystallography, using crystals grown from a concentrated hexane solution at -30 °C.

*Tert*butyl groups are associated in these systems with increased solubility, which might explain the comparatively low crystalline yield of **5.vii** (35 %) compared to **5.vi (**64 %**)**.

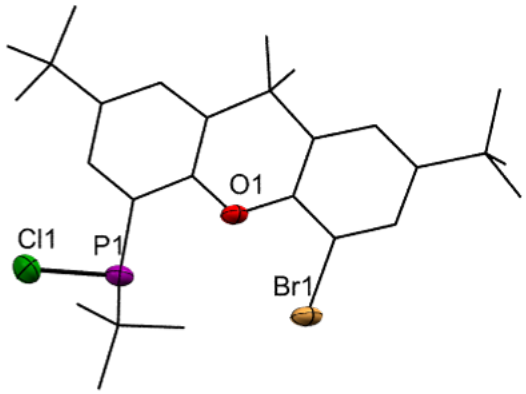

*Figure 5.8 – Molecular structure of **5.vii** as determined by X-ray crystallography. Ellipsoids are shown at 50% probability. Carbon atoms have been shown in wireframe format and hydrogen atoms are omitted for clarity.*

Subsequently, in analogous fashion to the chemistry outlined in **Scheme 5.6**, the syntheses of tethered phosphines **5.viii** and **5.ix** were attempted *via* the reactions of **5.vi** and **5.vii** with 4-lithioanisole.

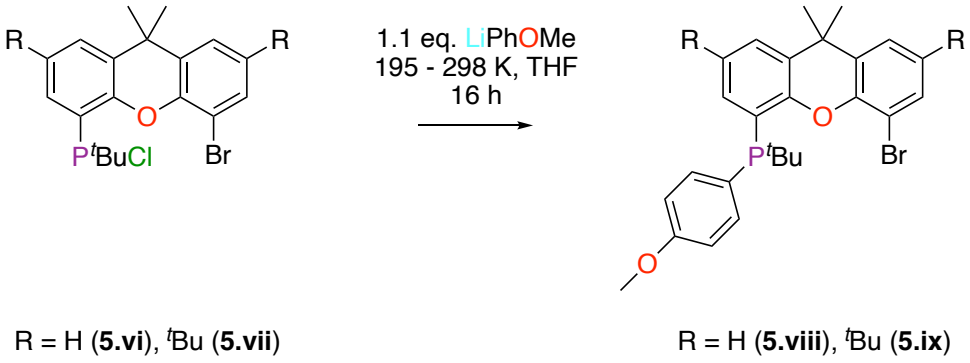

*Scheme 5.8 – Synthesis of methoxyphenol xanthene phosphines **5.viii** and **5.ix**.*

The reaction of **5.vi** with excess 4-lithioanisole to make **5.viii** does not occur in hydrocarbon or non-coordinating solvents and is both unselective and incomplete in ethereal solvents.

The synthesis of **5.ix** from **5.vii** can be inferred by a ^{31}P NMR resonance at 1.0 ppm – in the same region as the species **5.v** (3.4 ppm) which possesses a similar electronic environment about phosphorus. However, the reaction appears to be somewhat unselective, yielding multiple phosphorus-containing products. Purification of this oily mixture was found to be non-trivial, given the similar solubility of all components and the sensitivity of the phosphines to air. The crude yield of **5.ix** was 41 % assuming a density of 1 g cm^{-3}.

Metalation of **5.ix**, either through lithiation or by use of a Grignard proves to be unsuccessful in functionalising the 5 position. Here too, an intractable mixture of products is formed. Previous work in the Aldridge group has described the syntheses of xanthene-based FLPs with *tert*butyl groups in the 2 and 7 positions of the backbone as being far less selective than the unsubstituted analogues.[23] Additionally, recalling the work on derivatising Xantphos at its backbone as (**Section 1.6**), and the lack of success therein, far from being irrelevant, the functional groups in the 2 and 7 positions might have a decisive impact upon reactivity.

An examination of the literature relating to analogous systems reveals that there are numerous reports on the subsequent functionalisation of 9,9-dimethylxanthene bound to a dialkyl or diaryl phosphine.[7,24–28] In contrast, the sole communication of methoxyphenyl xanthene species concerns monodentate phosphine ligands (**Figure 5.9**).[29] Whilst it is possible that this appealing structural motif is coincidentally unexplored, the lack of literature on these systems could point to a synthetic challenge. These observations together indicate that incorporation of an oxygen-containing functional group *para*- to the phosphine yields multiple species which form unselectively and are unstable to the reagents required for addition of a Lewis acid. This underscores the impracticality of protected alcohols in this capacity.

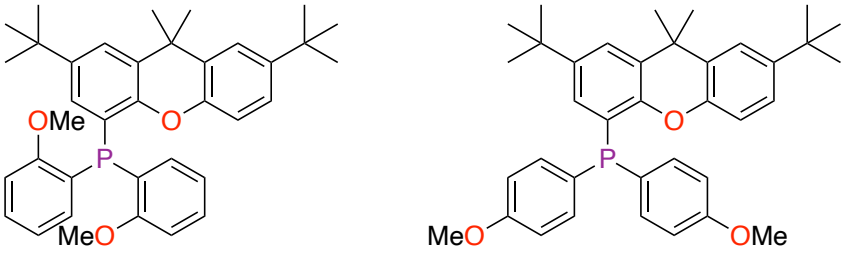

5.17 **5.18**

Figure 5.9 – Methoxyphenyl xanthene phosphines.

5.3.4 Dimethylaniline Tethered Phosphines

It is apparent that despite the literature precedent for alcohols as tethering groups, alternative functionalities might be apposite for the design of the desired FLPs. Within the boundaries of the synthetic chemistry required to subsequently introduce an acid (*i.e.* metalation) finding a functionality with a compatible protecting group is non-trivial. It was posited that instead of a group which must be deconstructed, it might be more facile to use one which can be post modified by protonation or alkylation. Rather than a covalent linker, this would yield a cationic species which could be electrostatically anchored to nanoporous silica (although this would add pH as a variable to be considered).[30] A derivative based on dimethyl aniline was chosen in the place of anisole to give a target phosphine **5.x** (**Figure 5.10**).

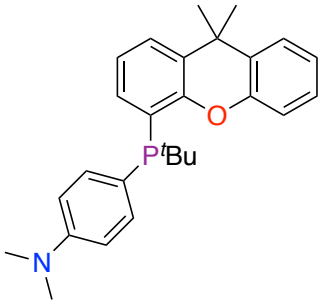

5.x

*Figure 5.10 – Envisaged dimethylaniline phosphine intermediate **5.x**.*

4-Lithio-*N,N*-dimethylaniline can be prepared *via* a modified literature procedure from 4-bromo-lithio-*N,N*-dimethylaniline, and slow addition of this lithiate to **5.ii** produces **5.x** as a viscous brown oil. The product is characterised by a singlet at -2.0 ppm in the ^{31}P NMR spectrum, *i.e.* somewhat upfield when compared to reasonably analogous phosphines such as *tert*butyldiphenylphosphine (17.1 ppm) and 4,4'-*tert*butylphosphinediyl*bisN,N*-dimethylaniline (15.3 ppm) – **Figure 5.11**.[31,32]

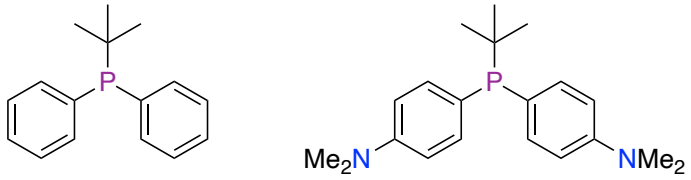

5.19 **5.20**

Figure 5.11 – Tertbutyldiarylphosphines.

The existence of **5.x** is most convincingly proven by its onward reactivity. Compound **5.x** was used without further work-up and lithiated with excess ^{n}BuLi to produce a fine off-white powder **5.xi** (**Scheme 5.9**).

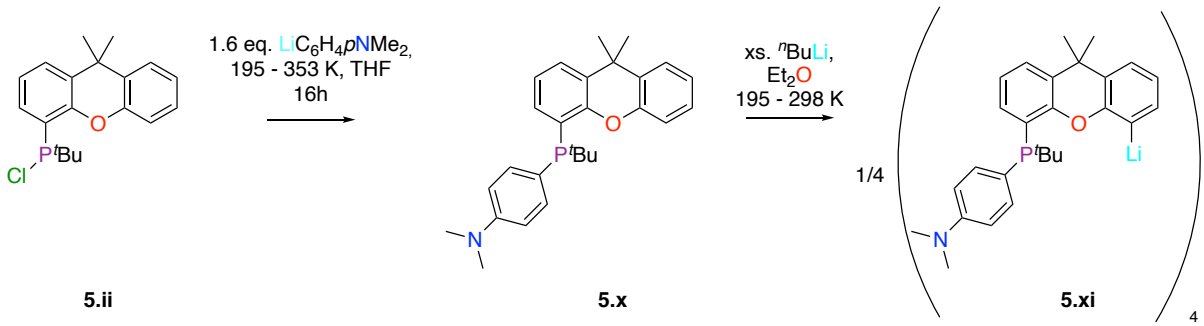

5.ii **5.x** **5.xi**

*Scheme 5.9 – Synthesis of lithiated FLP precursor **5.xi** from **5.ii**.*

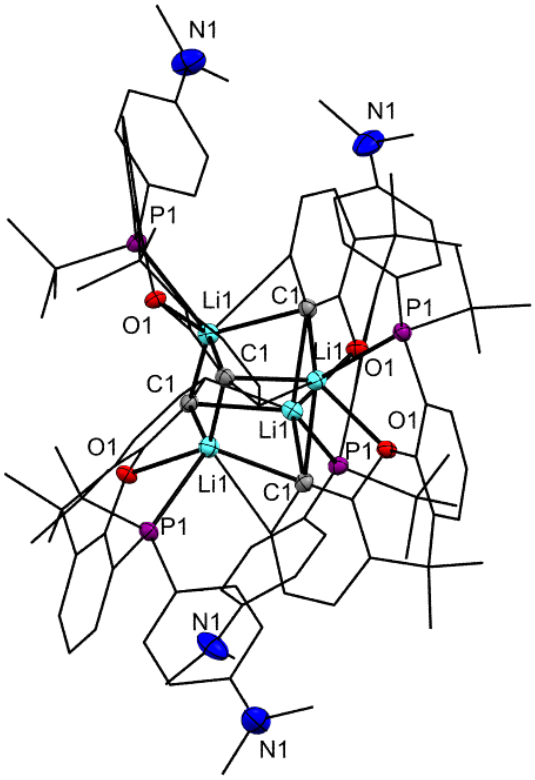

*Figure 5.12 – Molecular structure of **5.xi** as determined by X-ray crystallography. Ellipsoids are shown at 50% probability. Most carbon atoms have been shown in wireframe format and hydrogen atoms are omitted for clarity.*

Compound **5.xi** has been structurally characterised (**Figure 5.12**), using X-ray quality crystals grown from a concentrated benzene solution at room temperature. In the solid state, this complex is tetrameric, with C···Li contacts bridging the four substituted phosphines. In solution, **5.xi** appears to exist in various aggregated forms, as evidenced by two quartets in the ^{31}P NMR spectrum at -15.7 and -26.2 ppm respectively. This phenomenon is seen even in donor solvents, which are commonly used to de-aggregate organolithium reagents.[33] Additionally, the ^{1}H NMR spectrum of a crystalline sample of **5.xi**, redissolved in deuterated benzene, possesses two features, each corresponding to the six protons of the methyl groups at the 9 position of the xanthene backbone, suggesting that two species are present in solution in a 1:1 ratio. The yield of this lithiate from the initial xanthene precursor **4.4** is very low (ca. 20%) due

to the tendency of **5.ii** to sublime during work-up, making this step poorly yielding. This was improved by the preparation of **5.xi** directly from 9,9-dimethylxanthene, without purification of the intermediates. However, this procedure does require a somewhat more involved isolation protocol for **5.xi**, with multiple washes in different hydrocarbon solvents necessary to remove by-products.

5.3.5 Dimethylaniline Tethered FLPs

Compound **5.xi** was reacted with haloborane precursors $ClB(C_6F_5)_2$ **5.21**, $ClB(C_6Cl_5)_2$ **3.5** and $BrB(C_6Cl_5)(C_6F_5)$ **3.vi**, yielding phosphine boranes **5.xii** to **5.xiv** (**Scheme 5.10**). Both **5.21** and **3.5** were prepared *via* literature procedures, and **3.vi** as outlined in Chapter 3.[34,35]

*Scheme 5.10 – Syntheses of **5.xii** – **5.xiv** from **5.xi**.*

The syntheses of **5.xii** and **5.xiii** are both sensitive to solvent; when the reactions are carried out in fluorobenzene, toluene or benzene a mixture of products invariably forms, some of which contain a four-co-ordinate boron centre (as evidenced by ^{11}B NMR spectroscopy). Enhanced solvent polarity might be expected to favour a competing pathway where the borane attacks the Lewis basic dimethylamino nitrogen. The production of FLP **5.xii** through the reaction of

5.xi with $ClB(C_6F_5)_2$ (**5.21**) in hexane at high dilution is suggested by *in-situ* multinuclear NMR spectroscopy. A singlet in the ^{31}P NMR spectrum at -2.5 ppm is in the characteristic region for xanthene-backbone FLPs. A resonance in the ^{11}B NMR spectrum at 53.8 ppm indicates a three-co-ordinate borane function, and there are three resonances in the ^{19}F NMR spectrum of the reaction mixture at -129.0, -145.1 and -160.7 ppm, which can be attributed to **5.xii**. The reduction of the separation between the *ortho*- and *para*- multiplets in the fluorine spectrum compared to the free haloborane is typical of triaryl borane formation.[34] Nonetheless, clean isolation of this compound was not possible in our hands and it does not crystallise.

Compound **5.xiii** was synthesised through the reaction of **5.xi** with $BrB(C_6Cl_5)(C_6F_5)$ (**3.vi**) in toluene, in 50 % yield, and has been spectroscopically characterised. Although no resonance corresponding to the product can be assigned in the ^{11}B NMR spectrum, multiplet resonances at -128.6, -148.1 and -163.1 ppm in the ^{19}F NMR spectrum and a signal at -3.5 ppm in the ^{31}P NMR spectrum are consistent with the expected signals for the reaction product. Additionally, in the aliphatic region of the ^{1}H NMR spectrum, a singlet corresponding to the dimethylamino protons is seen at 2.43 ppm. The protons of the two methyl groups on the xanthene backbone resonate at 1.37 and 1.32 ppm respectively, and those on the *tert*-butyl group of the phosphine give rise to a doublet at 1.17 ppm ($^3J_{PH}$ = 12.5 Hz). In a similar fashion, reaction of **5.xi** with crystalline $ClB(C_6Cl_5)_2$ (**3.5**) occurs cleanly to form **5.xiv** in a range of hydrocarbon solvents, although toluene yields material which gives the best spectroscopic data. The ^{31}P NMR signal for **5.xiv** is observed in the expected region, at -5.3 ppm, although the resonance in the ^{11}B NMR spectrum is too broad to be located. X-ray quality crystals of **5.xiv** were obtained from a concentrated toluene solution stored at room temperature (**Figure 5.13**).

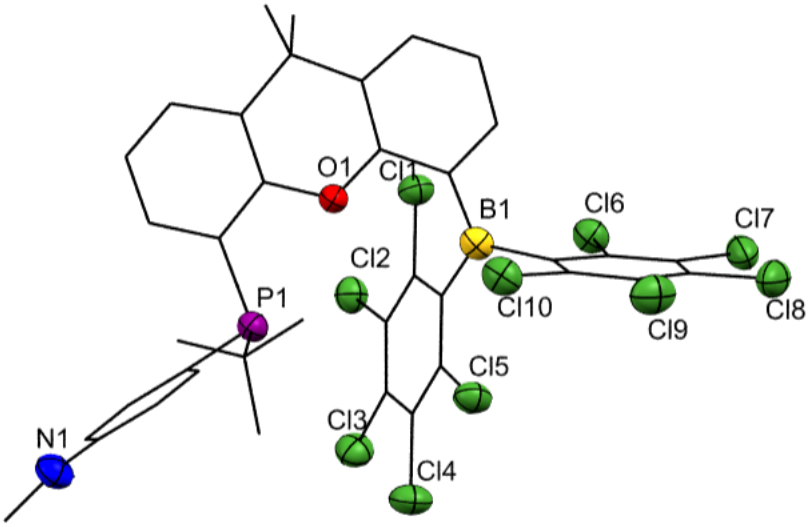

*Figure 5.13 – Molecular structure of **5.xiv** as determined by X-ray crystallography. Ellipsoids are shown at 50% probability. Carbon atoms have been shown in wireframe format and hydrogen atoms are omitted for clarity.*

It appears that the crystallinity conferred by the C_6Cl_5 substituents engenders more facile isolation of these FLPs but comes with a loss of useful ^{11}B spectroscopic data. This observation is in keeping with the multinuclear NMR spectra of perchlorinated FLPs reported in Chapter 4.

With the aim of obtaining a usefully functionalised tether, selective protonation of the dimethylaniline fragment on FLP **5.xiv** was attempted using the anilinium conjugate acid $[PhNHMe_2]Cl$ (**Scheme 5.11**).

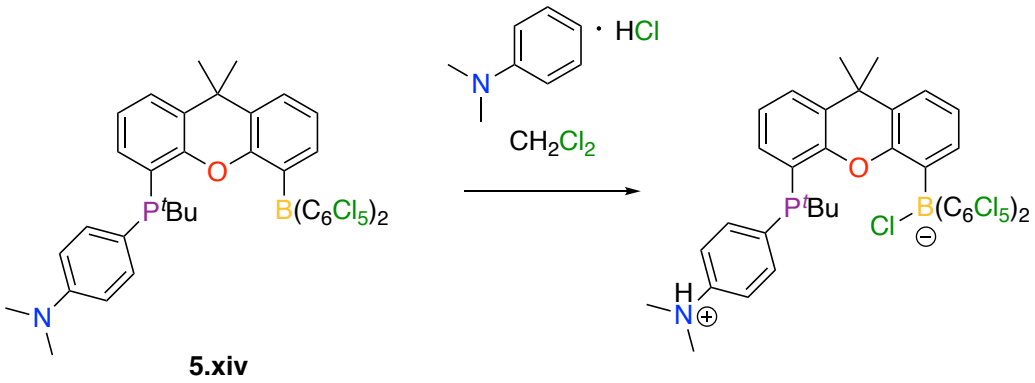

*Scheme 5.11 – Attempted protonation of aniline fragment on **5.xiv**.*

It was envisaged that if this were successful, a weakly coordinating $[B(C_6F_5)_4]^-$ anion would be exchanged in the place of the chloride, with its enhanced steric bulk reducing the likelihood of co-ordination of the liberated anion with the borane.

Unfortunately, this reaction does not yield the desired result – potentially due to a need for more significant discrimination in terms of basicity between the phosphine and amine. The pK_a of the amine is estimated to be around 12, based on the value for $PhNMe_2$ in MeCN.[36] For the phosphine, a reasonably comparable value might be that of Ph_2PMe in MeCN, which is approximately 10. However, the strongly electron donating *tert*-butyl group will elevate the basicity of the phosphine, which could conceivably put it in line with the amine. Similarly, attempted *N*-alkylation with isopropyl iodide or methyl triflate do not yield well a single product in either case.

5.3.6 Reactivity of FLP 5.xiv

As the ability of surface supported FLP systems to activate small molecules is crucial to their application, the reactivity of **5.xiv** was investigated. It was found that a solution of **5.xiv** in toluene reacts with hydrogen at 1 atm. pressure and room temperature (**Scheme 5.12**), as evidenced by an additional resonance in the $^{31}P\{^1H\}$ NMR spectrum at 5.7 in a 1:2 ratio with **5.xiv**, and a sharp peak at -9.7 in the $^{11}B\{^1H\}$ NMR spectrum of the reaction mixture.

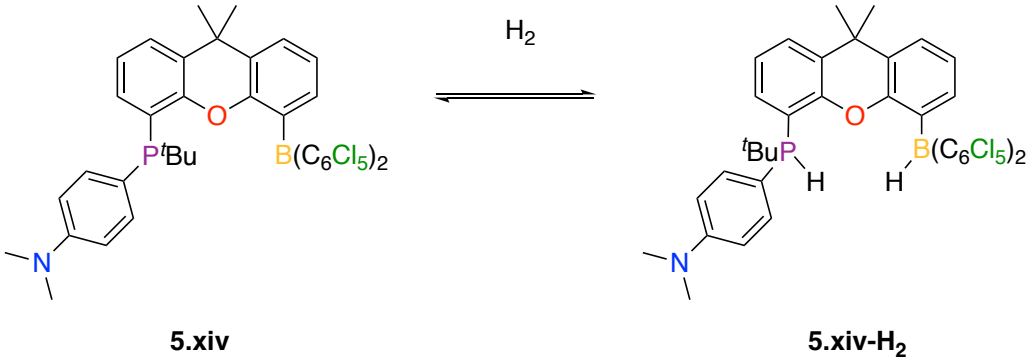

5.xiv **5.xiv-H_2**

*Scheme 5.12 – Hydrogen activation by **5.xiv**.*

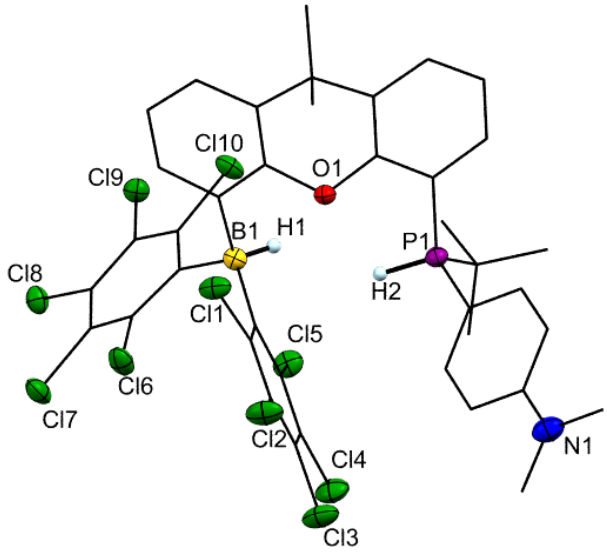

*Figure 5.14 – Molecular structure of **5.xiv-H_2** as determined by X-ray crystallography. Ellipsoids are shown at 50% probability. Carbon atoms are shown in wireframe format and most hydrogen atoms are omitted for clarity.*

The dihydrogen activation product **5.xiv-H_2** could be crystallographically characterised. The hydrogen atoms can be located in the difference map, and there is a characteristic change of geometry around boron corresponding to quaternisation. As such, while in the parent FLP **5.xiv** the average C_{phenyl}—B—$C_{phenyl'}$ bond angle is 119.9(6)°, in the activation product **5.xiv-H_2** the analogous metric is reduced to 113.8(5)°.

We attempted to ascertain whether the reaction of **5.xiv** with dihydrogen to make **5.xiv-H$_2$** is reversible *i.e.* whether it can be probed as an equilibrium between hydrogenated product and parent FLP. However, in contrast to the FLPs discussed in the Chapter 4, isolation of spectroscopically pure **5.xiv** is challenging. Also, upon introduction of hydrogen, multiple new products are observed in the ^{31}P NMR spectrum, which does not allow for a meaningful comparison of equilibrium concentrations by variable temperature NMR spectroscopy. This might be attributed, at least in part, to the stability of **5.xiv**; over the course of ca. 2 h in a sealed Youngs tap NMR tube, decomposition to around 8% protio precursor **5.x** is observed. Indeed, over the course of 72 h compound **5.xiv** decomposes almost entirely. Mitigation was attempted by re-examining conceivable routes for the entrance of air and moisture, such as wet solvent and glassware, all to no avail.

All further reactivity with **5.xiv** was conducted *in situ* from the reaction mixture. Reaction of this compound with N_2O or CO_2 instantaneously yielded crystalline products of unknown species in each case. In the reaction with N_2O, a new resonance in the ^{11}B NMR spectrum of the reaction mixture is observed at 2.8 ppm. This suggests an activation product on the basis of comparison with reactions of FLPs with N_2O (^{11}B resonance shift from 64.4 to 4.3 for reaction of FLP **1.55** with N_2O – **Scheme 5.13**).

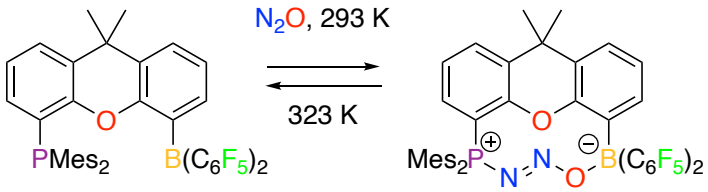

Scheme 5.13 – Previously reported FLP which reversibly forms a complex with N_2O.

In the case of the reaction with CO_2, no reaction can be observed by NMR spectroscopy. The crystalline products of both reactions do not yield structural solutions sufficient for even confirmation of connectivity.

5.3.6 Targeting a Dimethylbenzylamine Phosphine

In light of fruitless attempts to synthesise an ammonium cation from **5.xiv**, a more basic amine with a similar structure was sought, such as dimethylbenzylamine. 4-Lithio-dimethylbenzylamine was prepared by a modified literature procedure and added to **5.ii**. The phosphine product **5.xv** is a viscous brown oil, so it was used without purification, with conversion evidenced by a singlet in the ^{31}P NMR spectrum at 5.2 ppm. Reaction of **5.xv** with an excess of ^{t}BuLi did not solely give the xanthene phosphine lithiate **5.xvi**. The ^{31}P NMR spectrum becomes very poorly resolved, with additional resonances at -1.6 and -57.8 ppm.

The desired reaction is a metalation directed by the central xanthene oxygen to give product **5.xvi**, as illustrated in **Scheme 5.13**. It is possible that the benzylic protons adjacent to the tertiary amine group are of comparable acidity to that at the 5 position on xanthene, making this undesired side reaction competitive. Although the pK_a of aliphatic protons tends to be around 50 whereas aromatic pK_a values lie closer to 40, proximity to the electronegative nitrogen atom could inductively stabilise the conjugate base when a proton on the carbon adjacent to the dimethylamine group is lost.[37]

Metalation is, likewise, unsuccessful with the brominated analogues.

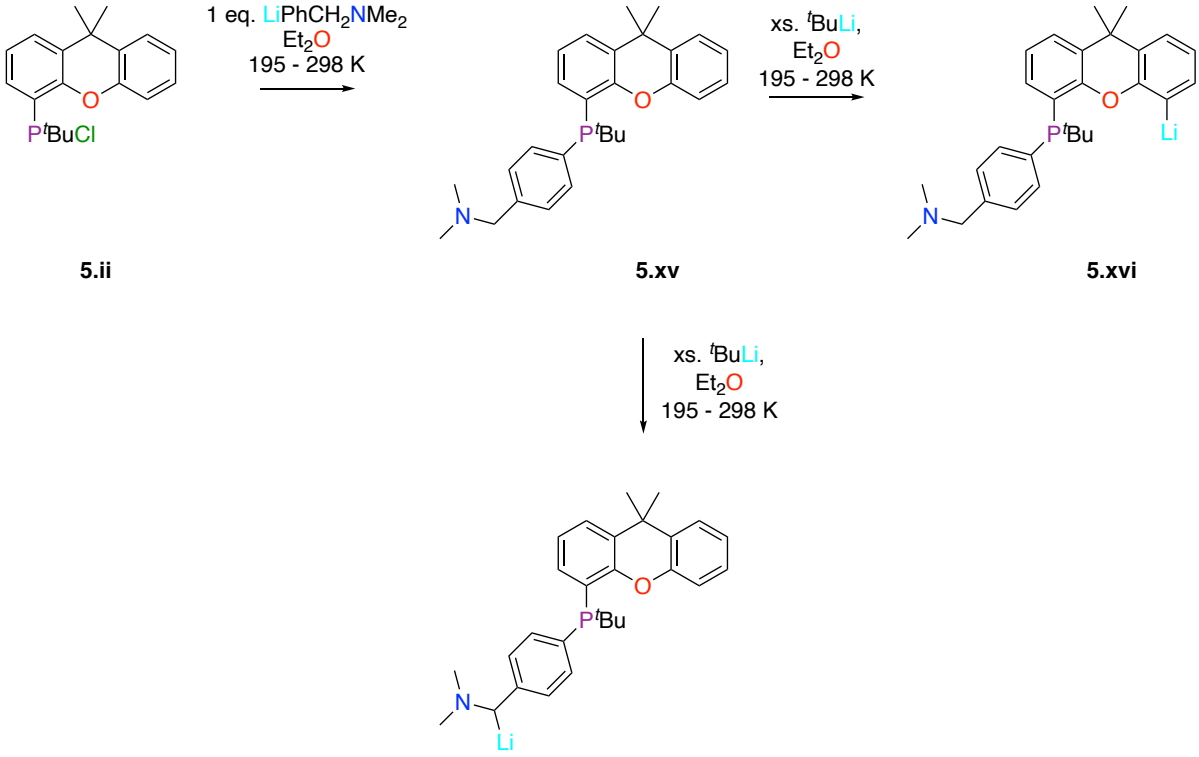

*Scheme 5.14 – Desired metalation of **5.xv** and proposed competing route.*

5.4 Conclusions

This chapter has primarily concerned the synthesis of xanthene-substituted phosphines incorporating either adjacent or remote tethering groups for attachment to a surface support. These species have been investigated with respect to their use as precursors for Frustrated Lewis Pairs. In terms of xanthene substituted phosphines with a direct bond to a leaving group, the third substituent have an appropriate steric profile in order to kinetically inhibit the co-ordination of more than one xanthene substituent, as seen in the structure of **5.i** versus **5.ii**.

Compound **5.ii** was used to prepare the benzyloxyphenol tethered phosphine **5.iii**, which did not react further *via* metalation. Due to concerns about the P—O electronic relationship altering reactivity by the aryloxy failing to act as an electron donating substituent, this tethering group was not explored further.

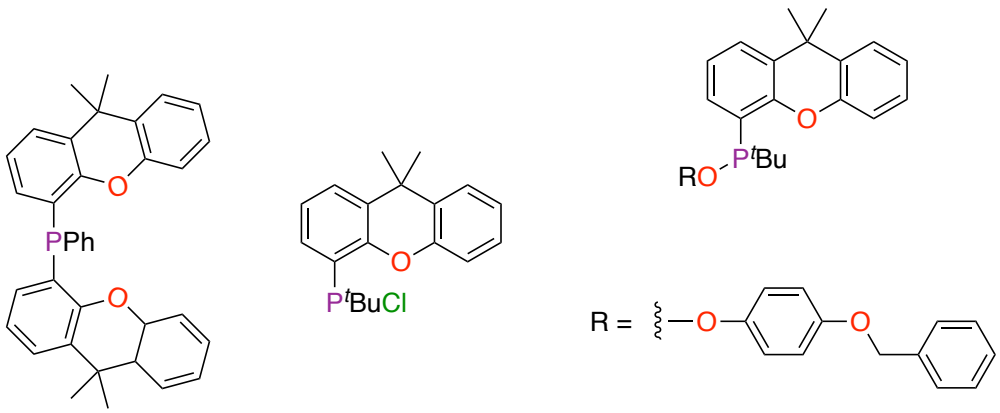

5.i **5.ii** **5.iii**

*Figure 5.15 – Phosphines **5.i - 5.iii**.*

A range of *tert*-butylated phosphines (**5.ii**, **5.vi** and **5.vii**) were prepared by substitution of the 4 position on xanthene, 4,5-dibromo 9,9-dimethylxanthene or 4,5-dibromo 2,7-di*tert*butyl-9,9-dimethylxanthene with dichlorophenylphosphine. Their structural similarities are useful in understanding the factors underpinning further reactivity. The synthesis of **5.v** was trialled by

two methods – from **5.ii** and 4-lithioanisole (Method A) or xanthene and **5.iv** (Method B). The second route was abandoned due to difficulties in handling and storage of **5.iv**. Method A was attempted to prepare **5.viii** and **5.ix** from **5.vi** and **5.vii** respectively, with limited success. Further work in this direction might therefore revisit pre-construction of phosphines. The properties of phosphines possessing substituents with greater structural complexity than anisole or might lend themselves to more facile synthesis.

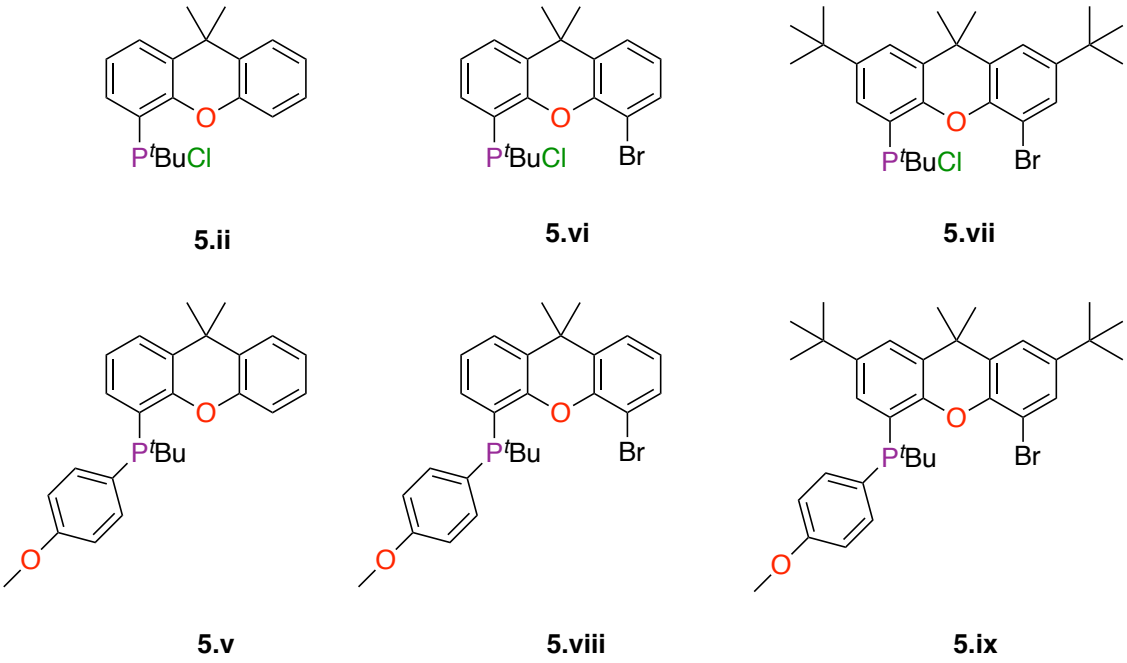

Figure 5.16 – Phosphines and their corresponding anisole tethered species.

In the case of **5.v**, the ethereal *para* group appears to have deactivated the next position to be functionalised on the xanthene ring. This stands in stark contrast to a tertiary amine functionality (**5.x**) where subsequent lithiation to form **5.xi** is facile.

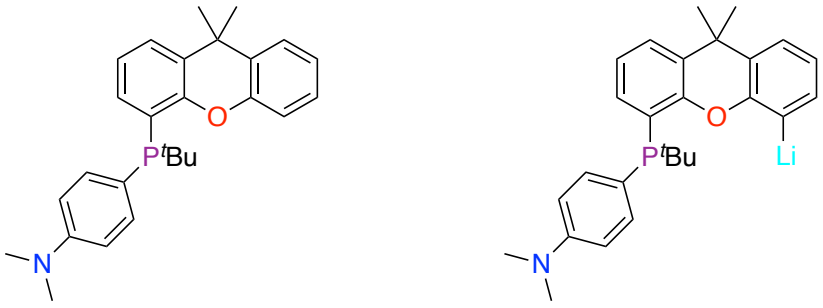

5.x **5.xi**

*Figure 5.17 – Phosphines **5.x** and **5.xi**.*

Looking at the *para* substituent constants (o_p)[1] for these functional groups (-0.830 for dimethylamino versus -0.268 for methoxy), the possibility exists that this could be the decisive factor in ease of further metalation.[38] This hypothesis could be tested by synthesising other phosphines with alternative *para* substituents. If facility for backbone lithiation is determined by this substituent constant, phenyls functionalised in this manner are likely unsuitable for this type of chemistry as most alternative groups possess an o_p value more positive than methoxy.

Phosphine compound **5.xi** was used to prepare FLPs **5.xii** – **5.xiv**.

[1] Substituent constant o is a measure of the electronic effect of replacing H by a given substituent.[39]

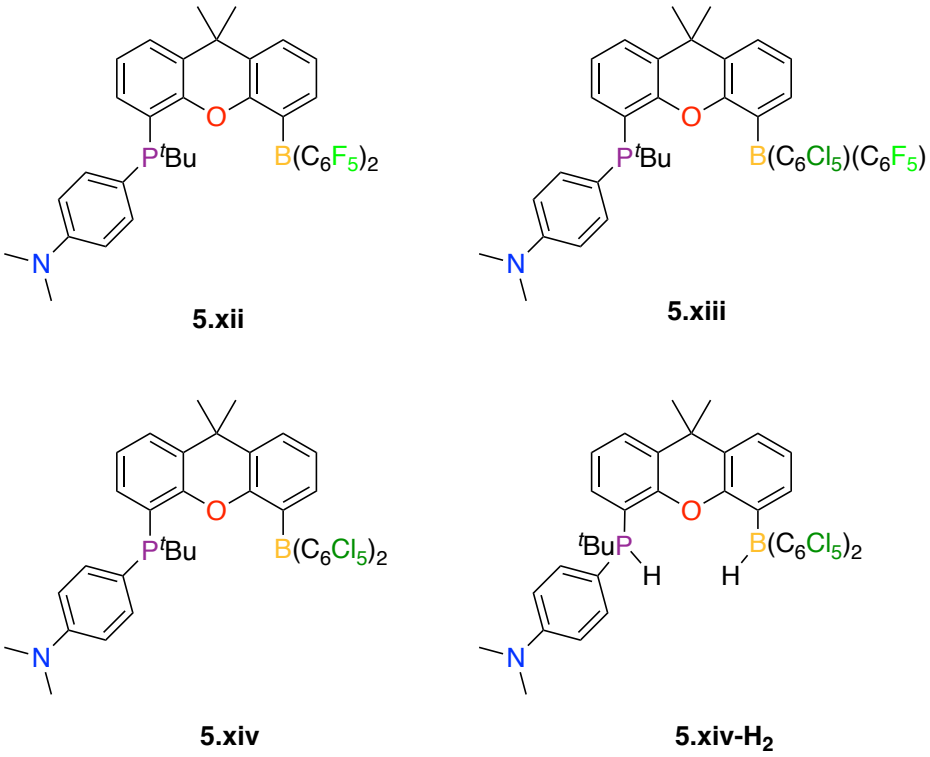

*Figure 5.18 – FLPs **5.xii** - **5.xiv** and H_2 activation product **5.xiv-H$_2$**.*

Having made these species, next steps should involve examining their reactivity. It would be interesting to look at any hydrogenation equilibrium via NMR spectroscopy in the same manner to Chapter 4, to see if a similar mechanistic probing is possible. The preparation of a hydrogen activation product **5.xiv-H$_2$** is encouraging, especially in the context of delivery to unsaturated small molecules. Due to difficulties in handling and storage, future work should first establish a means of obtaining clean material for a sufficient period to conduct reactivity studies.

It appears that incorporating a benzylic amine as a substituent on the phosphine (**5.xv**) acidified the adjacent carbon to nitrogen such that further reactivity at this point was competitive.

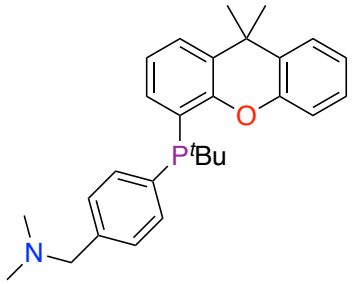

5.xv

*Figure 5.19 – Benzyl amine tethered phosphine **5.xv**.*

5.5 Synthetic Procedures and Spectroscopic Data for New Compounds

5.i - *Bis*(9,9-dimethyl-xanthen-4-yl)phenylphosphine

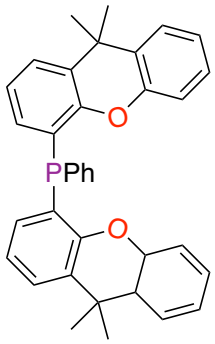

5.i

N,N,N,N,-tetramethylethylenediamine (3.6 mL, 23.75 mmol, 1 equiv.) was added to a solution of 9,9-dimethylxanthene (5g, 23.75 mmol, 1 equiv.) in Et_2O (50 mL) and cooled to -78 °C. ^{s}Buli (17 mL, 23.75 mmol of 1.4 M in cyclohexane, 1 equiv.) was added dropwise and the reaction mixture was warmed to room temperature then stirred for 16 h. The resulting suspension was cooled to -78 °C and neat $PhPCl_2$ (3.2 mL, 23.75 mmol, 1 equiv.) was added dropwise. After warming immediately to room temperature, the mixture was stirred for 16 h before volatiles were removed *in vacuo*. Extraction into Et_2O (30 mL) yielded crystals suitable

for X-ray structural determination. Yield: 2.6 g (42.5%). Anal calcd for $C_{36}H_{31}O_2P$ C: 82.11 H: 5.93. Found: C: 82.01 H: 6.04. ^{1}H NMR (500 MHz, C_7D_8) δ 7.61 – 7.54 (m, 2H, Ar*H*), 7.14 (dt, *J* = 7.8, 1.1 Hz, 2H, Ar*H*), 7.12 – 6.96 (m, 8H, Ar*H*), 6.85 – 6.75 (m, 3H, Ar*H*), 6.74 – 6.66 (m, 2H, Ar*H*), 1.40 (d, 6H, *J* = 12.1 Hz, XAN*CH*$_3$), 1.37 (d, 6H, *J* = 25.2 Hz, XAN*CH*$_3$). ^{13}C {^{1}H} NMR (126 MHz, C_7D_8) δ 152.8 (d, *J* = 15.0 Hz), 150.8, 134.5, 134.3, 132.0 (d, *J* = 4.5 Hz), 130.4, 130.2, 128.8, 128.4, 127.9, 127.1, 126.3, 125.1, 123.3, 123.1, 116.7 (Ar*C*), 34.2, 31.3, 30.9. ^{31}P NMR {^{1}H} (243 MHz, C_7D_8) δ -22.8.

5.ii - *Tert*-butylchloro(9,9-dimethyl-xanthen-4-yl)phosphine

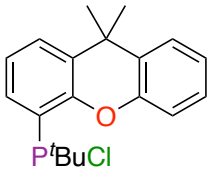

5.ii

N,N,N,N,-tetramethylethylenediamine (2.8 mL, 19 mmol, 1 equiv.) was added to a solution of 9,9-dimethylxanthene (4g, 19 mmol, 1 equiv.) in Et_2O (50 mL) and cooled to -78 °C. ^{s}Buli (13.6 mL, 19 mmol, 1 equiv. of a 1.6 M solution) was added dropwise and the reaction mixture was warmed to room temperature then stirred for 16 h. The suspension was cooled to -78 °C and a hexane (20 mL) solution of ^{t}BuPCl$_2$ (3 g, 19 mmol, 1 equiv.) was then added dropwise. After warming immediately to room temperature, the mixture was stirred for 16 h before extraction into hexane (30 mL) followed by crystallisation of **5.ii** in dichloromethane at -30 °C. Yield = 2 g, 32% Anal calcd for $C_{19}H_{22}ClOP$ C: 68.57 H: 6.66. Found: C: 68.51 H: 6.73 ^{1}H NMR (400 MHz, C_6D_6) δ 7.79 (ddd, *J* = 7.6, 3.5, 1.6 Hz, 1H), 7.11 (dt, *J* = 7.7, 1.9 Hz, 2H), 7.03 (dd, *J* = 8.0, 1.5 Hz, 1H), 6.98 – 6.87 (m, 3H), 1.33 (d, *J* = 15.3 Hz, 6H, XAN-CH_3), 1.13

(d, J = 13.1 Hz, 9H, ^{t}Bu-*CH*$_3$). ^{13}C{^{1}H} NMR (101 MHz, C_6D_6) δ 153.0, 152.8, 150.5, 131.3, 130.5, 130.5, 126.0, 124.0, 123.9, 123.5, 123.4, 116.7, (Ar*C*) 35.5 (d, J = 32.8 Hz, ^{t}Bu*C*), 34.4, (XAN*C*) 31.7 (d, J = 41.1 Hz, XAN*CH*$_3$), 25.9 (d, J = 17.2 Hz, ^{t}Bu*CH*$_3$). ^{31}P{^{1}H} NMR (162 MHz, C_6D_6) δ 104.3.

5.iii - *Tert*-butyl(9,9-dimethyl-xanthen-4-yl)(4-methoxyphenyl)phosphine

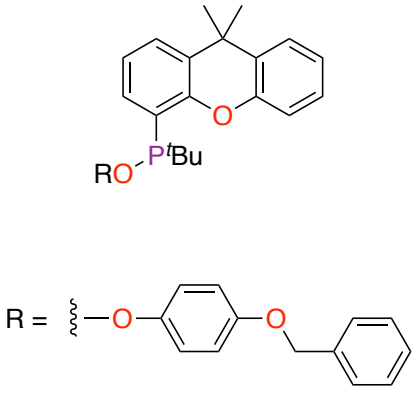

5.iii

4-Benzyloxyphenol (750 mg, 3.75 mmol, 1 equiv.) was dissolved in THF (25 mL) and cooled to -78 °C. A solution of NaH (90 mg, 3.75 mmol, 1 equiv.) in THF (40 mL) was added dropwise and the resulting pale blue suspension warmed to room temperature and stirred for 16 h. After again cooling to -78 °C, a solution of **5.ii** (1.25 g, 3.75 mmol, 1 equiv.) in THF (20 mL) was added dropwise. After warming rapidly to room temperature, **5.iii** was extracted into pentane from which it instantaneously crystallised. Yield = 1.45 g, 78 % Anal calcd for $C_{32}H_{33}O_3P$ C: 77.40 H: 6.70. Found C: 77.56 H: 6.89. ^{1}H NMR (400 MHz, C_6D_6) δ 7.73 (ddd, J = 7.4, 3.3, 1.6 Hz, 1H, Ar*H*), 7.25 – 6.94 (m, 10H, Ar*H*), 6.90 (td, J = 7.5, 1.4 Hz, 1H, Ar*H*), 6.76 – 6.68 (m, 2H, Ar*H*), 4.61 (s, 2H, Bn*H*), 1.40 (d, J = 11.1 Hz, 6H, XAN*CH*$_3$), 1.28 (d, J = 12.4 Hz, 9H, ^{t}Bu*CH*$_3$). ^{31}P{^{1}H} NMR (162 MHz, C_6D_6) δ 121.0.

5.iv - *Tert*-butylchloro(4-methoxyphenyl)phosphine

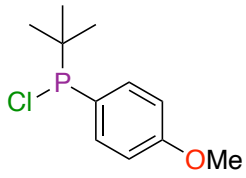

5.iv

A solution of chloro-diethylamino-tertbutyl phosphine (3.5 g, 17.9 mmol, 1 equiv.) in THF (40 mL) was added dropwise to a THF (20 mL) solution of 4-lithio-anisole (2.58g, mmol, 1.1 equiv.) at 0 °C. After warming to room temperature, the reaction mixture was stirred for 16 h. After cooling again to 0 °C an ethereal solution of HCl (18 mL, 36 mmol, 2 equiv. of a 2 M solution) was added. The reaction mixture was warmed to room temperature and stirred for 2 h before half of the solvent was removed *in vacuo*. The resulting suspension was filtered and extracted into diethyl ether. After being filtered once more, volatiles were removed *in vacuo* to yield a colourless oil which was used without further purification. Yield: 2 mL, 48 %. ^{1}H NMR (400 MHz, C_6D_6) δ 7.52 (dd, *J* = 8.9, 7.8 Hz, 2H, Ar*H*), 6.69 (d, *J* = 8.1 Hz, 2H, Ar*H*), 3.24 (s, 3H, OMe*CH*$_3$), 0.98 (d, *J* = 13.6 Hz, 9H, ^{t}Bu*CH*$_3$). ^{31}P{^{1}H} NMR (162 MHz, C_6D_6) δ 110.3.

5.vi - 5-bromo-9,9-dimethyl-xanthen-4-yl(*tert*-butyl)chlorophosphine

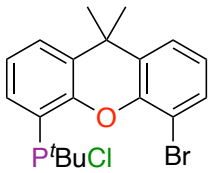

5.vi

4,5-dibromo-9,9-dimethylxanthene (1.89 g, 5.13 mmol, 1 equiv.) was slurried in Et_2O (25 mL) and cooled to -78 °C. ^{n}BuLi (3.2 mL, 5.13 mmol, 1 equiv. of a 1.6 M solution) was added dropwise. The reaction mixture was warmed to room temperature then stirred for 2h. The

resulting suspension was cooled to -78 °C and an ethereal (20 mL) solution of ^{t}BuPCl$_2$ (816 mg 5.13, 1 equiv.) added dropwise. This mixture was warmed to room temperature immediately and stirred for 16 h before the product was filtered and volatiles removed *in vacuo*. **5.vi** crystallised through sublimation at ambient pressure under a nitrogen atmosphere over the course of 48h. Yield: 1.35 g, 64 %. Anal calcd for $C_{19}H_{21}BrClOP$ C: 55.38 H: 5.10. Found: C: 55.30 H: 6.02 ^{1}H NMR (400 MHz, C_6D_6) δ 7.81 – 7.76 (m, 1H, Ar*H*), 7.27 (dd, *J* = 7.9, 1.4 Hz, 1H, Ar*H*), 7.05 – 7.00 (m, 1H, Ar*H*), 6.94 – 6.85 (m, 2H, Ar*H*), 6.54 (t, *J* = 7.9 Hz, 1H, Ar*H*), 1.27 – 1.17 (m, 16H, XAN-*CH$_3$* and ^{t}Bu-*CH$_3$*). ^{13}C{^{1}H} NMR (101 MHz, C6D6) δ 152.3, 152.1, 147.6, 132.1, 131.8, 131.6, 129.8, 127.9, 125.0, 124.4, 123.9, 111.3 (Ar*C*), 35.9 (d, *J* = 33.3 Hz, ^{t}Bu*C*), 34.8 (XAN-*C*), 33.6 (XAN*CH$_3$*), 30.1 (XAN*CH$_3$*), 25.9 (d, *J* = 17.2 Hz, ^{t}Bu*CH$_3$*) ^{31}P{^{1}H} NMR (162 MHz, C_6D_6) δ 103.2.

5.vii - 5-bromo-2,7-di-*tert*-butyl-9,9-dimethyl-xanthen-4-yl(*tert*-butyl)chlorophosphine

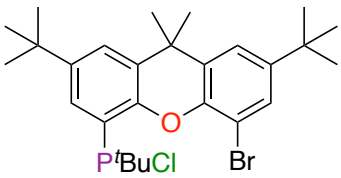

5.vii

4,5-dibromo-2,7-di*tert*butyl-9,9-dimethylxanthene (3g, 6.25 mmol, 1 equiv.) was slurried in Et_2O (50 mL) and cooled to -78 °C. ^{n}BuLi (3.9 mL, 6.25 mmol, 1 equiv. of a 1.6 M solution) was added dropwise. The reaction was warmed to room temperature and stirred for 2 h. The resulting suspension was cooled to -78 °C and a hexane (20 mL) solution of ^{t}BuPCl$_2$ (1.086g, 6.25 mmol, 1 equiv.) added dropwise. The reaction mixture was warmed to room temperature immediately and stirred for 16 h before **5.vii** was extracted into hexane, from which it crystallised at -30 °C. Yield: 1.15 g, 35%. Anal calcd. for $C_{27}H_{37}BrClOP$ C: 61.84 H: 7.06

Found: C: 61.05 H: 5.50. ^{1}H NMR (400 MHz, C_6D_6) δ 8.03 (dd, *J* = 3.4, 2.3 Hz, 1H, Ar*H*), 7.54 (d, *J* = 2.2 Hz, 1H, Ar*H*), 7.42 (d, *J* = 2.3 Hz, 1H, Ar*H*), 7.27 (d, *J* = 2.2 Hz, 1H, Ar*H*) 1.46 (s, 3H, XAN*CH₃*), 1.40 (s, 3H, XAN*CH₃*), 1.31 (s, 9H, ^{t}Bu*CH₃*), 1.28 (d, *J* = 13.0 Hz, 9H, ^{t}Bu*CH₃*), 1.13 (s, 9H, ^{t}Bu*CH₃*).^{31}P{^{1}H} NMR (162 MHz, C_6D_6) δ 103.2.

General Procedure for the synthesis of anisole tethered phosphines

A solution of the requisite chlorophosphine (0.96 mmol, 1 equiv.) in THF (20 mL) was cooled to -78 °C and a solution of 4-lithio-anisole (120 mg, 1.05 mmol, 1.1 equiv.) in THF (20 mL) was added dropwise. The resulting mixture was warmed to room temperature immediately and stirred for 16 h before the product was extracted into hexane to yield an oil in all cases, which was used assuming quantitative conversion.

5.v - *Tert*-butyl(9,9-dimethyl-xanthen-4-yl)(4-methoxyphenyl)phosphine

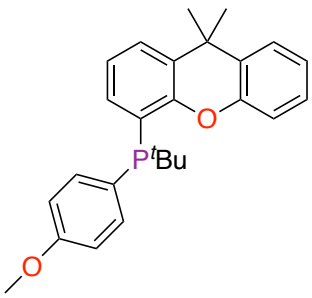

5.v

^{1}H NMR (400 MHz, C_6D_6) δ 7.64 (dd, *J* = 8.9, 6.9 Hz, 1H, Ar*H*), 7.56 (ddd, *J* = 7.5, 3.2, 1.5 Hz, 1H, Ar*H*), 7.11 (dd, *J* = 7.7, 1.7 Hz, 1H, Ar*H*), 7.01 – 6.84 (m, 6H, Ar*H*), 6.70 (d, *J* = 7.9 Hz, 2H, Ar*H*), 3.23 (s, 3H, OMe*CH₃*), 1.37 (d, *J* = 2.6 Hz, 9H, ^{t}Bu*CH₃*), 1.34 (s, 6H, XAN*CH₃*) ^{31}P NMR (162 MHz, C_6D_6) δ 3.4. Yield = 0.26 mL, 68 %

5.ix - *Tert*-butyl(5-bromo-2,7-di-*tert*-butyl-9,9-dimethyl-xanthen-4-yl)(4 methoxyphenyl)phosphine

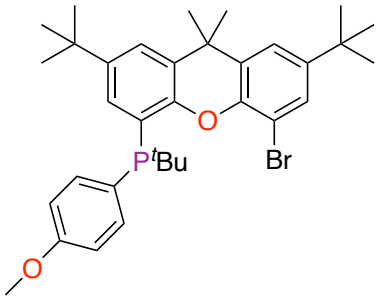

5.ix

Yield: 0.23 mL, 41 %. ^{31}P NMR (162 MHz, C_6D_6) δ 1.0.

5.x - *Tert*-butyl(9,9-dimethyl-xanthen-4-yl)phosphaneyl)-*N*,*N*-dimethylaniline

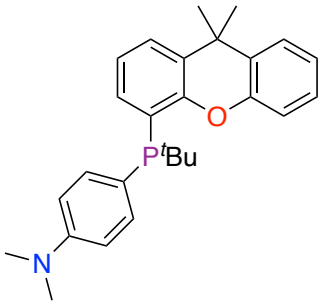

5.x

5.ii (3 g, 9 mmol, 1 equiv.) was dissolved in THF (25 mL) and cooled to -78 °C. 4-lithioaniline (2.21 g, 14.4 mmol, 1.6 equiv.) in THF (20 mL) was then added dropwise. The reaction mixture was then heated to 80 °C for 16 h. Following the removal of volatiles *in vacuo*, the resultant oil **5.x** was frozen in liquid nitrogen and dried under dynamic vacuum a further three times before being used assuming quantitative conversion $^{31}P\{^1H\}$ NMR (162 MHz, C_7H_8) δ 2.41.

5.xi - *tert*-butyl(4-(dimethylamino)phenyl)phosphaneyl)-9,9-dimethyl-xanthen-4-yl)lithium

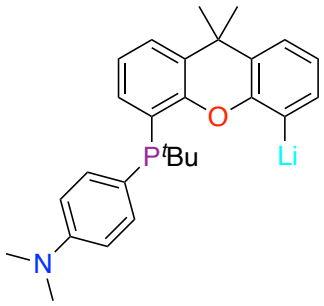

5.xi

5.x was dissolved in Et_2O (40 mL) and ^{n}BuLi (9.4 mL, 15 mmol, 1.7 equiv.) added dropwise at -78 °C. The reaction mixture was immediately warmed to room temperature and stirred for 24 h. **5.x** precipitated out from hexane (50 mL) at -30 °C and was isolated by filtration. Washing with cold (-78 °C) hexane until washes ran clear yielded a fine white powder which was recrystallised from toluene at -30 °C. Yield: 763 mg, 20 %. ^{1}H NMR (400 MHz, C_6D_6) δ 8.12 (d, *J* = 6.5 Hz, 1H), 7.69 – 7.61 (m, 1H, Ar*H*), 7.53 (dt, *J* = 7.6, 2.3 Hz, 1H, Ar*H*), 7.22 (d, *J* = 8.6 Hz, 1H, Ar*H*), 7.14 – 6.97 (m, 8H, Ar*H*), 6.65 – 6.56 (m, 1H, Ar*H*), 6.55 – 6.43 (m, 2H), Ar*H*) 2.59 – 2.51 (m, 6H, NMe$_2$*CH$_3$*), 1.93 (d, *J* = 8.2 Hz, 3H, XAN*CH$_3$*), 1.51 (s, 3H, XAN*CH$_3$*), 0.96 – 0.84 (m, 9H, ^{t}Bu*CH$_3$*). ^{7}Li NMR (156 MHz, C_6D_6) δ 3.6 (td, *J* = 28.6, 8.4 Hz), 2.03. ^{31}P{^{1}H} NMR (162 MHz, C_6D_6) δ -15.7 (dd, *J* = 56.2, 28.2 Hz), -26.2 (dd, *J* = 59.5, 29.7 Hz).

General procedure for the synthesis of FLPs 5.xii – 5.xiv

5.xi (200 mg, 0.47 mmol, 1 equiv.) was dissolved in toluene (20 mL) and the solution cooled to -78 °C. The respective haloborane (0.47 mmol, 1 equiv.) was dissolved in toluene (20 mL) and added dropwise. The resulting suspension was warmed to room temperature whereupon it

turned bright yellow. After stirring for 16 h, the product was isolated by filtration and volatiles removed *in vacuo*.

5.xii - *Bis*pentafluoro-borane-9,9-dimethyl-xanthen-4-yl)(*tert*-butyl)phosphineyl)-*N*,*N*-dimethylaniline

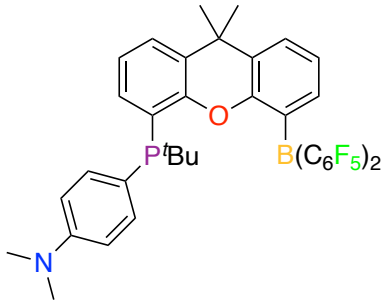

5.xii

$^{11}B\{^1H\}$ NMR (128 MHz, C_6D_6) δ 53.8. $^{19}F\{^1H\}$ NMR (377 MHz, C_6D_6) δ -128.6 to -129.3 (m), -145.1 (d, J = 22.8 Hz), -160.7 (td, J = 22.4, 9.0 Hz). ^{31}P NMR (162 MHz, C_6D_6) δ -2.5. The ^1H spectrum reveals a mixture of products and deconvolution is non-trivial.

5.xiii - Pentafluoro-pentachloro-borane-9,9-dimethyl-xanthen-4-yl)(*tert*-butyl)phosphineyl)-*N*,*N*-dimethylaniline

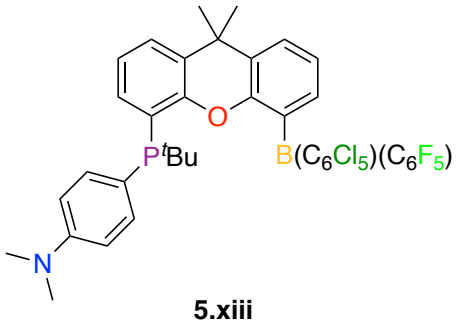

5.xiii

Yield = 198 mg, 50 %. Anal calcd for $C_{39}H_{31}BCl_5F_5NOP$ C: 55.52 H 3.70 Found C: 54.92 H: 3.41 ^1H NMR (500 MHz, C_6D_6) δ 7.47 (dt, *J* = 7.5, 2.0 Hz, 1H, Ar*H*), 7.31 (dd, *J* = 8.6, 6.5 Hz, 2H, Ar*H*), 7.24 (ddd, *J* = 9.8, 7.7, 1.7 Hz, 2H, Ar*H*), 7.10 – 7.06 (m, 1H), 6.87 (t, *J* = 7.7

Hz, 2H), 6.80 (t, *J* = 7.6 Hz, 1H), 6.49 (dd, *J* = 11.5, 8.5 Hz, 2H, Ar*H*), 2.43 (s, 6H, NMe_2*CH_3*), 1.35 (d, *J* = 27.8 Hz, 6H, XAN*CH_3*), 1.17 (d, *J* = 12.5 Hz, 9H, ^{t}Bu*CH_3*). Residual toluene and precursor are also seen in spectrum. $^{13}C\{^1H\}$ NMR (126 MHz, C_6D_6) δ 150.5, 136.5, 134.9, 134.8, 134.2, 133.9, 132.7, 132.2, 132.1, 130.1, 129.9, 129.3, 127.0, 125.7, 123.4, 123.2, 122.4, 122.3, 117.1, 112.6 (Ar*C*), 39.8 (NMe_2*CH_3*), 32.2 (XAN*CH_3*), 28.8 (d, *J* = 15.8 Hz, ^{t}Bu*CH_3*). No signals attributable to the quarternary xanthene or *tert*butyl phosphine carbon atoms can be seen. $^{19}F\{^1H\}$ NMR (470 MHz, C_6D_6) δ -128.4 – -128.8 (m, *o*-C_6F_5), -148.1 (tt, *J* = 21.4, 5.7 Hz, *p*-C_6F_5), -163.1 (dtd, *J* = 87.1, 22.7, 8.9 Hz, *m*-C_6F_5).$^{31}P\{^1H\}$ NMR (202 MHz, C_6D_6) δ -3.5.

5.xiv - *Bis*pentachloro-borane-9,9-dimethyl-xanthen-4-yl)(*tert*-butyl)phosphineyl)-*N*,*N*-dimethylaniline

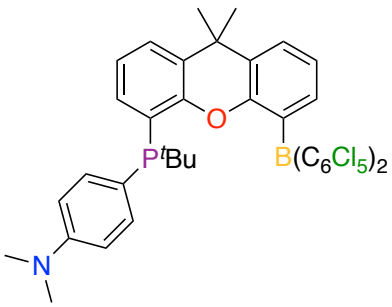

5.xiv

Yield: 279 mg, 64 %. Anal calcd for $C_{39}H_{31}BCl_{10}NOP$ C: 50.59 H: 3.37. Found: C: 51.05 H: 3.30 ^1H NMR (500 MHz, CD_2Cl_2) δ 7.75 (d, *J* = 7.6 Hz, 1H, Ar*H*), 7.41 – 7.35 (m, 1H, Ar*H*), 7.14 (ddd, *J* = 24.8, 11.9, 7.7 Hz, 4H, Ar*H*), 6.94 (s, 2H, Ar*H*), 6.67 (d, *J* = 8.4 Hz, 2H, Ar*H*), 2.95 (br. s, 6H, NMe_2*CH_3*), 1.72 – 1.58 (m, 6H, XAN*CH_3*), 1.07 (d, *J* = 12.1 Hz, 9H, ^{t}Bu*CH_3*). Residual toluene is also seen in spectrum. $^{13}C\{^1H\}$ NMR (126 MHz, CD_2Cl_2) δ 150.4, 138.4, 137.4, 137.2, 135.8, 134.9, 134.6, 129.4, 128.6, 127.4, 125.7, 123.7, 123.1, 112.5 (Ar*C*), 40.5

(NMe$_2$*CH$_3$*), 34.5 (XAN*C*) 32.8, (XAN*CH$_3$*), 28.5 (d, *J* = 15.5 Hz, ^{t}Bu*CH$_3$*) ^{31}P{^{1}H} NMR (202 MHz, CD_2Cl_2) δ -5.3. No signals attributable to the product can be seen in the ^{11}B spectrum.

5.xiv-H$_2$ - *Bis*pentachloro-borane-9,9-dimethyl-xanthen-4-yl)(*tert*-butyl)phosphaneyl)-*N*,*N*-dimethylaniline-H$_2$

Approx. 6 mg of compound was dissolved in 0.6 mL toluene and added to a Youngs-tap NMR tube through a syringe filter. The resulting solution was degassed by three freeze-pump-thaw cycles and 1 bar. H_2 was added. ^{11}B{^{1}H} NMR (128 MHz, C_7H_8) δ -9.7. ^{31}P{^{1}H} NMR (162 MHz, C_7H_8) δ 5.7.

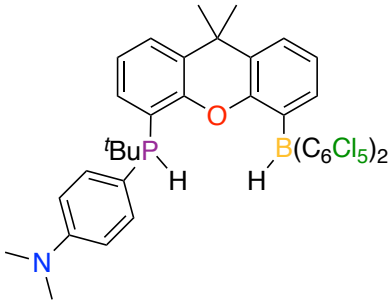

5.xiv-H$_2$

5.xv - *Tert*-butyl(9,9-dimethyl-xanthen-4-yl)phosphineyl)phenyl)-*N*,*N*-dimethylmethanamine

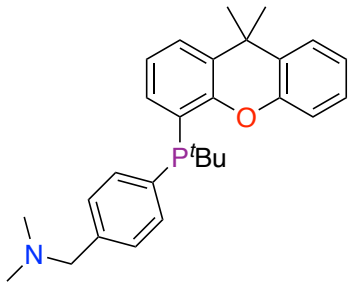

5.xv

N-butyllithium (0.6 mL, 0.93 mmol, 1.1 equiv. of a 1.6 M solution) was added dropwise at -78 °C to a solution of 4-bromo dimethylbenzylamine (0.15 mL, 0.94 mmol, 1.1 equiv.) in THF

(10 mL). This temperature was maintained and a THF (20 mL) solution of **5.ii** (283 mg, 0.85 mmol, 1 equiv.) was added before the reaction mixture was warmed to room temperature. Following the removal of volatiles *in vacuo*, the resulting oil **5.xv** was frozen in liquid nitrogen and dried under dynamic vacuum a further three times before being used. ^{1}H NMR (400 MHz, C_6D_6) δ 7.68 (t, *J* = 7.4 Hz, 2H, Ar*H*), 7.56 (ddd, *J* = 7.6, 3.8, 1.6 Hz, 1H, Ar*H*), 7.26 (dd, *J* = 12.6, 8.0 Hz, 2H, Ar*H*), 7.09 (dd, *J* = 6.7, 4.7 Hz, 2H, Ar*H*), 6.98 – 6.82 (m, 5H, Ar*H*), 3.62 (d, *J* = 6.2 Hz, 3H, NMe$_2$*CH$_3$*), 3.26 – 3.18 (m, 2H, Ph*CH$_2$*), 2.06 (s, 6H, XAN*CH$_3$*), 1.35 (d, *J* = 1.8 Hz, 9H, ^{t}Bu*CH$_3$*). ^{31}P NMR (162 MHz, C_6D_6) δ 5.2.

5.6 References

1 O. Karaman, G. A. Alkan, C. Kizilenis, C. C. Akgul and G. Gunbas, *Coord. Chem. Rev.*, 2023, **475**, 214841.

2 G. Shabir, A. Saeed and P. Ali Channar, *Mini. Rev. Org. Chem.*, 2018, **15**, 166–197.

3 J. Hicks, P. Vasko, J. M. Goicoechea and S. Aldridge, *Nature*, 2018, **557**, 92–95.

4 N. R. Andreychuk, B. Vidjayacoumar, J. S. Price, S. Kervazo, C. A. Peeples, D. J. H. Emslie, V. Vallet, A. S. P. Gomes, F. Réal, G. Schreckenbach, P. W. Ayers, I. Vargas-Baca, H. A. Jenkins and J. F. Britten, *Chem. Sci.*, 2022, **13**, 13748–13763.

5 A. J. Sandee, J. N. H. Reek, P. C. J. Kamer and P. W. N. M. Van Leeuwen, *J. Am. Chem. Soc.*, 2001, **123**, 8468–8476.

6 K. Škoch, C. G. Daniliuc, G. Kehr, S. Ehlert, M. Müller, S. Grimme and G. Erker, *Chem. – A Eur. J.*, 2021, **27**, 12104–12114.

7 P. Vasko, I. A. Zulkifly, M. Á. Fuentes, Z. Mo, J. Hicks, P. C. J. Kamer and S. Aldridge, *Chem. - A Eur. J.*, 2018, **24**, 10531–10540.

8 P. Vasko, M. Á. Fuentes, J. Hicks and S. Aldridge, *Dalt. Trans.*, 2019, **48**, 2896–2899.

9 Z. Mo, E. L. Kolychev, A. Rit, J. Campos, H. Niu and S. Aldridge, *J. Am. Chem. Soc*, 2015, **137**, 12227–2230.

10 V. T. Trepohl, R. Fröhlich and M. Oestreich, *Tetrahedron*, 2009, **65**, 6510–6518.

11 J. S. Han and W. Wolfsberger, *Zeitschrift fur Naturforsch. - Sect. B J. Chem. Sci.*, 1989, **44**, 502–504.

12 E. Bergin, C. T. O'Connor, S. B. Robinson, E. M. McGarrigle, C. P. O'Mahony and D. G. Gilheany, *J. Am. Chem. Soc.*, 2007, **129**, 9566–9567.

13 H. Lee and S. H. Hong, *Appl. Catal. A Gen.*, 2018, **560**, 21–27.

14 W. Tang and X. Zhang, *Chem. Rev.*, 2003, **103**, 3029–3069.

15 K. C. Szeto, W. Sahyoun, N. Merle, J. L. Castelbou, N. Popoff, F. Lefebvre, J. Raynaud, C. Godard, C. Claver, L. Delevoye, R. M. Gauvin and M. Taoufik, *Catal. Sci. Technol.*, 2016, **6**, 882–889.

16 M. Schelhaas and H. Waldmann, *Angew. Chemie Int. Ed. English*, 1996, **35**, 2056–2083.
17 P. W. Atkins, *Phys. Chemie*, 2010, 972.
18 J. S. Nowick, P. Ballester, F. Ebmeyer and J. Rebek, *J. Am. Chem. Soc.*, 1990, **112**, 8902–8906.
19 P. Devulapalli, B. Wang and R. H. Neilson, *Phosphorus. Sulfur. Silicon Relat. Elem.*, 2015, **190**, 2154–2163.
20 N. G. Andersen, P. D. Ramsden, D. Che, M. Parvez and B. A. Keay, *J. Org. Chem.*, 2001, **66**, 7478–7486.
21 W. Chodkiewicz, D. Guillerm, D. Jore, E. Mathieu and W. Wodzki, *J. Organomet. Chem.*, 1984, **269**, 107–114.
22 M. Z. Bani-Fwaz, A. E. Fazary and G. Becker, *J. Organomet. Chem.*, 2017, **846**, 51–65.
23 I. Zulkifly, University of Oxford, 2020.
24 S. H. Chikkali, R. Bellini, G. Berthon-Gelloz, J. I. Van Der Vlugt, B. De Bruin and J. N. H. Reek, *Chem. Commun.*, 2010, **46**, 1244–1246.
25 J. Zhou, E. D. Litle and F. P. Gabbaï, *Chem. Commun.*, 2021, **57**, 10154–10157.
26 L. A. D. Van Der Veen, P. K. Keeven, P. C. J. Kamer and P. W. N. M. Van Leeuwen, *Chem. Commun.*, 2000, 333–334.
27 F. Kutter, E. Lork, S. Mebs and J. Beckmann, *Organometallics*, 2018, **37**, 4287–4296.
28 P. Federmann, R. Müller, F. Beckmann, C. Lau, B. Cula, M. Kaupp and C. Limberg, *Chem. – A Eur. J.*, 2022, **28**, e202200404.
29 M. J. L. Tschan, H. Launay, H. Hagen, J. Benet-Buchholz and P. W. N. M. Van Leeuwen, *Chem. – A Eur. J.*, 2011, **17**, 8922–8928.
30 J. Yang, H. Su, C. Lian, Y. Shang, H. Liu and J. Wu, *Phys. Chem. Chem. Phys.*, 2020, **22**, 15373–15380.
31 M. Herberhold, C. Köhler, V. Tröbs and B. Wrackmeyer, *Zeitschrift fur Naturforsch. - Sect. B J. Chem. Sci.*, 2000, **55**, 939–945.
32 J. R. McAtee, G. P. A. Yap and D. A. Watson, *J. Am. Chem. Soc.*, 2014, **136**, 10166–10172.
33 H. J. Reich, *Chem. Rev.*, 2013, **113**, 7130–7178.
34 D. J. Parks and W. E. Piers, *Organometallics*, 1998, **17**, 5492–5503.
35 A. E. Ashley, T. J. Herrington, G. G. Wildgoose, H. Zaher, A. L. Thompson, N. H. Rees, T. Krämer and D. O'Hare, *J. Am. Chem. Soc.*, 2011, **133**, 14727–14740.
36 K. Haav, J. Saame, A. Kütt and I. Leito, *European J. Org. Chem.*, 2012, **2012**, 2167–2172.
37 J. Clayden, N. Greeves and S. Warren, *Organic Chemistry*, Oxford University Press, 2nd edn., 2012.
38 L. P. Hammett, *J. Am. Chem. Soc.*, 1937, **59**, 96–103.
39 L. Arnaut, *Chem. Kinet.*, 2021, 225–245.

Chapter 6 – Suggestions for Further Research

6.1 Future Work

Remaining true to the initial goal of designing a well-characterised surface supported intramolecular FLP, future work should look towards expanding upon the lessons learnt in Chapter 5. Although the approaches explored in this chapter can be reasonably conclusively ruled out, these investigations could prove a starting point for a variety of new directions.

One potential unexplored route is the employment of polyaromatic hydrocarbons as an aryl substituent on the phosphine, such as a substituted biphenyl or naphthalene. Creating a distinct separation between the FLP reactivity and surface tethering might enable them to function in a complementary manner.

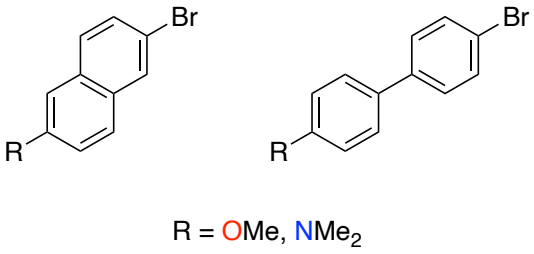

Figure 6.1 – Potential functionalised PAH tethers.

Additionally, only intramolecular pairs derived from xanthene have been explored. Other scaffolds might be conducive to more facile tethering. This could be especially true if the conditions required to introduce the Lewis acid and Lewis base in a stepwise manner are more benign than lithiation. A key tenet of xanthene based FLP chemistry is that the proximity of the Lewis acidic and basic centre determines the small molecule reactivity of these systems. Looking just at molecules which are known to reversibly activate hydrogen, there is a difference of just under 0.3 Å between the furthest and shortest acid/base separations.[1]

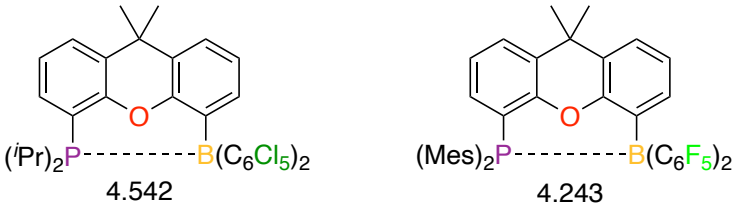

Figure 6.2 – Reversibly hydrogen activating FLPs with largest and smallest P...B separations.

What is more, xanthene and related backbones can distort something akin to butterfly wings flapping, which means that if targeted scaffolds have some degree of structural flexibility, they might be able to accommodate small molecule activation in some conformations. Given the breadth of bidentate phosphines based on similar backbones, it is helpful to look at structurally characterised complexes based on these motifs. For example, free thixantphos has a 4.025 Å P…P separation, although this is very can widen to 4.4512 Å in a palladium complex.[2,3] The analogous separation in sixantphos is 3.884 Å and it can form a ruthenium complex where the two phosphorous atoms on the bidentate phosphine ligand are 4.572(3) Å apart.[4,5]

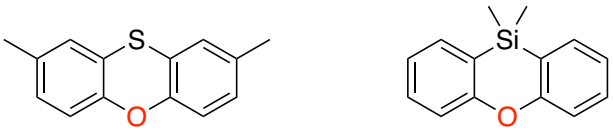

Figure 6.3 – Thixanthene (thixantphos precursor) and 10,10-dimethylphenoxasilin (sixantphos precursor).

In light of these considerations, synthetic routes towards surface supported intramolecular FLPs seem attainable in the medium term.

6.2 References

1 Z. Mo, E. L. Kolychev, A. Rit, J. Campos, H. Niu and S. Aldridge, *J. Am. Chem. Soc*, 2015, **137**, 12227–2230.

2 M. A. Zuideveld, B. H. G. Swennenhuis, M. D. K. Boele, Y. Guari, G. P. F. Van Strijdonck, J. N. H. Reek, P. C. J. Kamer, K. Goubitz, J. Fraanje, M. Lutz, A. L. Spek and P. W. N. M. Van Leeuwen, *J. Chem. Soc. Dalt. Trans.*, 2002, 2308–2317.

3 W. Goertz, W. Keim, D. Vogt, U. Englert, M. D. K. Boele, L. A. Van Der Veen, P. C. J. Kamer and P. W. N. M. Van Leeuwen, *J. Chem. Soc. Dalt. Trans.*, 1998, 2981–2988.

4 D. Pingen, T. Lebl, M. Lutz, G. S. Nichol, P. C. J. Kamer and D. Vogt, *Organometallics*, 2014, **33**, 2798–2805.

5 T. Marimuthu, M. D. Bala and H. B. Friedrich, *J. Chem. Crystallogr.*, 2012, **42**, 251–257.